C(sp^3)-H Fluorination with a Copper(II)/(III) Redox Couple

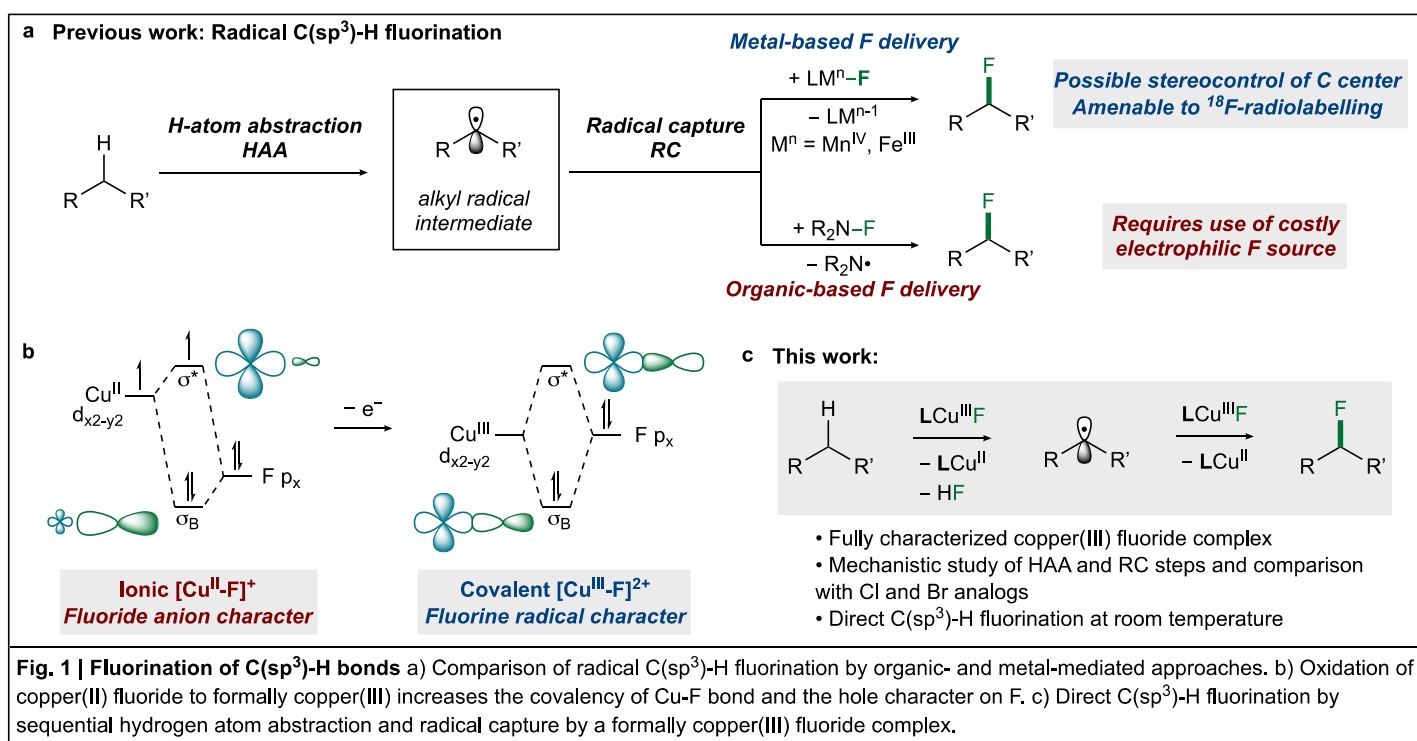Jamey K. Bower,[a] Andrew D. Cypcar,[a] Brenda Henriquez,[b] S. Chantal E. Stieber,[b]* Shiyu Zhang[a]*

[a] Department of Chemistry & Biochemistry, The Ohio State University, 100 West 18th Ave, Columbus, OH 43210
[b] Department of Chemistry & Biochemistry, California State Polytechnic University, Pomona, 3801 W. Temple Ave, Pomona, California 91768

Abstract

Despite the growing interest in the synthesis of fluorinated organic compounds, few methods are able to incorporate fluoride ion directly into alkyl C-H bonds. Here, we report the C(sp^3)-H fluorination reactivity of a formally copper(III) fluoride complex. The C-H fluorination intermediate, **L**CuF, along with its chloride and bromide analogs, **L**CuCl and **L**CuBr, were prepared directly from halide sources with a chemical oxidant and fully characterized. While all three copper(III) halide complexes capture carbon radicals efficiently to afford C(sp^3)-halogen bonds, **L**CuF is two orders of magnitude more efficient at hydrogen atom abstraction (HAA) than **L**CuCl and **L**CuBr. Alongside reported kinetic data for other **L**Cu(III) species, we established a positive correlation between ligand basicity and the rate of HAA. The capability of **L**CuF to perform both hydrogen atom abstraction and radical capture was leveraged to enable fluorination of allylic and benzylic C-H bonds and α-C-H bonds of ethers at room temperature.

Carbon-fluorine bonds are becoming increasingly prevalent in pharmaceuticals and agrochemicals.[1] The value of fluorinated compounds in these applications stems from their enhancement of lipophilicity, metabolic stability, and receptor binding affinity.[2] Given the abundance of C(sp^3)-H bonds in organic molecules, the atom-efficient conversion of C(sp^3)-H to C(sp^3)-F bonds has been a prominent goal for synthetic methodology development.[3–6] The majority of C(sp^3)-H fluorination methods depend on electrophilic fluorination reagents (F$^+$), e.g. Selectfluor,[7,8] N-fluorosulfonimide (NFSI),[9] N-fluoro-2,4,6-trimethylpyridinium,[10] which are hazardous to synthesize and costly to use on large scale (Fig. 1a). Few C(sp^3)-H fluorination protocols employ nucleophilic fluorine (F$^-$) sources, e.g. metal fluorides[3,11] or HF.[4] Most notably, Groves and co-workers developed several manganese catalysts that fluorinate C(sp^3)-H bonds using fluoride salts.[11] In these and several other examples,[9] the C(sp^3)-F bond was furnished by metal fluorides, e.g. Mn^{IV}-F and Fe^{III}-F, that capture the alkyl radical generated from C(sp^3)-H activation (Fig. 1a). Not all C(sp^3)-H fluorination methods, however, deliver the F atom to alkyl radicals through a metal-centered mechanism. Alkyl radicals can also react with Selectfluor and NFSI to afford C(sp^3)-F bonds.[7–9,12–14] Practically, the metal-mediated process is advantageous, since it is more suitable for ^{18}F radiolabeling and controlling

Fig. 1 | Fluorination of C(sp^3)-H bonds a) Comparison of radical C(sp^3)-H fluorination by organic- and metal-mediated approaches. b) Oxidation of copper(II) fluoride to formally copper(III) increases the covalency of Cu-F bond and the hole character on F. c) Direct C(sp^3)-H fluorination by sequential hydrogen atom abstraction and radical capture by a formally copper(III) fluoride complex.

2

the stereochemistry of the C(sp^3)-F center.[10,15] Despite this progress, a remaining challenge is improving the selectivity of alkyl fluorination.[1] As chiral copper complexes are well-known asymmetric catalysts for radical C-H functionalization,[16–18] the use of tunable copper fluoride complexes, in principle, would provide the opportunity to further improve the selectivity of C(sp^3)-H fluorination. However, the mechanistic step of R• capture at a copper fluoride complex to afford C(sp^3)-F bonds has yet to be established.

While copper(II) chloride and bromide are well-documented C(sp^3)-H halogenating reagents,[19–21] copper(II) fluoride is not amenable to analogous fluorination reactivity, likely due to the highly ionic nature of the Cu^{II}-F bond (Fig. 1b). Therefore, we questioned whether a formally [Cu^{III}-F]$^{2+}$ complex might be suited for C(sp^3)-H fluorination, as oxidation would increase the copper effective nuclear charge and lower the Cu d orbital energy to allow for increased fluorine contribution to the lowest unoccupied molecular orbital (LUMO) of the [Cu^{III}-F]$^{2+}$ motif (Fig. 1b). Consistent with this hypothesis, recent X-ray absorption spectroscopy studies on formally copper(III) complexes showed that a majority of LUMOs are located on the ligand instead of the metal, resulting in an inverted ligand field.[22,23] The increased hole character on the ligand has been invoked to explain the C(sp^3)-H amination reactivity of Cu nitrene complexes.[24,25] Thus, we propose that the introduction of fluorine hole character will allow a [Cu^{III}-F]$^{2+}$ complex to perform both hydrogen atom abstraction (HAA) and radical capture (RC) to furnish the C(sp^3)-F bond (Fig 1c). Herein, we report the synthesis and C(sp^3)-H halogenation reactivity of formally copper(III) fluoride, chloride, and bromide complexes. While all [Cu^{III}-X]$^{2+}$ complexes are proficient at radical capture, the [Cu^{III}-F]$^{2+}$ complex is faster at HAA than [Cu^{III}-Cl]$^{2+}$ and [Cu^{III}-Br]$^{2+}$ complexes by two orders of magnitude. Leveraging these mechanistic insights, we demonstrate that the copper(III) fluoride is capable of directly fluorinating allylic and benzylic C(sp^3)-H bonds as well as α-C-H bonds of ethers using F$^-$ as the fluorine source.

Results and discussion

Synthesis, Characterization, and Electronic Structure. To examine the ability of the $[Cu^{III}-F]^{2+}$ motif to fluorinate $C(sp^3)$-H bonds, we set out to synthesize a discrete $[Cu^{III}-F]^{2+}$ complex. Additionally, we targeted copper(III) chloride and bromide analogs to provide a detailed understanding of how electronic structure affects reactivity relevant to $C(sp^3)$-H halogenation across the copper(III) halide series. As copper(III) halides are often speculated products of oxidative addition of aryl halides to a copper(I) center, the traditional Cu^I/Cu^{III} redox cycles are more amenable to C-X bond cleavage instead of C-X bond formation.[26,27] To support the one-electron Cu^{II}/Cu^{III} redox couple central to our hypothesis, we selected the bis-carboxamidopyridine ligand (**L** = [N-N'-bis(2,6-diisopropylphenyl)-2,6-pyridinedicarboxamido]$^{2-}$) based on the work by Tolman and co-workers.[28] Reaction of **L**Cu^{II}(MeCN) with tetrabutylammonium halide salts in tetrahydrofuran afforded the corresponding anionic copper(II) halide complexes [TBA]**L**Cu^{II}X (X = F, Cl, Br) in 88%, 83%, and 84% yield, respectively (Fig. 2a). All [TBA]**L**Cu^{II}X complexes were characterized by X-ray crystallography and electron paramagnetic resonance (see Supplementary Information), confirming copper $S = \frac{1}{2}$ centers. Samples of [TBA]**L**Cu^{II}F were unsuitable for single crystal X-ray diffraction, therefore, the bis(triphenylphosphine)iminium (PPN) salt, [PPN]**L**Cu^{II}F, was prepared to obtain structural characterization (Supplementary Fig. 1). The copper(II) halide structures exhibit similar Cu-N distances between **L** and copper center (Cu-N$_{(avg)}$ (Å) = 1.977 for [**L**Cu^{II}F]$^-$, 1.987 for [**L**Cu^{II}Cl]$^-$, 1.982 for [**L**Cu^{II}Br]$^-$). All copper(II) centers adopt a distorted square planar geometry (τ_4 = 0.15 for [**L**Cu^{II}F]$^-$), 0.20 for [**L**Cu^{II}Cl]$^-$), 0.20 for [**L**Cu^{II}Br]$^-$, τ_4 = 0 for square planar, τ_4 = 1 for tetrahedral)[29] with the halide positioned slightly out of the N$_3$Cu plane. Seeking to access copper(III) halides by one-electron oxidation, we measured the Cu^{II}/Cu^{III} redox potential in solution. The cyclic voltammograms of [TBA]**L**Cu^{II}X complexes in CH$_2$Cl$_2$ exhibit quasi-reversible redox couples at $E_{1/2}$ = 0.465 V for [**L**Cu^{II}F]$^-$, 0.525 V for [**L**Cu^{II}Cl]$^-$, and 0.525 V for [**L**Cu^{II}Br]$^-$ (vs Ag/AgNO$_3$, Fig. 2b), respectively. As expected, [TBA]**L**Cu^{II}F features the most cathodic redox potential due to the high electronegativity of
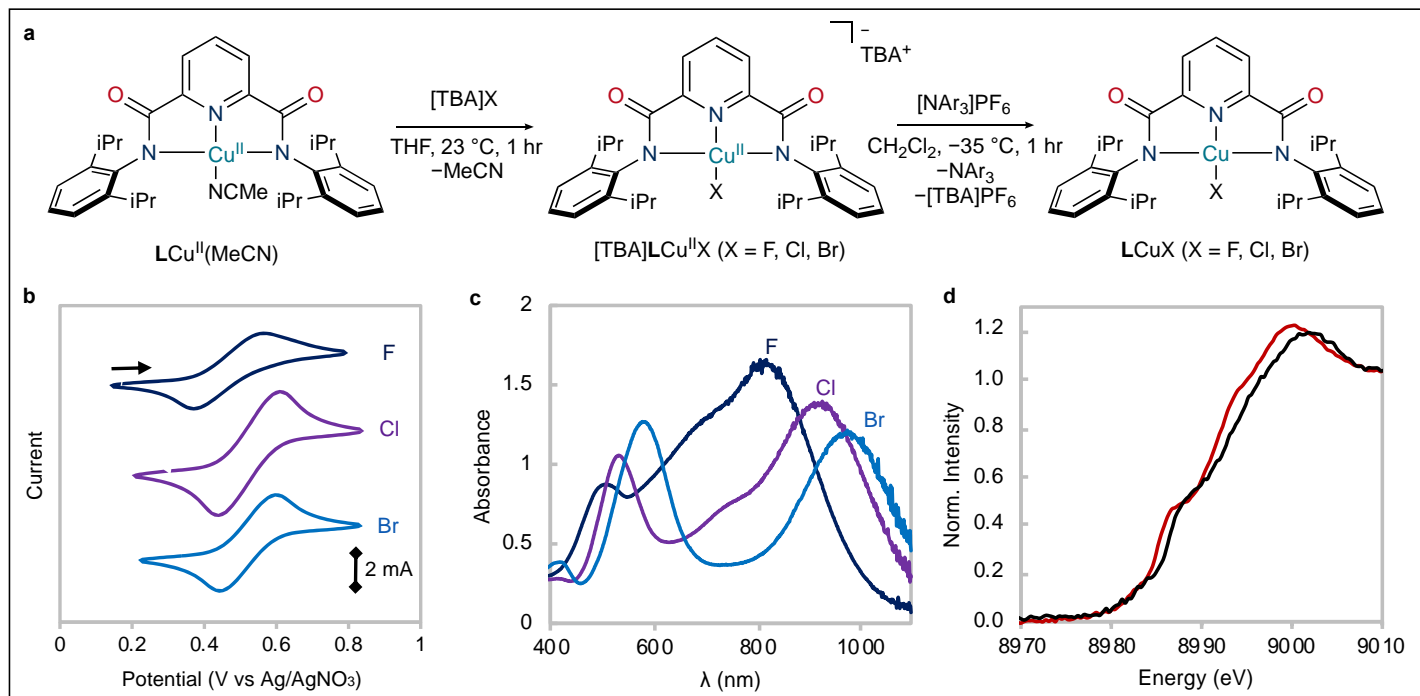
Fig. 2 | Synthesis and characterization of copper(III) halides a) Two-step synthesis of copper(III) halides via halide addition and chemical oxidation. b) Cyclic voltammograms of [TBA]**L**CuX complexes (0.3mM in 0.1 M [TBA]ClO$_4$ in CH$_2$Cl$_2$). c) UV-vis spectra of **L**CuX complexes at −80 °C (0.1mM in CH$_2$Cl$_2$). c) Copper K-edge X-ray absorption spectra of [TBA]**L**Cu^{II}F (red) and **L**CuF (black) in CH$_2$Cl$_2$ at 10K.

fluoride. Interestingly, [TBA]**L**Cu^{II}Br is oxidized at nearly the same potential as [TBA]**L**Cu^{II}Cl but features the most reversible redox profile of the series, with a peak-to-peak separation of 160 mV.

Variable temperature UV-Vis spectrophotometry was utilized to study the thermal stability of the copper(III) fluoride complex, **L**CuF (Fig. 2b). Based on the CV profiles of [TBA]**L**Cu^{II}X, the aminium radical cation, [NAr$_3$]PF$_6$ (Ar = 4-bromophenyl; $E_{1/2}$ = 0.66 V vs Ag/AgNO$_3$ in MeCN) was selected as the chemical oxidant to prepare **L**CuX complexes. Treatment of [TBA]**L**Cu^{II}F with [NAr$_3$]PF$_6$ at −80 °C in CH$_2$Cl$_2$ resulted in the rapid formation of a new species with intense absorptions at 520 nm (ε = 9100 M^{-1} cm^{-1}) and 820 nm (ε = 18600 M^{-1} cm^{-1}), which were attributed to the **L**CuF complex (Fig. 2c). The UV-Vis spectra of **L**CuCl and **L**CuBr, prepared analogously via chemical oxidation, share the two main charge transfer bands (Fig. 2c). Both UV-Vis bands red-shift along the series from **L**CuF to **L**CuCl to **L**CuBr in accordance with the donating ability of the halide ligands, indicating that these transitions correspond to ligand-to-metal charge transfer (LMCT).[27] Time-dependent density functional theory (TD-DFT) calculations at B3LYP/def2-TZVP(-f) level reproduced the two intense features as well as their red-shifting trends (Supplementary Fig. 46). Both absorptions originate from charge transfers from halide/**L** based orbitals to the LUMO, which features
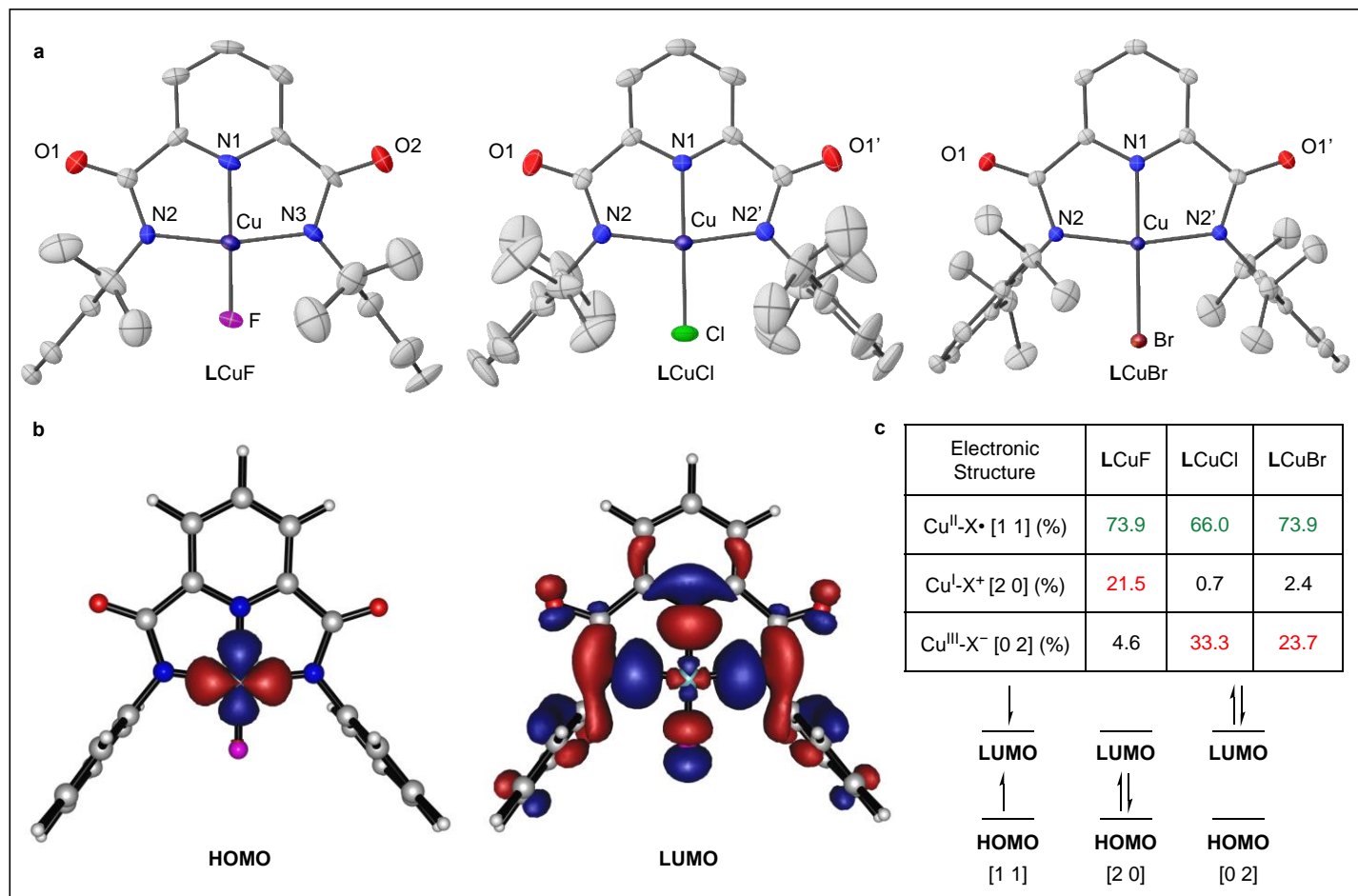
5

Fig. 3 | Physical and electronic structures of copper(III) halides a) Solid-state structures of **L**CuF, **L**CuCl, and **L**CuBr with thermal ellipsoids shown at 50% level of probability. Cocrystallized solvents and minor components of disorder are omitted for clarity. Selected bond lengths (Å) and angles (°): **L**CuF Cu-F = 1.755(3); Cu -N_1 =1.841(4); Cu-N_2 = 1.901(4) ; N_1-Cu-F =179.68(17). **L**CuCl Cu-Cl = 2.1085(8); Cu-N_1 = 1.859(2); Cu-N_2 = 1.9132(16); N_1-Cu-Cl = 180. **L**CuBr Cu-Br = 2.2562(4); Cu-N_1 = 1.8623(18); Cu-N_2 = 1.9159(13); N_1-Cu-Br = 180. b) Localized HOMO and LUMO from the CASSCF(2 electrons, 2 orbitals) calculation of a truncated model of **L**CuF in which isopropyl groups are substituted with hydrogens. Orbitals are shown at an isovalue of 0.03. c) Contributions of electronic configurations to the ground state of **L**CuX complexes determined by CASSCF calculation.

the σ* interaction of the Cu $d_{x2−y2}$ and the halide/**L**. The TD-DFT calculations also suggest that

decreasing peak intensity from **L**CuF to **L**CuCl to **L**CuBr correlates to the reducing contribution of **L** to

the donor orbital (Supplementary Tables 7-9). While **L**CuCl and **L**CuBr are stable in solution at 20 °C,

LCuF undergoes slow decay at temperatures above −20 °C in CH_2Cl_2. The ^{1}H nuclear magnetic

resonance (NMR) spectra of **L**CuX in CD_2Cl_2 show sharp resonances within the 0-9 ppm range that

account for all ligand protons (Supplementary Figs. 17-22), consistent with a diamagnetic ground

state for **L**CuX complexes. Additionally, a ^{19}F NMR signal at −209.4 ppm is observed for **L**CuF.

Single crystal X-ray diffraction confirmed the formation of [Cu^{III}-X]$^{2+}$ species (Fig. 3a). The Cu-

N and Cu-X bond distances contract by 0.07-0.1 Å upon oxidation from Cu^{II} to the formally Cu^{III} state.

All copper(III) complexes exhibit more rigid square planar geometries (τ_4 = 0.09 for **L**CuF, 0.10 for

LCuCl, 0.10 for **L**CuBr) compared to their copper(II) counterparts. Overall, the structural reorganization upon oxidation is minimal, consistent with the highly reversible redox couples observed by CV (Fig. 2b). **L**CuF is, to our best knowledge, the first structurally characterized copper(III) fluoride and features the shortest Cu-F distance (1.755(3) Å) reported in the Cambridge Structural Database. Furthermore, **L**CuCl and **L**CuBr feature shorter Cu-Cl (2.1085(8) Å) and Cu-Br (2.2562(4) Å) bonds than previously reported five-coordinate copper(III) halide complexes (Cl: 2.2011(18) – 2.468(1) Å; Br: 2.3842(5) – 2.600(1) Å).[23,27,30,31]

X-ray absorption spectroscopy of the copper K-edge shows a rising edge shift of 1.4 eV upon oxidation of both the Cu^{II}-F and Cu^{II}-Cl precursors, consistent with a more oxidized copper center (Fig. 2d, Supplementary Fig. 36). The edge shift of 1-2 eV is in the range of reported values for oxidation from Cu^{II} to Cu^{III}.[32,33] The edges of both F complexes are also shifted to higher energy than the analogous Cl complexes, consistent with the shorter Cu-F bonds observed crystallographically. Lancaster and coworkers have argued that most formally copper(III) complexes have a LUMO that resides predominantly on the ligands instead of the Cu d_{x2-y2} orbital, suggesting a physical *d*-electron count higher than 8.[23] Following the experimentally-calibrated computational approach employed by Lancaster, we found that the LUMOs of **L**CuX complexes are 62.5%, 64.8% and 66.1% ligand-based for **L**CuF, **L**CuCl, and **L**CuBr, respectively (Supplementary Fig. 48), indicative of significant **L** and halide hole character.

Multireference calculations with the complete active space-self consistent field (CASSCF)[34] method lend further insight into the electronic structure of the $[Cu^{III}-X]^{2+}$ unit as a function of halide identity. Some of us[35] and others[36] have shown that CASSCF computations can provide valuable insights into the electronic structure of highly covalent metal-ligand interactions. An active space of 2e, 2o (2 electrons, 2 orbitals) comprised of σ bonding and antibonding interactions between the Cu d_{x2-y2} and **L**/halides orbitals (Supplementary Fig. 47) was found to be optimal for this system (see Supplementary Information). State-specific CASSCF calculations reveal that singlet **L**CuX complexes exhibit increasing multireference character (Supplementary Table 10) from **L**CuF to **L**CuCl to **L**CuBr

with increasing σ^* population: 0.155 e$^-$ (**L**CuF), 0.172 e$^-$ (**L**CuCl), and 0.189 e$^-$ (**L**CuBr). Consistent with this trend, natural atomic charges[37] show decreasing positive charge on Cu and decreasing negative charge on the halogen, indicating increasing covalency from **L**CuF to **L**CuCl to **L**CuBr (Supplementary Table 11). To assist a valence bond-like interpretation of CASSCF wave function, the CASSCF(2,2) orbitals were localized with an intrinsic atomic orbitals (IAO) localization method (Fig. 3b). Subsequent recalculation of the CAS wavefunction permit delineation of **L**CuX CAS wavefunction as a combination various resonance structures: Cu^{III}-X$^-$, Cu^{II}-X•, and Cu^{I}-X$^+$.[38] In all cases, the leading electronic configuration is copper(II) bound to a ligand-centered radical, denoted Cu^{II}-X• (Fig. 3c). Interestingly, while the second leading configuration of **L**CuCl and **L**CuBr is Cu^{III}-X$^-$, that of **L**CuF is Cu^{I}-X$^+$, despite the highest electronegativity of fluoride. Taken together, the XAS data and CASSCF calculation supports that the oxidation of [**L**CuX]$^-$ to **L**CuX is well distributed over metal and ligand.

HAA and RC Reactivity of [Cu^{III}-X]$^{2+}$. The presence of fluorine radical character in **L**CuF motivated us to explore C(sp^3)-H fluorination reactivity by the proposed HAA/RC mechanism. To first understand how electronic structures govern HAA reactivity across the copper(III) halide series, we investigated the reaction of **L**CuX complexes with the hydrogen atom donor, 9,10-dihydroanthracene (DHA). Addition of 100 equivalents of DHA to **L**CuX complexes at −30 °C leads to their consumption with formation of anthracene as revealed by UV-Vis spectroscopy (Supplementary Fig. 12). To confirm that the **L**Cu^{II} core remains intact after HAA, the reaction of **L**CuF with DHA was repeated in a scintillation vial. Following workup in acetonitrile, the brown-colored **L**Cu^{II}(MeCN) complex was isolated in 84% spectroscopic yield (Supplementary Fig. 13). The second-order rate constant (k) of HAA was obtained by monitoring the decay of LMCT bands of **L**CuX (820 nm for **L**CuF, 920 nm for **L**CuCl, 980 nm for **L**CuBr, respectively) under pseudo-first-order conditions (see Supplementary Information). The rate of HAA from DHA for **L**CuF is $k = 0.668$ M^{-1} s^{-1}, which is 230 times higher than
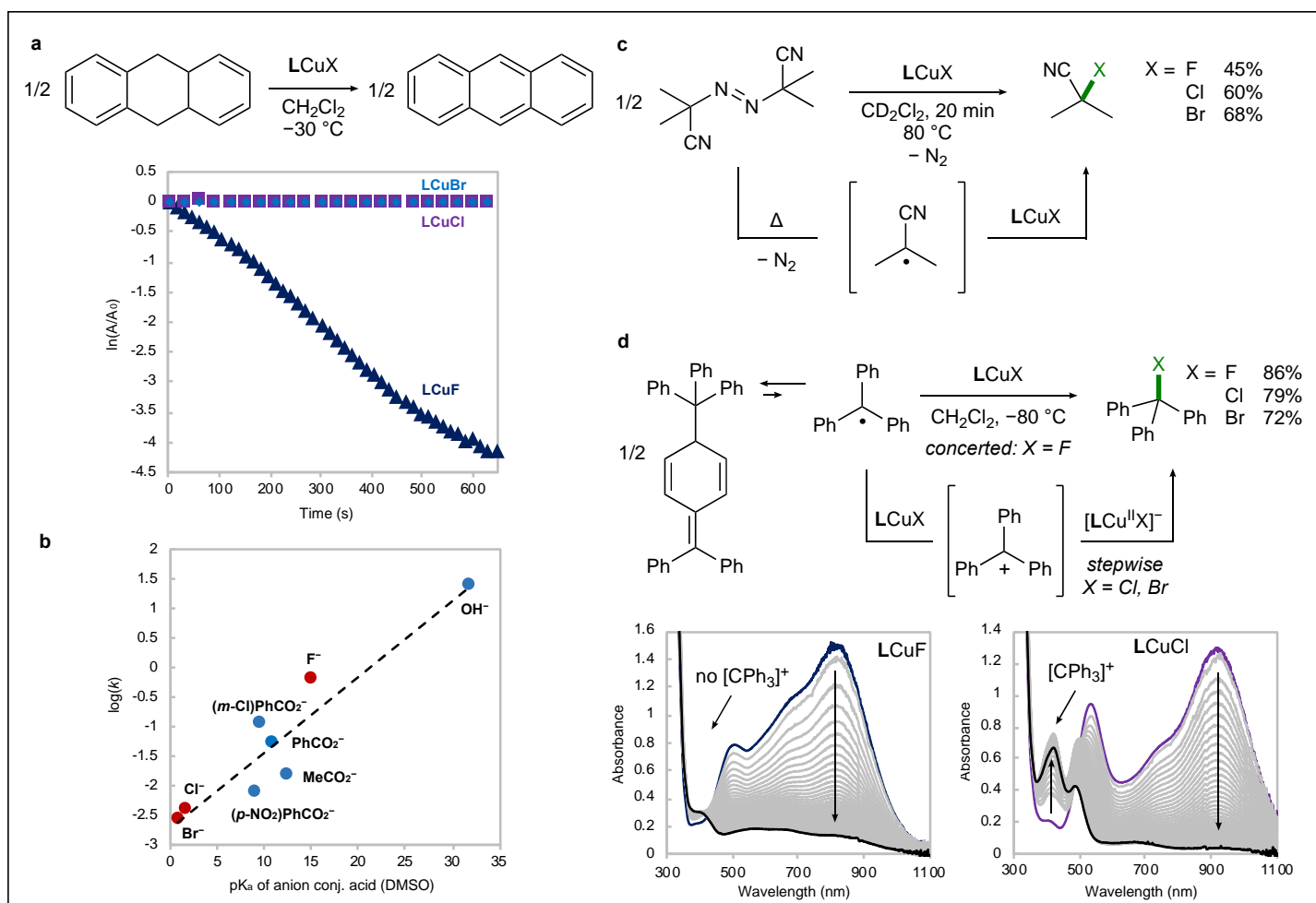
Fig. 4 | Mechanistic study of hydrogen atom abstraction and radical capture. a) Kinetic traces of the reaction between copper(III) halides and 9,10-dihydroanthracene (100 eq, −30 °C) b) Plot of the log of second-order rate constants for HAA from DHA versus pK_a of the conjugate acid of the anion (in DMSO) bound to **L**Cu complexes. Data for **L**CuOH (Ref. 28) was collected at −30 °C in acetone, and data for **L**Cu(O₂CR) complexes (Refs. 39 & 48) were collected at −25 °C in 1,2-difluorobenzene. c) Reaction of azobisisobutyronitrile with **L**CuX complexes at elevated temperatures furnishes the corresponding C(sp³)-X bonds. d) Radical capture reactivity study with triphenylmethyl radical at −80 °C reveals the intermediacy of triphenylmethyl cation for **L**CuCl, but not for **L**CuF. Scans were recorded every 15 seconds.

LCuCl and 280 times higher than **L**CuBr (Fig. 4a). The rapid rate of HAT by **L**CuF is intriguing considering **L**CuF is a weaker oxidant than **L**CuCl and **L**CuBr. Since **L**CuF is expected to be more basic than **L**CuCl and **L**CuBr, the higher HAA reactivity of **L**CuF can be attributed to the underlying correlation between HAA and basicity of the complex, which was first demonstrated by Tolman's highly basic **L**CuOH complexes.[28]

The difference in HAA reactivity of **L**CuF and **L**CuOH (36x higher) was further probed with an Eyring analysis (ln(k/T) vs 1/T). Although **L**CuF exhibits a slightly lower activation enthalpy than **L**CuOH (ΔH‡(**L**CuF) = 3.8(2); ΔH‡(**L**CuOH) = 5.4(2) kcal mol⁻¹), there is a greater entropic penalty for **L**CuF (ΔS‡(**L**CuF) = −10(1) cal K⁻¹ mol⁻¹; ΔS‡(**L**CuOH) = −7.2(5) cal K⁻¹ mol⁻¹; see Supplementary Information). Despite **L**CuF being ~450 mV more oxidizing than **L**CuOH, the lower basicity of fluoride

9

results in a lower HAA rate, clearly emphasizing the importance of the proton transfer over electron transfer for the overall rate of HAA by formally $\mathbf{L}Cu^{III}$ species. In this context, it is informative to compare the HAA rate constants of $\mathbf{L}CuX$ with $\mathbf{L}CuOH$[28] and $\mathbf{L}Cu(O_2CR)$[39] complexes. Despite the different solvents used for HAA kinetic study, a positive correlation of $\log(k)$ from HAA by $\mathbf{L}Cu^{III}$ species with the pK_a of the ligand is observed (Fig. 4b).

Having established the high rate of HAA by $\mathbf{L}CuF$, we were eager to explore the possibility of radical capture as the terminating step in a $C(sp^3)$-H fluorination sequence. A common strategy to explore the capture of alkyl radical ($R\bullet$) is to examine the reaction of metal complexes with carbon-centered radical precursors e.g. azo compounds and acyl peroxides.[40,41] Heating $\mathbf{L}CuX$ complexes in the presence of azobisisobutyronitrile (AIBN) at 80 °C in CD_2Cl_2 results in the formation of 2-haloisobutyronitriles in 45% ($\mathbf{L}CuF$), 60% ($\mathbf{L}CuCl$), and 68% ($\mathbf{L}CuBr$) yield, respectively (Fig. 4a). In contrast, treatment of [TBA]$\mathbf{L}Cu^{II}X$ complexes with AIBN at 80 °C for 2 hours does not furnish halogenated products, consistent with the increased hole character on halides upon oxidation of Cu^{II} to Cu^{III}. The lower yield of halogenated product for $\mathbf{L}CuF$ relative to $\mathbf{L}CuCl$ and $\mathbf{L}CuBr$ is likely due to its higher rate of self-decomposition at 80 °C (Supplementary Fig. 15). These results show that discrete $[Cu^{III}\text{-}X]^{2+}$ complexes mediate carbon radical capture, which has been previously proposed in copper-catalyzed $C(sp^3)$-H halogenation reactions.[21]

To gain insights into the mechanism of radical capture by $\mathbf{L}CuX$ complexes, we employed trityl radical, generated from the dissociation of Gomberg's dimer.[42,43] Contrary to the two-hundred-fold rate difference for HAA, all $\mathbf{L}CuX$ complexes react with trityl radical at similar rates at −80 °C. ^{1}H NMR analysis of the same reactions at a larger scale confirms the formation of the corresponding Ph_3C-F, Ph_3C-Cl, and Ph_3C-Br products in 86%, 79% and 72% yield, respectively (Supplementary Figs. 26-28). Despite the similar efficiency of RC for all three $\mathbf{L}CuX$ complexes, there are key mechanistic differences. Careful examination of *in situ* UV-Vis profiles reveals that trityl radical capture by $\mathbf{L}CuCl$ and $\mathbf{L}CuBr$ proceeds through the trityl cation intermediate (λ_{max} = 415 nm), while that by $\mathbf{L}CuF$ does not (Fig. 4c, Supplementary Fig. 16). This result suggests a stepwise electron transfer-halide transfer

(ET-XT) mechanism for **L**CuCl and **L**CuBr and a synchronous fluorine atom transfer mechanism for

LCuF. These observations are consistent with the lower redox potential and higher nucleophilicity of

LCuF compared to **L**CuCl and **L**CuBr. There is ambiguity in the literature about the suitability of

copper(III) versus copper(II) for alkyl radical capture and whether the precise mechanism is concerted

or stepwise.[21,44] Further kinetic studies to quantitate the synchronicity of radical capture by formally

copper(III) species are ongoing and will be reported in due course.

Fluorination reactivity. The proficiency of **L**CuF for both hydrogen atom abstraction and radical capture led us to envision the possibility of direct $C(sp^3)$-H fluorination by a sequential HAA/RC mechanism. Treatment of **L**CuF with 100 equivalents of tetrahydrofuran at room temperature for 3 hours resulted in the selective formation of 2-fluorotetrahydrofuran in 69% yield based on the requirement of two **L**CuF complexes to furnish one fluorinated product.

Table 1 | Direct $C(sp^3)$-H fluorination by **L**CuF[a]

[a]Yields determined by $^{19}F\{^1H\}$ NMR analysis with 100 equivalents of substrate. [b]With 16 equivalents of substrate. [c]Combined yield of branched and linear isomers. [d]After 64 hours.

Fluorination of 1,4-dioxane and 18-crown-6 with **L**CuF proceeds selectively to furnish

monofluorinated products formed in 45% and 35% yield, respectively (Table 1). Fluorine atom

transfer from a metal fluoride to the α-position of ether, to our knowledge, has yet to be

demonstrated. Such direct fluorination by **L**CuF is also amenable to other activated $C(sp^3)$-H bonds.

Treatment of **L**CuF with allylic and benzylic substrates selectively afforded the corresponding allylic or

benzylic fluorinated compounds, albeit in moderate to low yields (8 − 42%, Table 1). The low yield of

benzylic substrates suggests that steric hinderance by the four iPr moieties around the $[Cu^{III}\text{-}F]^{2+}$ unit

might be detrimental to $C(sp^3)$-H fluorination reactivity. This demonstration of $C(sp^3)$-H fluorination,

despite requiring stoichiometric amount of **L**CuF, suggests that copper fluoride complexes that support the Cu^{II}/Cu^{III} redox couple, in principle, are suitable for fluorination of C(sp^3)-H bonds with an oxidant and F$^-$ source.

Conclusion

In summary, we have synthesized a series of formally copper(III) halide complexes, **L**CuX (X = F, Cl, Br), by the use of halide (X$^-$) sources and an oxidant. The electronic structure of these species, as shown by a suite of spectroscopic and computational techniques, features significant halogen radical character, which correlates to their ability to perform hydrogen atom abstraction and radical capture. Expanding on these insights, **L**CuF was employed for direct fluorination of a variety of alkyl substrates with allylic and benzylic C-H bonds as well as C(sp^3)-H bonds alpha to ethers. With the establishment of a radical capture mechanism at a copper(III) fluoride center, the use of tunable copper complexes, in principle, can provide further practicality and generality to C(sp^3)-H fluorination, i.e. regioselectivity and stereoselectivity.

Our demonstration of C(sp^3)-H fluorination with **L**CuF adds to the growing list of formally copper(III) intermediates in biological[45,46] and abiological[26,47] copper-mediated carbon-heteroatom bond-forming reactions. Alongside kinetic data reported by Tolman,[28,48] we established a correlation between the ligand basicity and the rate of HAA (Fig. 4b). Our findings open the possibility of other carbon-heteroatom bond-forming reactions employing **L**Cu^{III} complexes bearing other basic functional groups (FG), e.g. alkoxide, amide, and thiolate. Conceivably, the generality of this Cu^{II}/Cu^{III} C(sp^3)-H functionalization paradigm relies on the ability of **L**Cu-FG to abstract H atoms (depending on pK_a) and capture R• (depending on redox potential, $E_{1/2}$).[43] Therefore, an interesting mechanistic question arises from the inverse correlation of pK_a and $E_{1/2}$ of **L**Cu-FG – can the **L**Cu-FG complex be efficient at RC and HAA at the same time? As shown by our study, the efficiency of R• capture remains high even with less oxidizing **L**Cu-FG, e.g. **L**CuF. Albeit through two different mechanisms (concerted for **L**CuF, stepwise ET-XT for **L**CuCl and **L**CuBr), the high proficiency of RC at different **L**CuX further

underscores the possibility of other mechanistically related $C(sp^3)$-H functionalization with $[Cu^{III}\text{-}FG]^{2+}$ species.

Acknowledgements

Author contributions

J.K.B. and S.Z. conceived and designed the research; J.K.B., A.D.C, B.H., and S.C.E.S. collected and analyzed the data. J.K.B., S.C.E.S., and S.Z. wrote the paper.

Competing Interests

The authors declare no competing financial interests.

References

1.   Cheng, Q. & Ritter, T. New directions in C–H fluorination. *Trends Chem.* **1**, 461–470 (2019).

2.   Müller, K., Faeh, C. & Diederich, F. Fluorine in pharmaceuticals: Looking beyond intuition. *Science* **317**, 1881–1886 (2007).

3.   McMurtrey, K. B., Racowski, J. M. & Sanford, M. S. Pd-catalyzed C–H fluorination with nucleophilic fluoride. *Org. Lett.* **14**, 4094–4097 (2012).

4. Braun, M.-G. & Doyle, A. G. Palladium-catalyzed allylic C–H fluorination. *J. Am. Chem. Soc.* **135**, 12990–12993 (2013).

5. Zhu, R.-Y. *et al.* Ligand-enabled stereoselective β-C(sp^3)–H fluorination: Synthesis of unnatural enantiopure anti-β-fluoro-α-amino acids. *J. Am. Chem. Soc.* **137**, 7067–7070 (2015).

6. Zhang, Q., Yin, X.-S., Chen, K., Zhang, S.-Q. & Shi, B.-F. Stereoselective synthesis of chiral β-fluoro α-amino acids via Pd(II)-catalyzed fluorination of unactivated methylene C(sp^3)–H bonds: Scope and mechanistic studies. *J. Am. Chem. Soc.* **137**, 8219–8226 (2015).

7. Bloom, S. *et al.* A polycomponent metal-catalyzed aliphatic, allylic, and benzylic fluorination. *Angew. Chem. Int. Ed.* **51**, 10580–10583 (2012).

8. Bloom, S. *et al.* Iron(II)-catalyzed benzylic fluorination. *Org. Lett.* **15**, 1722–1724 (2013).

9. Groendyke, B. J., AbuSalim, D. I. & Cook, S. P. Iron-catalyzed, fluoroamide-directed C–H fluorination. *J. Am. Chem. Soc.* **138**, 12771–12774 (2016).

10. Park, H., Verma, P., Hong, K. & Yu, J.-Q. Controlling Pd(IV) reductive elimination pathways enables Pd(II)-catalysed enantioselective C(sp^3)−H fluorination. *Nat. Chem.* **10**, 755–762 (2018).

11. Liu, W. *et al.* Oxidative aliphatic C-H fluorination with fluoride ion catalyzed by a manganese porphyrin. *Science* **337**, 1322–1325 (2012).

12. Xia, J.-B., Zhu, C. & Chen, C. Visible light-promoted metal-free C–H activation: Diarylketone-catalyzed selective benzylic mono- and difluorination. *J. Am. Chem. Soc.* **135**, 17494–17500 (2013).

13. Rueda-Becerril, M. *et al.* Fluorine transfer to alkyl radicals. *J. Am. Chem. Soc.* **134**, 4026–4029 (2012).

14. Pitts, C. R. *et al.* Direct, catalytic monofluorination of sp^3 C–H Bonds: A radical-based mechanism with ionic selectivity. *J. Am. Chem. Soc.* **136**, 9780–9791 (2014).

15. Liu, J., Yuan, Q., Toste, F. D. & Sigman, M. S. Enantioselective construction of remote tertiary carbon–fluorine bonds. *Nat. Chem.* **11**, 710–715 (2019).

16. Kainz, Q. M. *et al.* Asymmetric copper-catalyzed C-N cross-couplings induced by visible light. *Science* **351**, 681–684 (2016).

17. Zhang, W. *et al.* Enantioselective cyanation of benzylic C–H bonds via copper-catalyzed radical relay. *Science* **353**, 1014–1018 (2016).

18. Zhang, Z., Zhang, X. & Nagib, D. A. Chiral piperidines from acyclic amines via enantioselective, radical-mediated δ C−H cyanation. *Chem* **5**, 3127–3134 (2019).

19. Kochi, J. K. The reduction of cupric chloride by carbonyl compounds. *J. Am. Chem. Soc.* **77**, 5274–5278 (1955).

20. Castro, C. E., Gaughan, E. J. & Owsley, D. C. Cupric halide halogenations. *J. Org. Chem.* **30**, 587–592 (1965).

21. Liu, T., Myers, M. C. & Yu, J. Copper-catalyzed bromination of $C(sp^3)$−H bonds distal to functional groups. *Angew. Chem. Int. Ed.* **56**, 306–309 (2017).

22. Hoffmann, R. *et al.* From Widely Accepted Concepts in Coordination Chemistry to Inverted Ligand Fields. *Chem. Rev.* **116**, 8173–8192 (2016).

23. DiMucci, I. M. *et al.* The myth of d^8 copper(III). *J. Am. Chem. Soc.* **141**, 18508–18520 (2019).

24. Carsch, K. M. *et al.* Synthesis of a copper-supported triplet nitrene complex pertinent to copper-catalyzed amination. *Science* **365**, 1138–1143 (2019).

25. Badiei, Y. M. *et al.* Copper–nitrene complexes in catalytic C–H amination. *Angew. Chem. Int. Ed.* **47**, 9961–9964 (2008).

26. Hickman, A. J. & Sanford, M. S. High-valent organometallic copper and palladium in catalysis. *Nature* **484**, 177–185 (2012).

27. Casitas, A. *et al.* Direct observation of Cu^I/Cu^{III} redox steps relevant to Ullmann-type coupling reactions. *Chem. Sci.* **1**, 326–330 (2010).

28. Donoghue, P. J. *et al.* Rapid C–H bond activation by a monocopper(III)–hydroxide complex. *J. Am. Chem. Soc.* **133**, 17602–17605 (2011).

29. Yang, L., Powell, D. R. & Houser, R. P. Structural variation in copper(i) complexes with

pyridylmethylamide ligands: structural analysis with a new four-coordinate geometry index, τ4. *Dalt. Trans.* 955–964 (2007). doi:10.1039/B617136B

30. Santo, R. *et al.* Diamagnetic–paramagnetic conversion of tris(2-pyridylthio)methylcopper(III) through a structural change from trigonal bipyramidal to octahedral. *Angew. Chem. Int. Ed.* **45**, 7611–7614 (2006).

31. Chang, H.-C. *et al.* Ambient stable trigonal bipyramidal copper(III) complexes equipped with an exchangeable axial ligand. *Inorg. Chem.* **54**, 5527–5533 (2015).

32. DuBois, J. L. *et al.* A systematic K-edge X-ray absorption spectroscopic study of Cu(III) sites. *J. Am. Chem. Soc.* **122**, 5775–5787 (2000).

33. Tomson, N. C. *et al.* Re-evaluating the Cu K pre-edge XAS transition in complexes with covalent metal–ligand interactions. *Chem. Sci.* **6**, 2474–2487 (2015).

34. Werner, H. J. & Knowles, P. J. A second order multiconfiguration SCF procedure with optimum convergence. *J. Chem. Phys.* **82**, 5053–5063 (1985).

35. Bower, J. K., Sokolov, A. Y. & Zhang, S. Four-coordinate copper halonitrosyl {CuNO}[10] complexes. *Angew. Chem. Int. Ed.* **58**, 10225–10229 (2019).

36. In-Iam, A. *et al.* {FeNO}[7]-type halogenido nitrosyl ferrates: Syntheses, bonding, and photoinduced linkage isomerism. *Chem. Eur. J.* **25**, 1304–1325 (2019).

37. Reed, A. E., Weinstock, R. B. & Weinhold, F. Natural population analysis. *J. Chem. Phys.* **83**, 735–746 (1985).

38. Radoń, M., Broclawik, E. & Pierloot, K. Electronic structure of selected {FeNO}[7] complexes in heme and non-heme architectures: A density functional and multireference ab initio study. *J. Phys. Chem. B* **114**, 1518–1528 (2010).

39. Mandal, M. *et al.* Mechanisms for hydrogen-atom abstraction by mononuclear copper(III) cores: Hydrogen-atom transfer or concerted proton-coupled electron transfer? *J. Am. Chem. Soc.* **141**, 17236–17244 (2019).

40. Salvador, T. K. *et al.* Copper catalyzed sp^3 C–H etherification with acyl protected phenols. *J.*

Am. Chem. Soc. **138**, 16580–16583 (2016).

41. Bour, J. R., Ferguson, D. M., McClain, E. J., Kampf, J. W. & Sanford, M. S. Connecting organometallic Ni(III) and Ni(IV): Reactions of carbon-centered radicals with high-valent organonickel complexes. *J. Am. Chem. Soc.* **141**, 8914–8920 (2019).

42. Jang, E. S. *et al.* Copper(II) anilides in sp^3 C-H amination. *J. Am. Chem. Soc.* **136**, 10930–10940 (2014).

43. Zaragoza, J. P. T. *et al.* Direct observation of oxygen rebound with an iron-hydroxide complex. *J. Am. Chem. Soc.* **139**, 13640–13643 (2017).

44. Kochi, J. K. Mechanisms of organic oxidation and reduction by metal complexes. *Science* **155**, 415–424 (1967).

45. Abad, E., Rommel, J. B. & Kästner, J. Reaction mechanism of the bicopper enzyme peptidylglycine α-hydroxylating monooxygenase. *J. Biol. Chem.* **289**, 13726–13738 (2014).

46. Cao, L., Caldararu, O., Rosenzweig, A. C. & Ryde, U. Quantum refinement does not support dinuclear copper sites in crystal structures of particulate methane monooxygenase. *Angew. Chem. Int. Ed.* **57**, 162–166 (2018).

47. Casitas, A. & Ribas, X. The role of organometallic copper(III) complexes in homogeneous catalysis. *Chem. Sci.* **4**, 2301–2318 (2013).

48. Elwell, C. E. *et al.* Carboxylate structural effects on the properties and proton-coupled electron transfer reactivity of $[CuO_2CR]^{2+}$ cores. *Inorg. Chem.* **58**, 15872–15879 (2019).

Supplementary Information for:

C(sp^3)-H fluorination with a copper(II)/(III) redox couple

Jamey K. Bower,[a] Andrew D. Cypcar,[a] Brenda Henriquez,[b] S. Chantal E. Stieber,[b*] Shiyu Zhang[a*]

[a] Department of Chemistry & Biochemistry, The Ohio State University, 100 West 18th Ave, Columbus, OH 43210
[b] Department of Chemistry & Biochemistry, California State Polytechnic University, Pomona, 3801 W. Temple Ave, Pomona, CA 91768

*Correspondence to: zhang.8941@osu.edu, sestieber@cpp.edu

Contents

General Experimental Details

All syntheses and experiments were performed under a nitrogen atmosphere in an MBraun glovebox or using standard Schlenk techniques unless otherwise noted. Dichloromethane, tetrahydrofuran, acetonitrile, fluorobenzene, pentane, and diethyl ether were dried and degassed under nitrogen using a Pure Process Technologies (PPT, Nashua, NH) solvent purification system, and stored over 4 Å molecular sieves. Chloroform-d_1 and dichloromethane-d_2 (Cambridge Isotope Laboratories, Inc.) were dried over 4Å molecular sieves prior to use. All glassware was dried at 120 °C prior to use. Elemental analysis was performed by Midwest Micro Lab (Indianapolis, IN, http://midwestlab.com/). All reagents were obtained from reputable suppliers and used without further purification. [N,N'-bis(2,6-diisopropylphenyl)-2,6-pyridinedicarboxamido] copper(II) acetonitrile complex (**L**Cu^{II}(MeCN)),[1] bis(triphenylphosphine)iminium fluoride ([PPN]F),[2] and Gomberg's dimer[3] were synthesized according to literature procedures. NMR spectra were recorded on a Bruker Avance NEO 400 MHz instrument, Bruker Avance III HD 600 MHz instrument, or a Bruker Ascend 850 MHz instrument and referenced to residual solvent peaks. UV-vis spectra were collected on an Agilent Cary 60 spectrophotometer outfitted with a Unisoku Unispeks cryostat (−100 °C to + 100 °C).

Preparation of Compounds

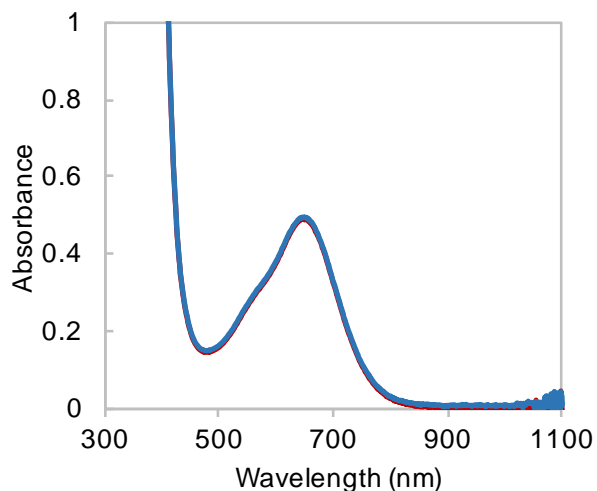## Synthesis and Characterization of [TBA]LCu^{II}F
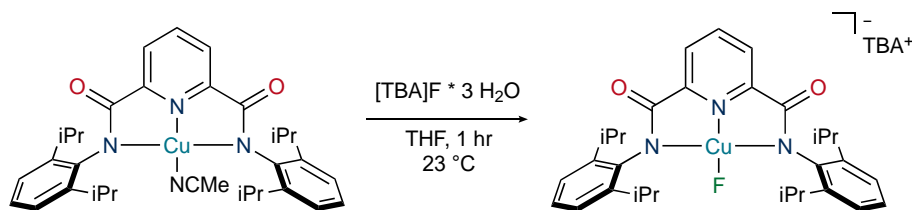
This compound was prepared by adaptation of a literature report for the copper(II) chloride complex, [TBA]**L**Cu^{II}Cl (L = N,N'-bis(2,6-diisopropylphenyl)-2,6-pyridinedicarboxamido).[1] Tetrabutylammonium fluoride trihydrate (112.2 mg, 0.3556 mmol) was dissolved in tetrahydrofuran (4 mL) and added to stirring solution of **L**Cu^{II}(MeCN) (209.3 mg, 0.3558 mmol) in tetrahydrofuran (5 mL). The solution rapidly became a deep navy blue as was allowed to stir for an hour at room temperature. The solution was concentrated to ca. 1 mL, filtered, and placed in a −35 °C freezer. After chilling, diethyl ether was layered to the solution and deep blue crystals were formed overnight. The supernatant was decanted and the crystals washed with diethyl ether (ca. 1 mL) three times. The crystals were dried in vacuo for 8 hours to yield [TBA]**L**Cu^{II}F (254.1 mg, 88.4%). Attempts of structural characterization by X-ray diffraction were frustrated by the poor crystallinity of the sample when removed from solution and exposed to ambient conditions. Analysis, calculated for $C_{47}H_{73}N_4O_2FCu \cdot 2H_2O$: C, 66.83; H, 9.19; N, 6.63. Found: C, 66.51; H, 8.87; N, 6.51. UV-vis: CH_2Cl_2 @ 23 °C: λ_{max} = 360 nm (ε = 2230 M^{-1} cm^{-1}), 655 nm (ε = 292 M^{-1} cm^{-1}).

Synthesis and Characterization of [PPN]LCu^{II}F
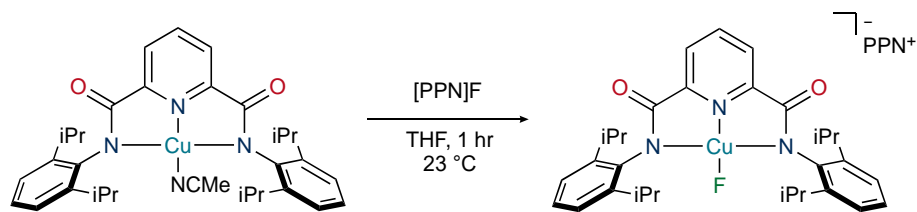
To a suspension of bis(triphenylphosphine)iminium fluoride ([PPN]F, 19.0 mg, 0.0341 mmol) in tetrahydrofuran (1 mL) was added a homogenous tetrahydrofuran solution of **LCu^{II}**(MeCN) (20.0 mg, 0.0340 mmol). The color of the solution changed to navy blue. The reaction was allowed to stir for one hour, and then placed in a −35 °C freezer. Overnight, deep blue crystals were deposited on the bottom of the vial, which proved suitable for single-crystal X-ray diffraction analysis. Decanting of the supernatant and the removal of volatiles for 3 hours resulted in the isolation of [PPN]**LCu^{II}**F (24.8 mg, 66.0%). The UV-vis features of the title compound precisely match those of [TBA]**LCu^{II}**F, supporting the formation of the same molecular structure at the copper center. Anal. Calcd. For $C_{67}H_{67}N_4O_2FP_2Cu$ * C_4H_8O • H_2O: C, 71.37; H, 6.50; N, 4.69. Found: C, 71.75; H, 6.59; N, 4.72. UV-vis: CH_2Cl_2 @ 23 °C: λ_{max} = 360 nm, 655 nm.

Supplementary Fig. 1: Overlay of UV-vis spectra of [TBA]**LCu^{II}**F (red trace) and [PPN]**LCu^{II}**F (blue trace). Concentration: 1.8 mM; Temperature: 23 °C; Solvent: MeCN.

Synthesis and Characterization of [TBA]LCu^{II}Cl
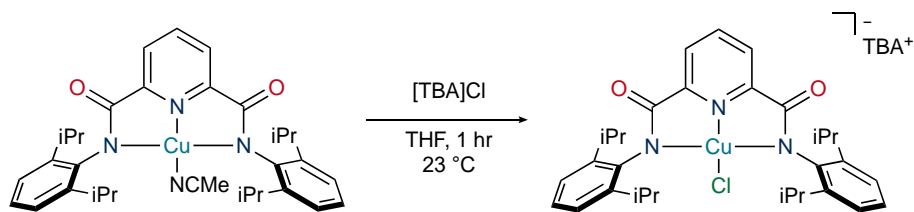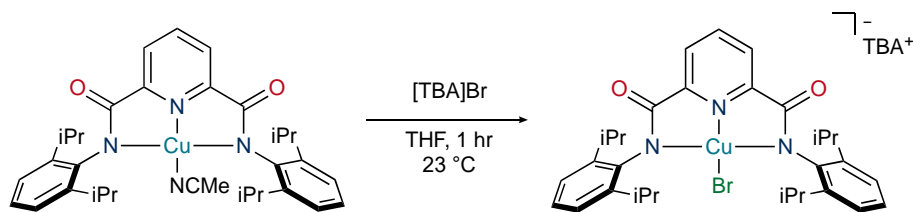

The title compound was prepared by adaptation of a literature report.[1] A homogenous solution of **LCu^{II}**(MeCN) (71.3 mg, 0.121 mmol) in tetrahydrofuran (5 mL) was added to a stirring tetrahydrofuran (5 mL) suspension of tetrabutylammonium chloride (33.7 mg, 0.121 mmol). The solution rapidly became deep forest green as it was allowed to stir for an hour at room temperature. The resulting solution was concentrated in vacuo to ca. 4 mL and placed in a −35 °C freezer. After chilling, diethyl ether (ca. 3 mL) was layered to the solution and deep green block crystals formed overnight. The supernatant was decanted and the crystals were washed with 1 mL diethyl ether three times. The crystals were dried in vacuo for 3 hours to yield [TBA]**LCu^{II}**Cl (82.5 mg, 82.5%). Single-crystals suitable for X-ray diffraction analysis were obtained by vapor diffusion of diethyl ether to a THF solution of [TBA]**LCu^{II}**Cl at −35 °C. The optical and EPR spectra of the title compound match those reported by Tolman.[1] UV-vis: CH_2Cl_2 @ 23 °C: λ_{max} = 400 nm (ε = 2640 M^{-1} cm^{-1}), 635 nm (ε = 343 M^{-1} cm^{-1}).

Synthesis and Characterization of [TBA]LCu^{II}Br

    The title compound was prepared by adaptation of a literature report for the chloride complex, [TBA]**L**Cu^{II}Cl.[1] A homogenous solution of **L**Cu^{II}(MeCN) (64.8 mg, 0.110 mmol) in tetrahydrofuran (5 mL) was added to a stirring tetrahydrofuran (5 mL) suspension of tetrabutylammonium bromide (35.5 mg, 0.110 mmol). The solution rapidly became a deep brown-green as it was allowed to stir for an hour at room temperature. The resulting solution was layered with diethyl ether (ca. 2 mL) and placed in a −35 °C freezer overnight, resulting in the formation of deep green crystals. The supernatant was decanted and the crystals were washed with diethyl ether (ca. 1 mL) three times. The crystals were dried in vacuo for 3 hours to yield [TBA]**L**Cu^{II}Br (80.2 mg, 83.7%). Single-crystals suitable for X-ray diffraction analysis were obtained by vapor diffusion of diethyl ether to a THF solution of [TBA]**L**Cu^{II}Br at −35 °C. Anal. Calcd. For C$_{47}$H$_{73}$N$_4$O$_2$BrCu • 2H$_2$O: C, 62.34; H, 8.57 N, 6.19. Found: C, 62.23; H, 8.12; N, 6.38. UV-vis: CH$_2$Cl$_2$ @ 23 °C: λ_{max} = 420 nm (ε = 2640 M^{-1}cm^{-1}), 625 nm (ε = 333 M^{-1}cm^{-1}).

Synthesis and Characterization of tris(4-bromophenyl)aminium hexafluorophosphate
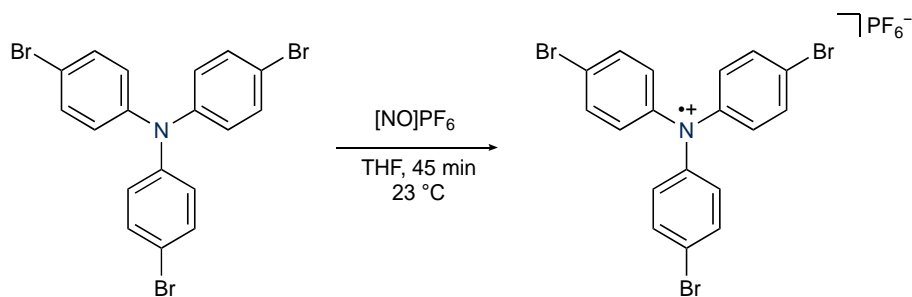
The title compound was prepared by adaptation of a literature report.[4] Inside the glovebox, nitrosonium hexafluorophosphate ([NO]PF$_6$) was added to a 250-mL round bottom flask, to which dichloromethane (15 mL) was added. A homogenous solution of tris(4-bromophenyl)amine in dichloromethane was added dropwise to the stirring [NO]PF$_6$ suspension in dichloromethane over the course of 30 minutes. *Note: the rate of addition is critical to the success of the reaction. After half of the amine solution had been added,* the headspace of the flask was evacuated for 3 minutes, and then the addition was resumed. Following the addition, the mixture was allowed to stir for 15 minutes while volatiles were removed in vacuo. Diethyl ether (ca. 200 mL) was subsequently added to precipitate the product. Following three washes with diethyl ether (5 mL), a violet powder was isolated and dried in vacuo for three hours (294 mg, 75.3%). The isolated solid can be stored indefinitely at low temperature (−35 °C) without decomposition. The UV-vis spectrum of the product in MeCN matches the literature report.[4] UV-vis: MeCN @ 23 °C: λ_{max} = 705 nm (ε = 28000 $M^{-1}cm^{-1}$), 605 nm (ε = 8100 $M^{-1}cm^{-1}$), 363 nm (ε = 21000 $M^{-1}cm^{-1}$).

Synthesis and Characterization of LCuF
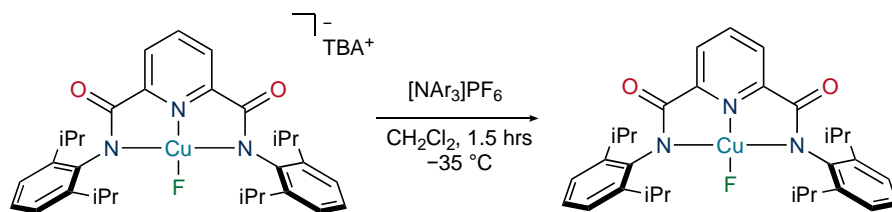
A solution of [TBA]**L**Cu^{II}F (15.1 mg, 0.0187 mmol) was dissolved in dichloromethane (2 mL) and cooled in a −35 °C freezer. A solution of [NAr$_3$]PF$_6$ (11.7 mg, 0.0187 mmol) was weighed into a vial equipped with a stir bar cooled in a −35 °C freezer. The chilled solution of [TBA]**L**Cu^{II}F was added to a stirring solid [NAr$_3$]PF$_6$ to afford a homogenous deep blue solution. Cold dichloromethane (ca. 2 mL) was used to rinse the vial of [TBA]**L**Cu^{II}F to assist quantitative transfer. Immediately after addition, the vial was placed into the freezer for 5 minutes, whereupon it was removed and allowed to stir for 1 minute. This process was repeated twice more. The vial was then left undisturbed for 1 hour in the freezer. Volatiles were then removed in vacuo and the dark solid residue was extracted with cold fluorobenzene and rapidly filtered through a cold, Celite-filled pipette. The solution was concentrated to ca. 2 mL and layered with cold pentane and allowed to sit undisturbed in the freezer. A few dark blue block crystals suitable for X-ray diffraction were formed overnight. We were unable to be prepared analytically pure sample on preparative scale due to its low thermal stability. ^{1}H NMR (600 MHz, CD$_2$Cl$_2$): δ 8.50 (t, J = 7.5, 1H), 8.07 (d, J = 7.6 Hz, 2H), 7.47 (t, J = 7.7 Hz, 2H), 7.09 (d, J = 7.7 Hz, 4H), 4.93 (m, J = 6.8 4H), 1.29 (d, J = 6.8 Hz, 12H), 1.19 (d, J = 6.8 Hz, 12H). UV-vis: CH$_2$Cl$_2$ @ −80 °C: λ_{max} = 520 nm (ε = 9070 M^{-1} cm^{-1}), 820 nm (ε = 18600 M^{-1} cm^{-1}).

Synthesis and Characterization of LCuCl
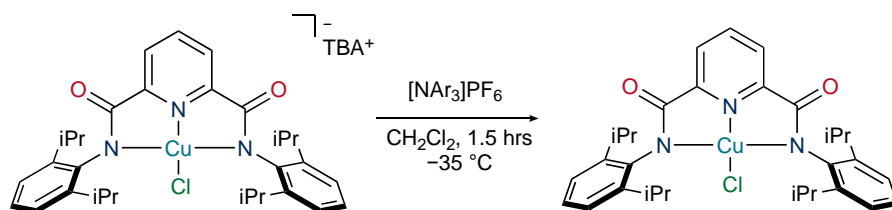
A solution of [TBA]**L**Cu^{II}Cl (31.8 mg, 0.0385 mmol) was dissolved in dichloromethane (1 mL) and cooled in a −35 °C freezer. A vial containing [NAr$_3$]PF$_6$ (23.7 mg, 0.0378 mmol) was equipped with a stir bar and cooled in a −35 °C freezer. The chilled solution of [TBA]**L**Cu^{II}Cl was added to stirring solid [NAr$_3$]PF$_6$. Cold dichloromethane (ca. 2 mL) was used to rinse the vial of [TBA]**L**Cu^{II}Cl to assist quantitative transfer. Immediately after addition, the vial was placed into the freezer for 5 minutes, whereupon it was removed and allowed to stir for 1 minute. This process was repeated twice more. The vial was then left undisturbed for 1 hour in the freezer. Volatiles were then removed in vacuo and the dark solid residue was extracted with diethyl ether and rapidly filtered through a cold, Celite-filled pipetted. The Celite pad was washed with cold diethyl ether (~2 mL) to facilitate quantitative transfer. The solution was concentrated to ~2 mL and allowed to sit undisturbed in the freezer. Dark purple block crystals suitable for X-ray diffraction were formed after approximately two days. The supernatant was decanted and the crystals were dried in vacuo for 3 hours to yield the title compound (19.0 mg, 86.6%). The isolated solid can be stored indefinitely at low temperature (−35 °C) without decomposition. ^{1}H NMR (600 MHz, CD$_2$Cl$_2$): δ 8.55 (t, J = 7.6 Hz, 1H), 8.15 (d, J = 7.0 Hz, 2H), 7.46 (t, J = 7.5 Hz, 2H), 7.14 (d, J = 7.6 Hz, 4H), 3.48 (m, J = 7.0 Hz, 4H), 1.36 (d, J = 6.8 Hz, 12H), 1.21 (d, J = 6.4 Hz, 12H); ^{13}C NMR (214 MHz, CD$_2$Cl$_2$): δ 169.9, 149.2, 147.6, 146.9, 146.6, 130.9, 128.7, 124.0, 30.38, 24.3, 23.2; Anal. Calcd. For C$_{31}$H$_{37}$N$_3$O$_2$ClCu • 0.5 H$_2$O: C, 62.93; H, 6.47; N, 7.10. Found: C, 63.04; H, 6.55; N, 6.94. UV-vis: CH$_2$Cl$_2$ @ −80 °C: λ$_{max}$ = 530 nm (ε = 8530 M^{-1} cm^{-1}), 920 nm (ε = 13400 M^{-1} cm^{-1}).

Synthesis and Characterization of LCuBr
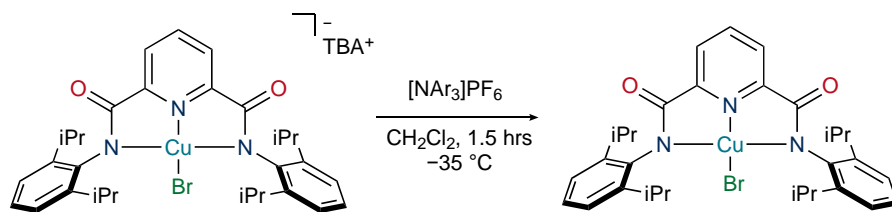
A solution of [TBA]**L**Cu^{II}Br (35.3 mg, 0.0406 mmol) was dissolved in dichloromethane (2 mL) and cooled in a −35 °C freezer. A vial containing [NAr$_3$]PF$_6$ (25.2 mg, 0.0402 mmol) was equipped with a stir bar and cooled in a −35 °C freezer. The chilled solution of [TBA]**L**Cu^{II}Br was added to stirring solid [NAr$_3$]PF$_6$. Cold dichloromethane (ca. 2 mL) was used to rinse the vial of [TBA]**L**Cu^{II}Br to assist quantitative transfer. Immediately after addition, the vial was placed into the freezer for 5 minutes, whereupon it was removed and allowed to stir for 1 minute. This process was repeated twice more. The vial was then left undisturbed for 1 hour in the freezer. Volatiles were then removed in vacuo and the dark solid residue was extracted with diethyl ether and rapidly filtered through a cold. The Celite pad was washed with cold diethyl ether (ca. 2 mL) to facilitate quantitative transfer. The solution was concentrated to ca. 2 mL and allowed to sit undisturbed in the freezer. Dark purple block crystals suitable for X-ray diffraction were formed after approximately two days. The supernatant was decanted and the crystals were dried in vacuo for 6 hours to yield the title compound (18.8 mg, 74.6%). The isolated solid can be stored indefinitely at low temperature (−35 °C) without decomposition. ^{1}H NMR (600 MHz, CD$_2$Cl$_2$): δ 8.54 (t, J = 7.5 Hz, 1H), 8.15 (s, 2H), 7.46 (s, 2H), 7.14 (d, J = 7.1 Hz, 4H), 3.49 (m, J = 6.4 Hz, 4H), 1.42 (d, J = 6.6 Hz, 12H), 1.21 (d, J = 6.2 Hz, 12H); ^{13}C NMR (214 MHz, CD$_2$Cl$_2$): δ 170.9, 152.2, 146.9, 146.5, 146.3, 130.59, 128.6, 123.57, 30.4, 24.7, 23.0; Anal. Calcd. For C$_{31}$H$_{37}$N$_3$O$_2$BrCu • H$_2$O: C, 57.72; H, 6.09; N, 6.51. Found: C, 57.86; H, 5.83; N, 6.74. UV-vis: CH$_2$Cl$_2$ @ −80 °C: λ$_{max}$ = 580 nm (ε = 12500 M^{-1} cm^{-1}), 980 nm (ε = 9110 M^{-1} cm^{-1}).

Electrochemical Measurements

Cyclic voltammograms were recorded under nitrogen atmosphere with a Biologic SP-150 potentiostat using a three-electrode system comprised of glassy carbon working electrode, platinum wire counter electrode, and nonaqueous silver nitrate reference electrode. All cyclic voltammograms were recorded at room temperature with a scan rate of 100 mV/s. Compounds (3 mM) were dissolved in an electrolyte solution consisting of 0.1 M electrochemical grade tetrabutylammonium perchlorate in dichloromethane.
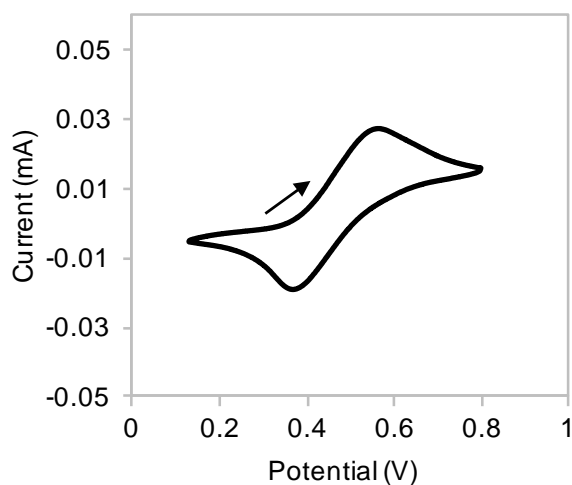
Supplementary Fig. 2: Cyclic voltammogram of [TBA]**L**Cu^{II}F. $E_{1/2}$ = 0.465 V vs Ag/AgNO$_3$; Peak-to-peak separation = 200 mV
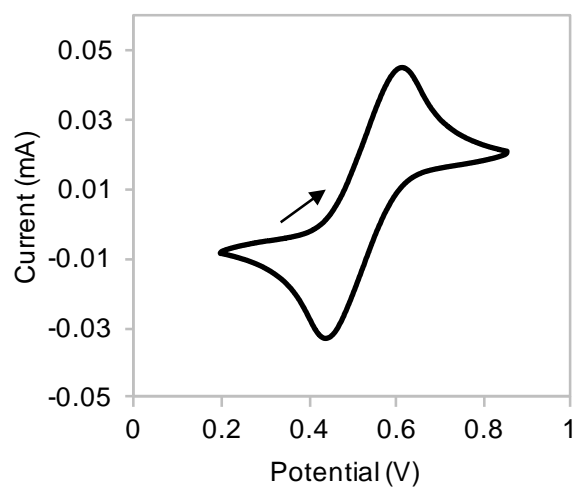
Supplementary Fig. 3: Cyclic voltammogram of [TBA]**L**Cu^{II}Cl. $E_{1/2}$ = 0.525 V vs Ag/AgNO$_3$; Peak-to-peak separation = 180 mV
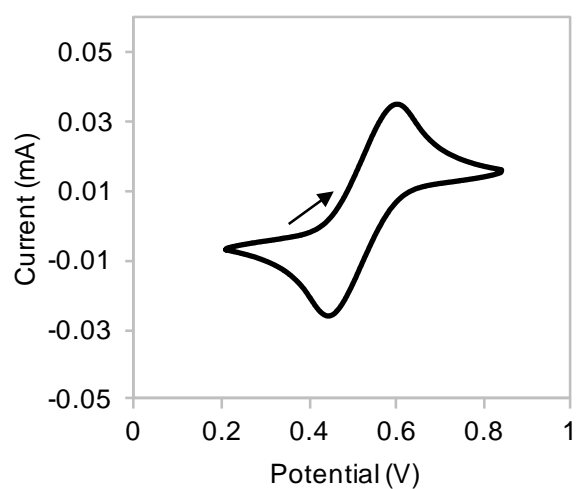
Supplementary Fig. 4: Cyclic voltammogram of [TBA]**L**Cu^{II}Br. $E_{1/2}$ = 0.525 V vs Ag/AgNO$_3$; Peak-to-peak separation = 160 mV

UV-vis Spectrophotometry Studies

Synthesis of LCuX complexes *in situ* for UV-vis experiments

A dichloromethane solution of [TBA]**L**Cu^{II}X (2.900 mL, 0.103 mM, 0.300 μmol) was placed in a quartz cuvette with septum attachment under a nitrogen atmosphere. The cuvette was sealed and cooled to −80 ℃ in the UV-vis spectrometer. A dichloromethane solution of [NAr$_3$]PF$_6$ (0.100 mL, 3.00 mM, 1 equivalent) was injected into the cuvette with a syringe, resulting in the rapid formation of peaks assigned to the corresponding **L**CuX complex.
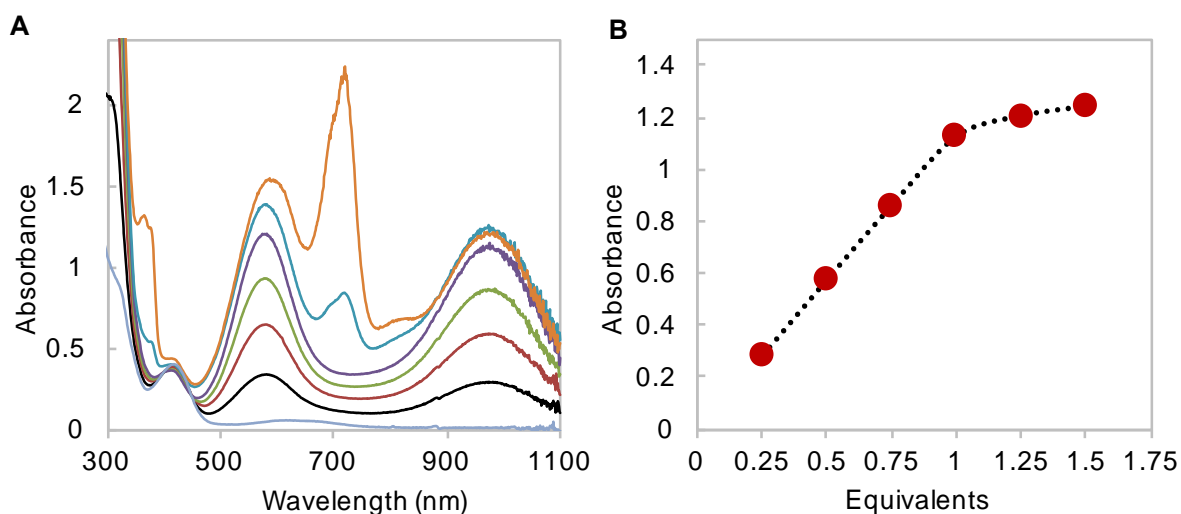
Supplementary Fig. 5. Job plot for the formation of **L**CuBr by titration of [NAr$_3$]PF$_6$ to a solution of [TBA]**L**Cu^{II}Br. Concentration @ 1 equivalent of oxidant: 0.1 mM; Temperature: −80 ℃; Solvent: CH$_2$Cl$_2$. The sharp peak at 700 nm is due to excess [NAr$_3$]PF$_6$.

Beer's Law plots

For LCu^{II}X[TBA] complexes: A dichloromethane solution of [TBA]**L**Cu^{II}X (2.700 mL, 0.333 mM, 0.899 μmol) was placed in a quartz cuvette with septum attachment under a nitrogen atmosphere at room temperature. A UV-vis spectrum was taken. Then, four 0.1 mL portions of dichloromethane were added to the cuvette to dilute the solution sequentially. UV-vis spectra were taken in between additions after the solution is completely equilibrated.
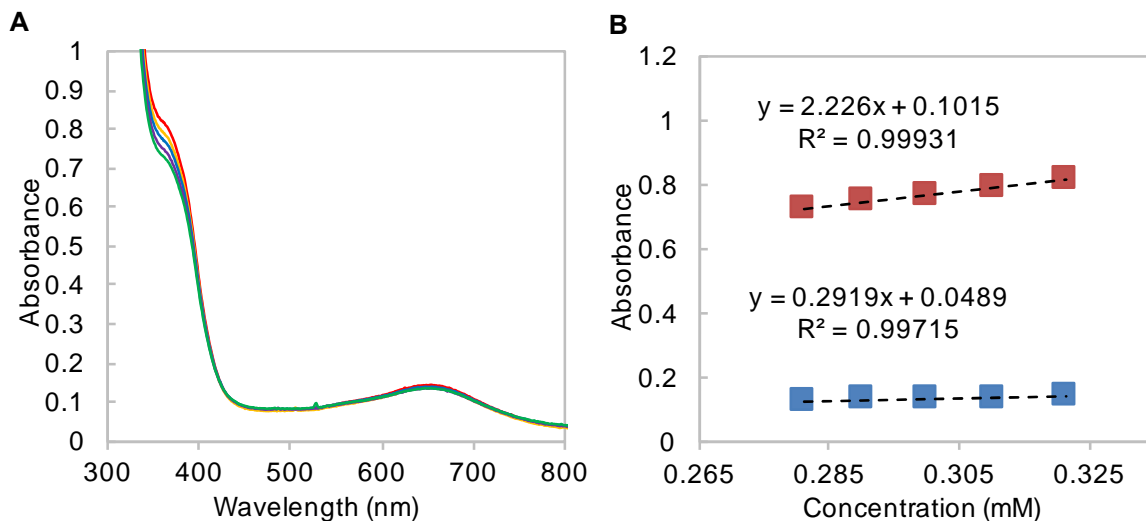
Supplementary Fig. 6. (A) UV-vis spectra obtained from the dilution of [TBA]**L**Cu^{II}F at 23 °C in CH$_2$Cl$_2$. (B) Beer's law plot for [TBA]**L**Cu^{II}F: 360 nm (2230 M^{-1} cm^{-1}); 655 nm (290 M^{-1} cm^{-1}).
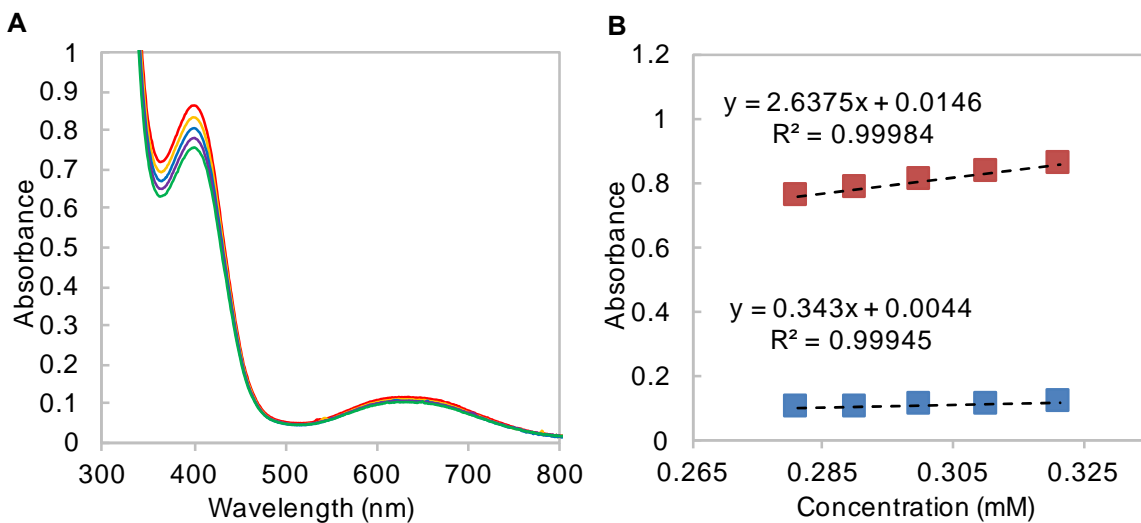
Supplementary Fig. 7. (A) UV-vis spectra obtained from the dilution of [TBA]**L**Cu^{II}Cl at 23 °C in CH$_2$Cl$_2$. (B) Beer's law plot for [TBA]**L**Cu^{II}Cl: 400 nm (2640 M^{-1} cm^{-1}); 635 nm (340 M^{-1} cm^{-1}).
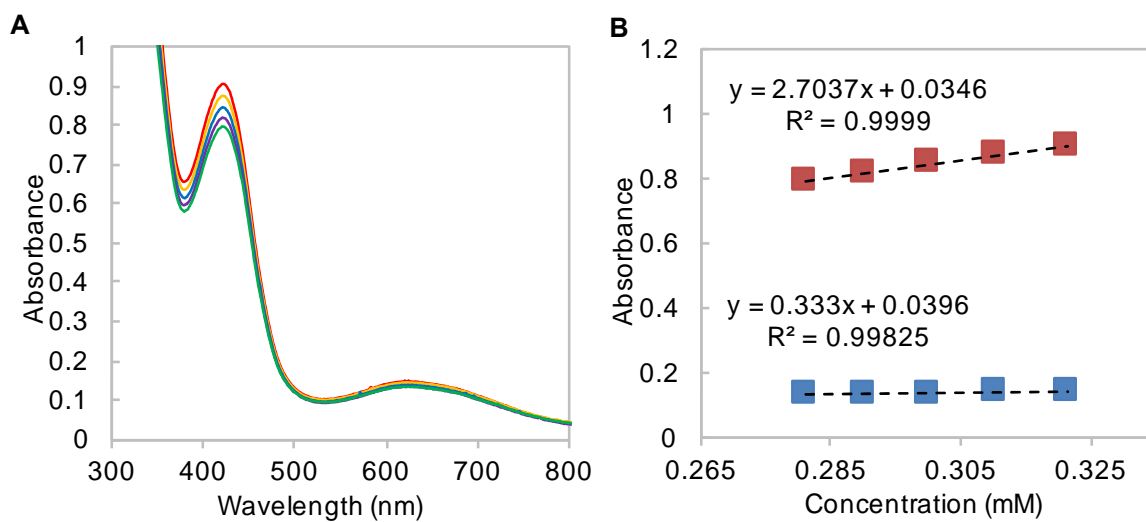
Supplementary Fig. 8. (A) UV-vis spectra obtained from the dilution of [TBA]**L**Cu^{II}Br at 23 °C in CH$_2$Cl$_2$. (B) Beer's law plot for [TBA]**L**Cu^{II}Br: 420 nm (2640 M^{-1} cm^{-1}); 625 nm (330 M^{-1} cm^{-1}).

For LCuX complexes: A dichloromethane solution of [TBA]**LCu**^{II}X (2.700 mL, 0.111 mM, 0.300 µmol) was placed in a quartz cuvette with septum attachment under a nitrogen atmosphere. The cuvette was sealed and cooled to −80 ℃ in the UV-vis spectrometer. A dichloromethane solution of [NAr$_3$]PF$_6$ (0.100 mL, 3.00 mM, 1 equivalent) was injected to the cuvette with a syringe, resulting in the rapid formation of peaks assigned to the corresponding **LCuX** complex. A UV-vis spectrum was taken. Then, four 0.1 mL portions of dichloromethane were added to the cuvette to dilute the solution sequentially. UV-vis spectra were taken in between additions after the solution is completely equilibrated.
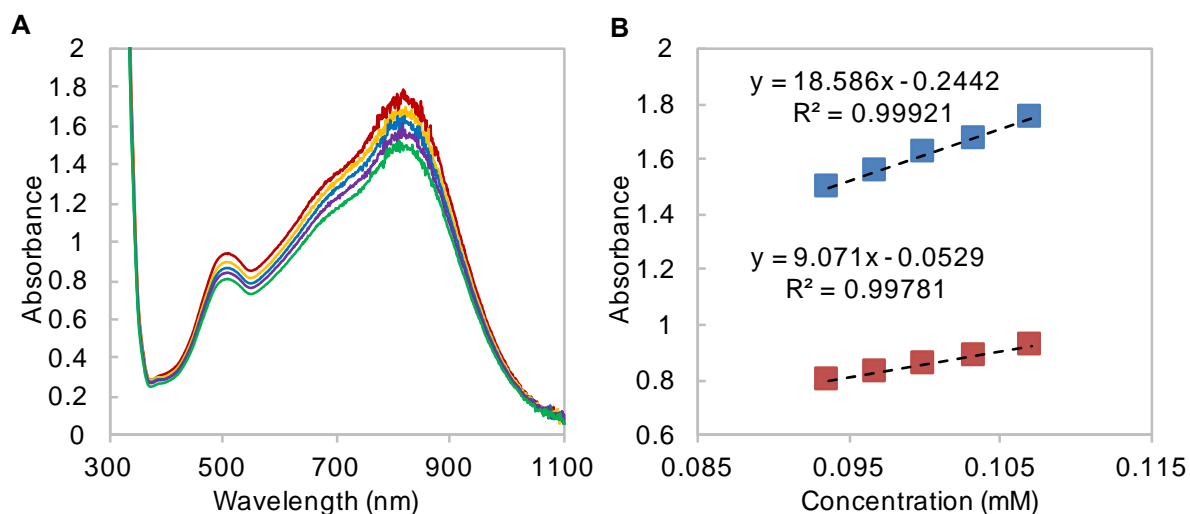
Supplementary Fig. 9. (A) UV-vis spectra obtained from the dilution of **LCuF** at −80 ℃ in CH$_2$Cl$_2$. (B) Beer's law plot for **LCuF**: 520 nm (9070 M^{-1} cm^{-1}); 820 nm (18600 M^{-1} cm^{-1}).
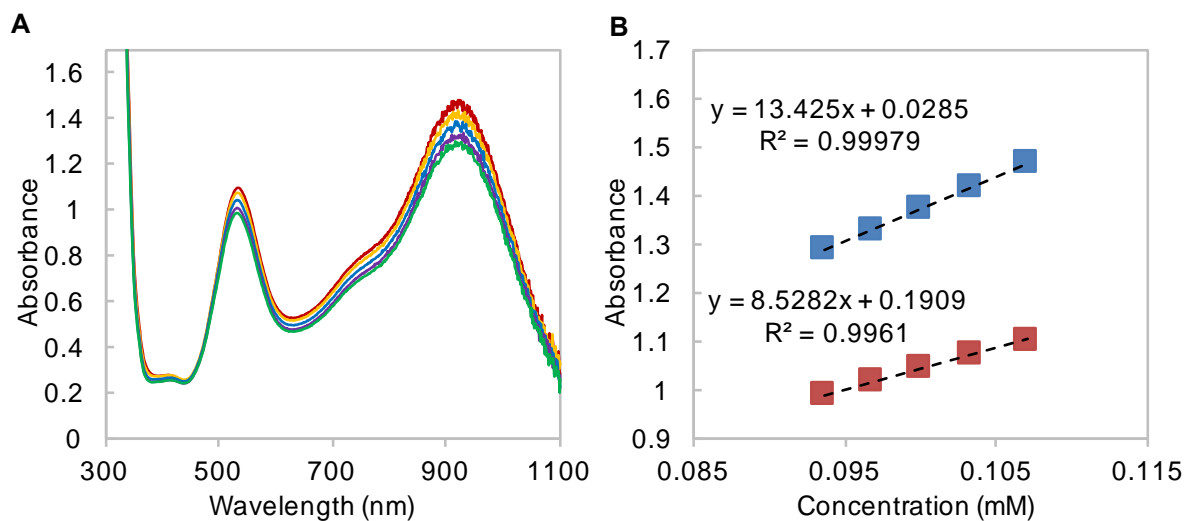
Supplementary Fig. 10. (A) UV-vis spectra obtained from the dilution of **L**CuCl at −80 ℃ in CH$_2$Cl$_2$. (B) Beer's law plot for **L**CuCl: 530 nm (8530 M^{-1} cm^{-1}); 920 nm (13400 M^{-1} cm^{-1}).
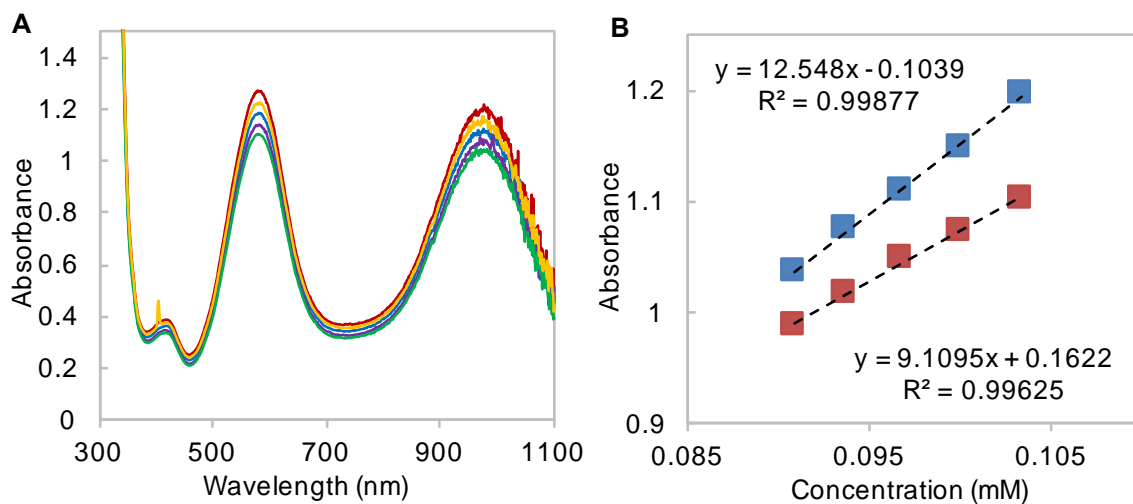
Supplementary Fig. 11. (A) UV-vis spectra obtained from the dilution of **L**CuBr at −80 ℃ in CH$_2$Cl$_2$. (B) Beer's law plot for **L**CuBr: 580 nm (12500 M^{-1} cm^{-1}); 980 nm (9110 M^{-1} cm^{-1}).

Kinetic studies of hydrogen atom abstraction

A dichloromethane solution of [TBA]**L**Cu^{II}X (2.800 mL, 0.107 mM) was placed in a quartz cuvette with septum attachment under a nitrogen atmosphere. The cuvette was sealed and cooled to −40 ℃ in the UV-vis spectrometer. A dichloromethane solution of [NAr$_3$]PF$_6$ (0.100 mL, 3.00 mM, 1 equivalent) was injected to the cuvette with a syringe, resulting in the rapid formation of peaks assigned to the corresponding **L**CuX complex. The solution was warmed to −30 °C and allowed to equilibrate for 5 minutes. Then, a dichloromethane solution of 9,10-dihydroanthracene (0.1 mL, 300 mM, 100 equivalents) was injected to the cuvette by syringe. The decay of characteristic peaks at 820 nm (**L**CuF), 920 nm (**L**CuCl) and 980 nm (**L**CuBr) was monitored for up to 3 hours. The rate of decay to **L**CuF reflects the full consumption to at least four half-lives, while **L**CuCl and **L**CuBr reflect the initial rate of decay to 25-35% consumption due to the significantly decreased reactivity at the same conditions.
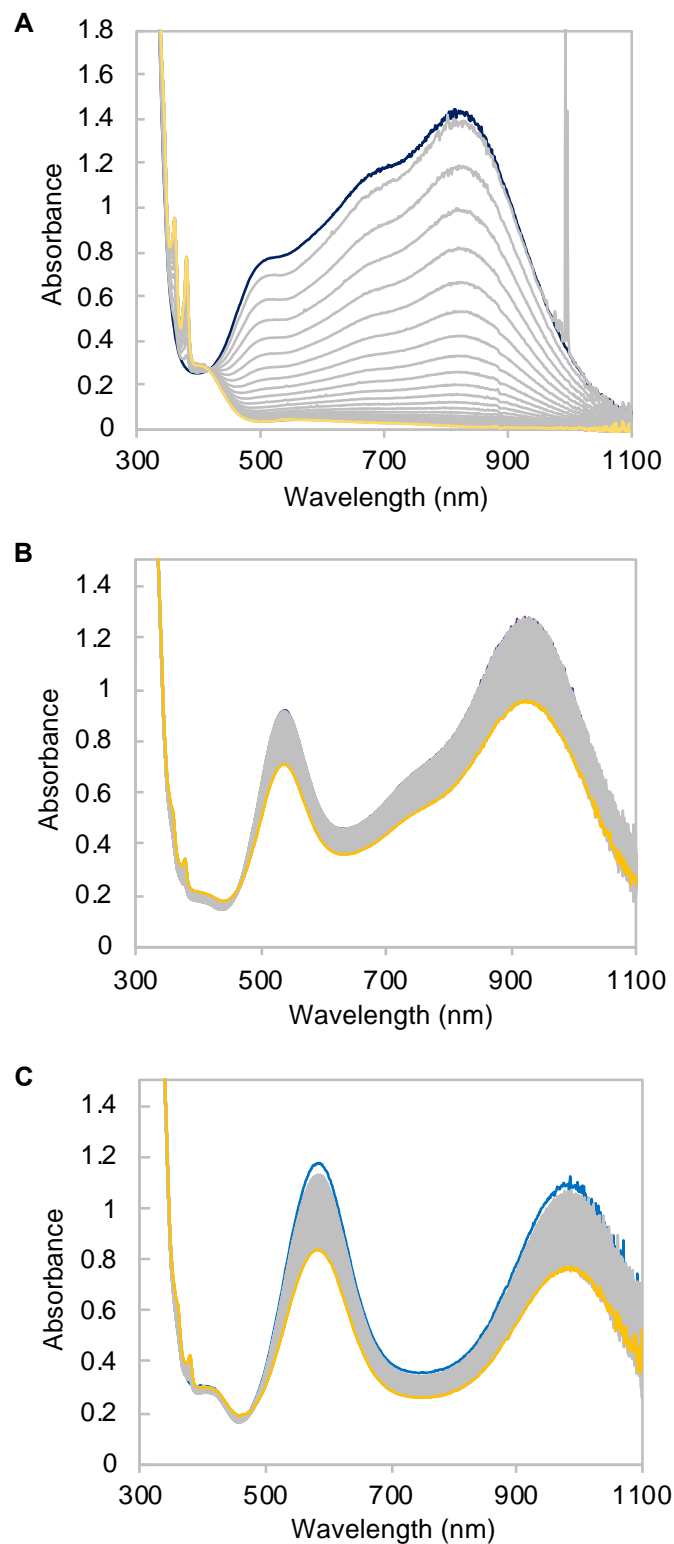
Supplementary Fig. 12. Example UV-vis spectra decay of a) **L**CuF (4 scans/minute), b) **L**CuCl (1 scan/minute), and c) **L**CuBr (1 scan/minute) when treated with 100 equivalents of 9,10-dihydroanthracene at −30 °C. The final spectrum is shown in yellow.
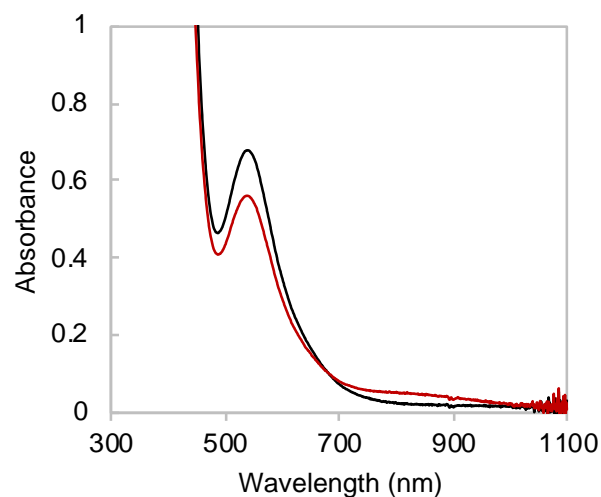
Supplementary Fig. 13. The UV-vis spectrum of **LCu**^{II}(MeCN) following the reaction of **LCuF** with 10 equivalents of DHA at −35 °C is shown (red trace). After the reaction, the volatiles were removed in vacuo and the remaining solids dissolved in MeCN. An aliquot was taken and diluted for UV-vis analysis. The overlaid black trace shows the spectrum of an authentic sample of **LCu**^{II}(MeCN) (0.3 mM), revealing the formation of **LCu**^{II}(MeCN) from HAA in 84% yield by comparison of the 535 nm peak.

Supplementary Table 1. Second-order rate constants (k, $M^{-1}\,s^{-1}$) from the reaction of **LCuX** complexes with 100 equivalents of 9,10-dihydroanthracene at −30 °C.

Compound	Trial 1	Trial 2	Trial 3	Average	Std. Dev.
LCuF	0.6784	0.6525	0.6718	0.6676	0.0135
LCuCl	0.00289	0.00223	0.00344	0.00285	0.00061
LCuBr	0.00257	0.00283	0.00163	0.00234	0.00063
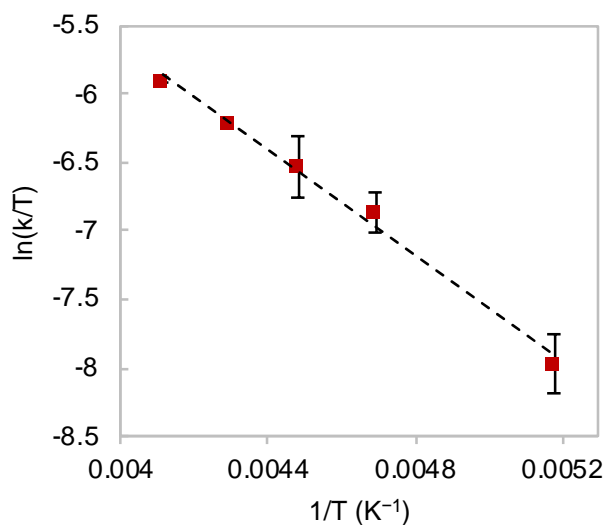
Supplementary Fig. 14. Eyring plot of reaction between **LCuF** and 9,10-dihydroanthracene. Calculated activation parameters are: $\Delta H^{\ddagger} = 3.8(2)$ kcal mol^{-1}, $\Delta S^{\ddagger} = -43(2)$ cal K^{-1}mol^{-1}. $R^2 = 0.9638$.

Supplementary Table 2. Second-order rate constants (k, $M^{-1}\,s^{-1}$) from the reaction of **LCuF** with 100 equivalents of 9,10-dihydroanthracene at various temperatures used to construct the Eyring plot.

Temperature (°C)	Trial 1	Trial 2	Trial 3	Average	Std. Dev.
−30	0.6784	0.6525	0.6718	0.6676	0.0135
−40	0.4559	0.4552	0.4873	0.4661	0.0183
−50	0.3980	0.3353	0.2565	0.3299	0.0709
−60	0.1898	0.2328	0.2501	0.2242	0.0310
−80	0.0801	0.0533	0.0701	0.0678	0.0134

Supplementary Table 3. Data used for the construction of Fig. 4b in the main text.

Anion bound to LCu	pK_a of anion conj. acid in DMSO	Source	Second-order rate constant ($M^{-1}\,s^{-1}$)	Temperature (° C), Solvent	Source	Log(k)
F	15	Ref. 5	0.668	−30 °C, CH_2Cl_2	This work	−0.175
Cl	1.8	Ref. 5	0.00389	−30 °C, CH_2Cl_2	This work	−2.41
Br	0.9	Ref. 5	0.00285	−30 °C, CH_2Cl_2	This work	−2.55
OH	32	Ref. 6	24.2	−30 °C, acetone	Ref. 1	1.38
$O_2CPh(m\text{-Cl})$	9.8	Ref. 7	0.11	−25 °C, 1,2-difluorobenzene	Ref. 8	−0.957
$O_2CPh(p\text{-NO}_2)$	9.1	Ref. 9	0.0079	−25 °C, 1,2-difluorobenzene	Ref. 10	−2.10
O_2CPh	11.1	Ref. 11	0.05	−25 °C, 1,2-difluorobenzene	Ref. 10	−1.30
O_2CMe	12.6	Ref. 12	0.015	−25 °C, 1,2-difluorobenzene	Ref. 10	−1.82

Thermal decomposition of LCuX complexes

LCuX complexes were generated in the UV-vis under standard conditions (see above) inside a quartz cuvette with Schlenk attachment at −80 °C, and warmed to room temperature. The cuvette was removed from the instrument while the cryostat was heated to 80 °C. Once the temperature was stabilized at 80 °C, the cuvette was inserted back to the cryostat and data collection was initiated.
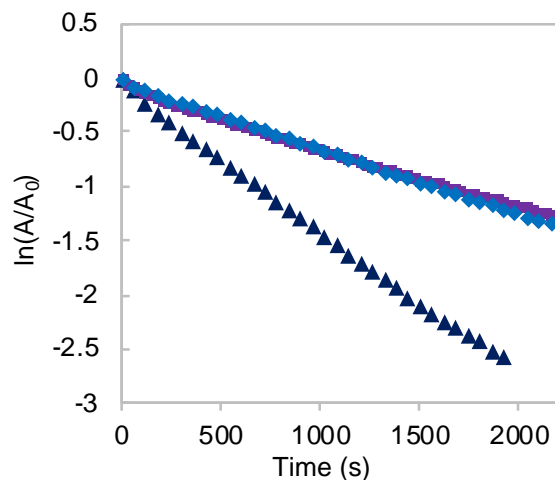
Supplementary Fig. 15. Overlay of kinetic traces of first order self-decay of **LCuF** (dark blue triangles, λ_{max} = 820 nm), **LCuCl** (purple squares, λ_{max} = 920 nm), **LCuBr** (light blue diamonds, λ_{max} = 980 nm) at 80 °C in CH_2Cl_2. **LCuF:** k_{obs} = 1.3 × 10^3 s^{-1} (R^2 = 0.9988); **LCuCl:** k_{obs} = 4.8 × 10^4 s^{-1} (R^2 = 0.9930); **LCuBr:** k_{obs} = 4.8 × 10^4 s^{-1} (R^2 = 0.9858).
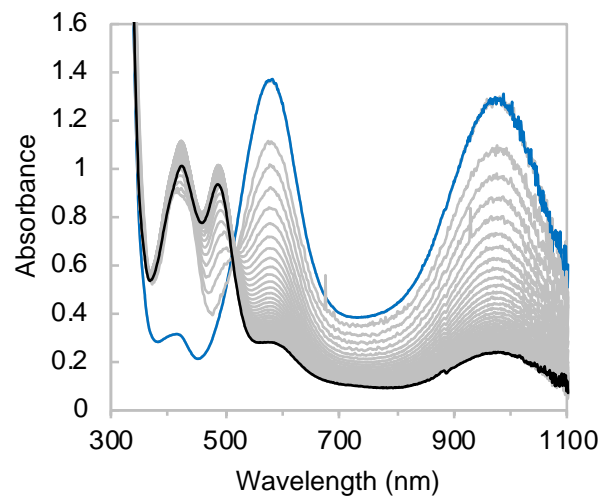
Supplementary Fig. 16. UV-vis spectra of the reaction between **L**CuBr (0.1 mM) and Gomberg's dimer (0.5 eq) in CH$_2$Cl$_2$ at −80 °C.

Nuclear Magnetic Resonance Spectra
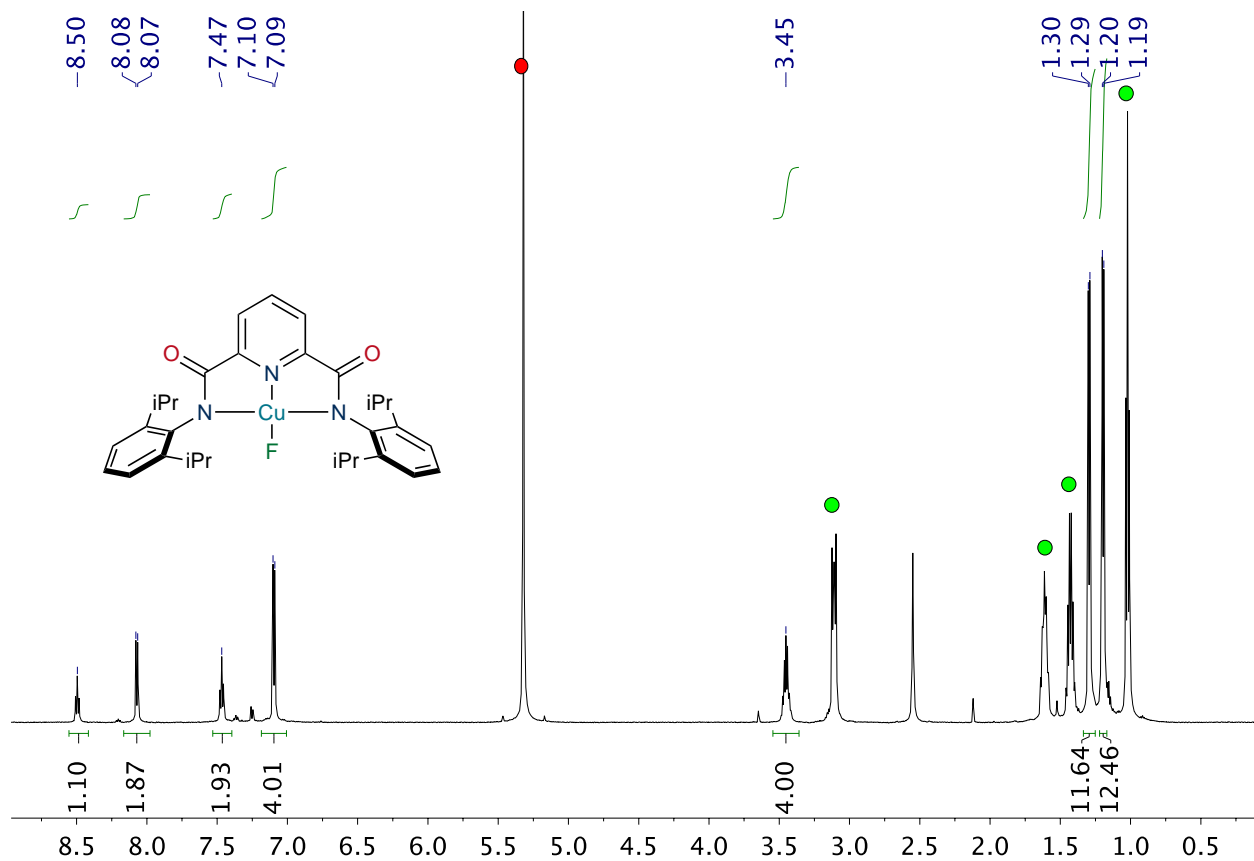
Supplementary Fig. 17. ^{1}H NMR (600 MHz, CD$_2$Cl$_2$, 27 °C) of **LCuF** generated from [TBA]**LCu^{II}F** and [NAr$_3$]PF$_6$. The sample was prepared in situ at −35 °C due to its thermal sensitivity. The red dot indicates the solvent residual peaks, and green dots indicate the tetrabutylammonium cation of tetrabutylammonium hexafluorophosphate.
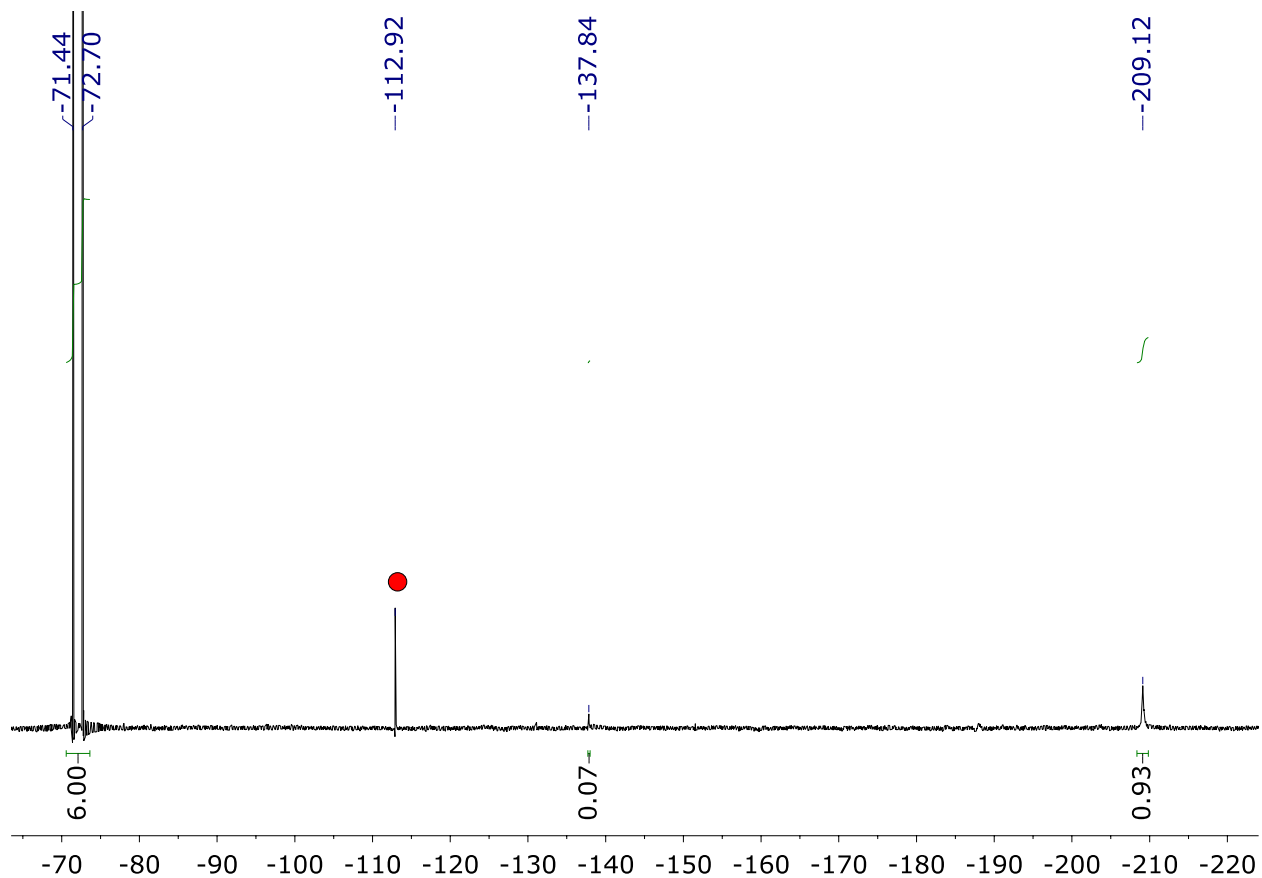
Supplementary Fig. 18. ^{19}F{^{1}H} NMR (565 MHz, CDCl$_3$/CH$_2$Cl$_2$ (1:1), 27 °C) of **LCuF** generated from [TBA]**LCu^{II}F** and [NAr$_3$]PF$_6$. The sample was prepared in situ at −35 °C due to its thermal sensitivity. The red dot indicates fluorobenzene which was used as an internal reference standard. The peak at −138 ppm corresponds to HF, which is the decomposition product of **LCuF**.
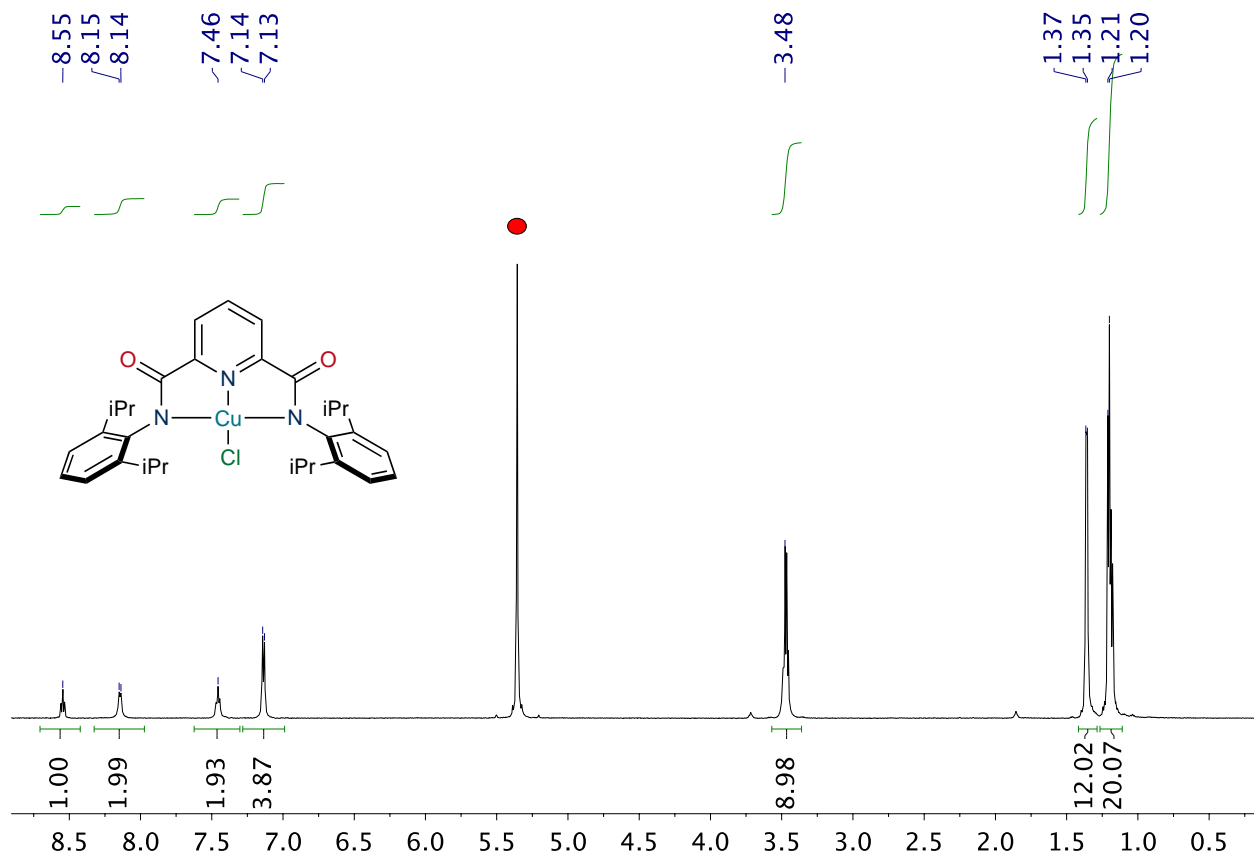
Supplementary Fig. 19. ¹H NMR (600 MHz, CD$_2$Cl$_2$, 27 °C) of **LCuCl**. The red dot indicates the solvent residual peaks. The integration of the peaks at 3.48 ppm and 1.21 ppm is skewed due to overlap with residual diethyl ether, which could not be removed despite prolonged application of vacuum to the solid sample.
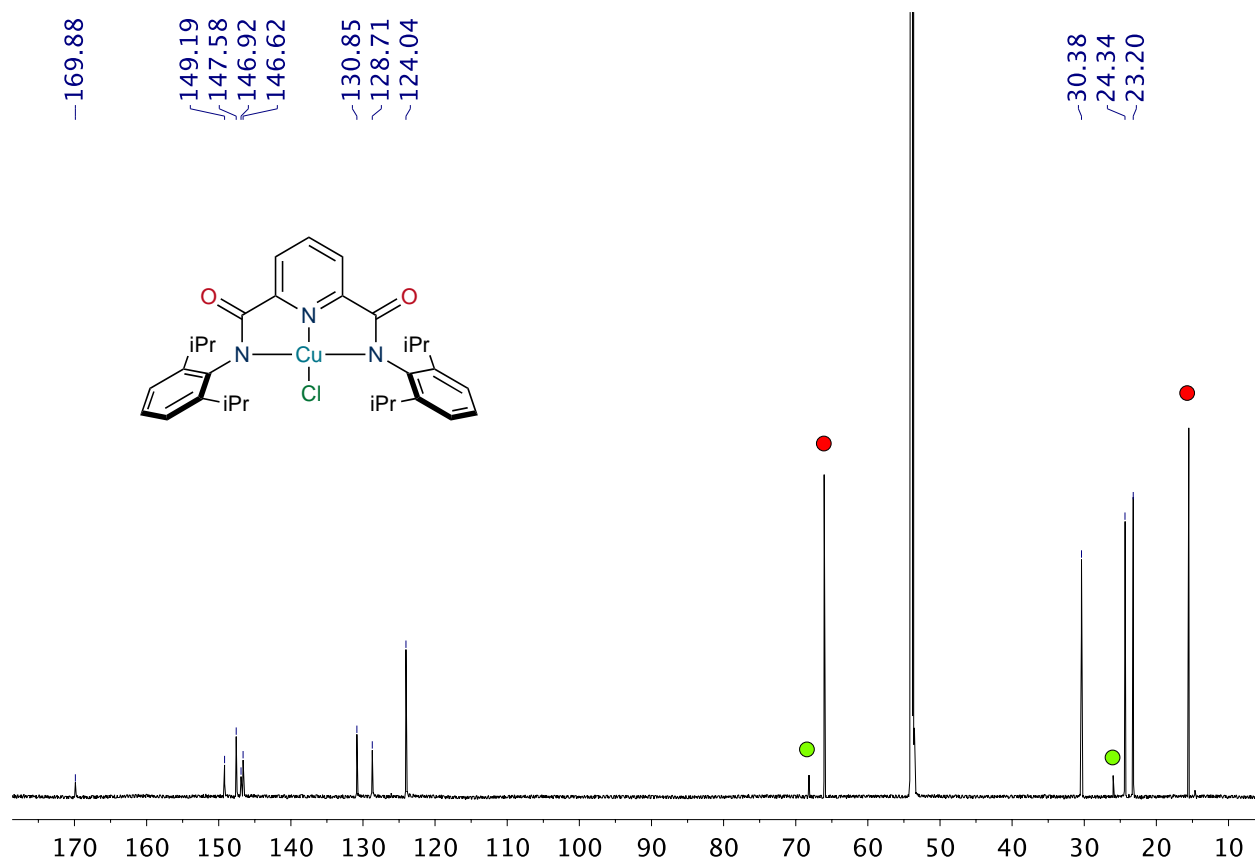
Supplementary Fig. 20. ^{13}C{^{1}H} NMR (214 MHz, CD$_2$Cl$_2$, 27 °C) of **LCuCl**. Red dots indicate diethyl ether signals, which could not be removed despite prolonged application of vacuum to the solid sample. Green dots indicate a small amount of residual tetrahydrofuran from the starting material.
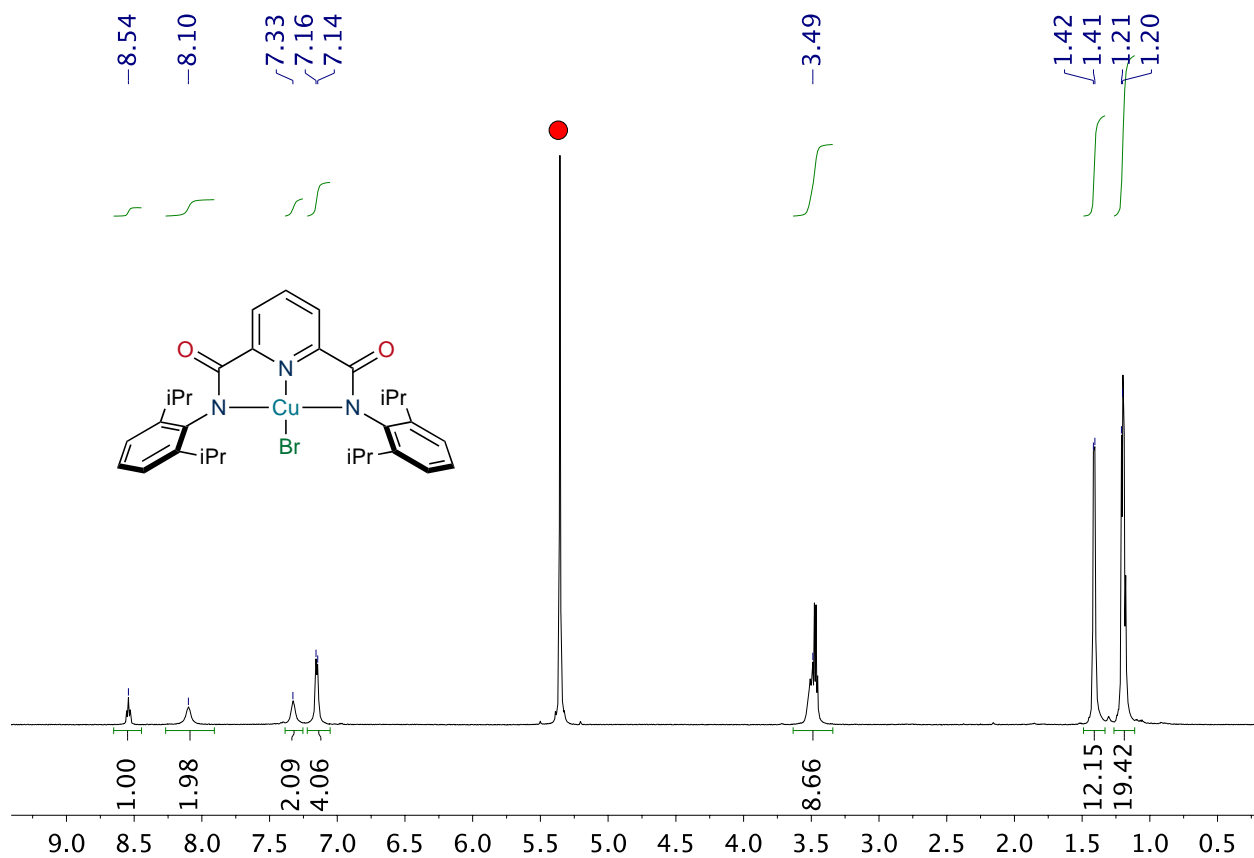
Supplementary Fig. 21. ^{1}H NMR (600 MHz, CD$_2$Cl$_2$, 27 °C) of **LCuBr**. The red dot indicates the solvent residual peaks. The integration of the peaks at 3.49 ppm and 1.21 ppm is skewed due to overlap with residual diethyl ether, which could not be removed despite prolonged application of vacuum to the solid sample.
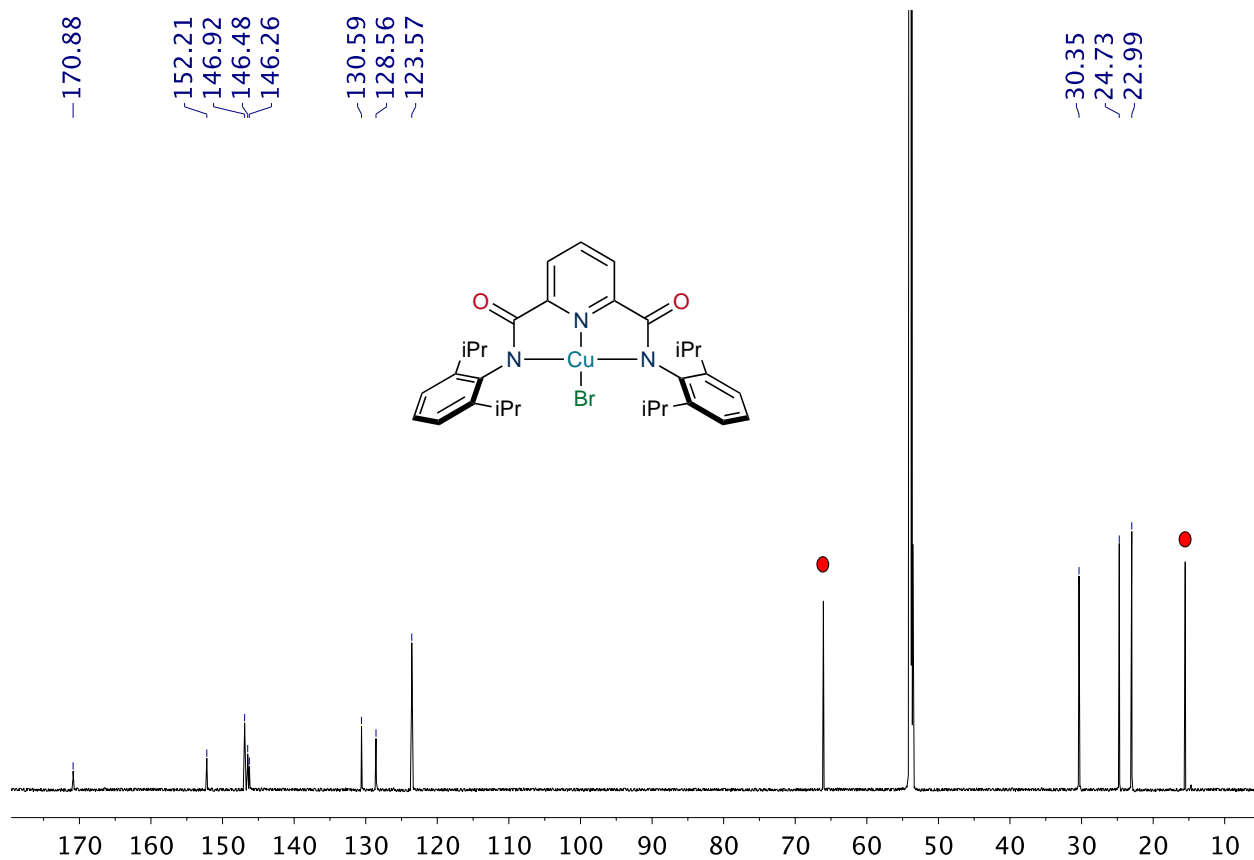
Supplementary Fig. 22. $^{13}C\{^1H\}$ NMR (214 MHz, CD$_2$Cl$_2$, 27 °C) of **LCuBr**. Red dots indicate diethyl ether signals, which could not be removed despite prolonged application of vacuum to the solid sample.

Radical capture from AIBN decomposition
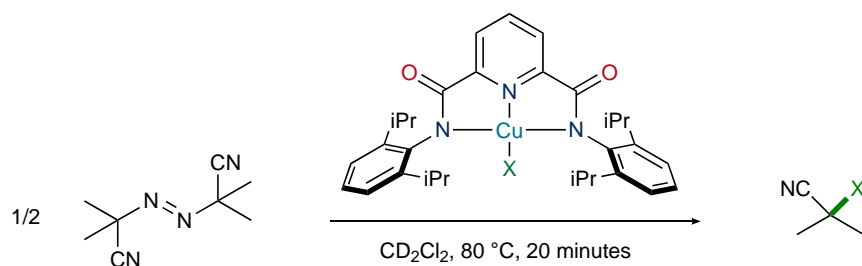
Procedure for LCuF: [TBA]**LCu**^{II}**F** (4.3 mg, 5.3 μmol) and azobisisobutyronitrile (2.6 mg, 15.8 μmol) were dissolved in 0.600 mL of CD$_2$Cl$_2$. The solution was added to a J-Young NMR tube and placed in a −35 °C freezer inside the glovebox. A chilled solution of [NAr$_3$]PF$_6$ in 0.400 mL CD$_2$Cl$_2$ was added, the tube inverted, and the sample was quickly returned to the freezer for five minutes. The sample was removed from the glovebox and placed into a preheated oil bath at 80 °C for 20 minutes. The reaction was indicated complete by the disappearance of the dark blue color of **LCuF** and the appearance of a red-brown solution, indicative of a nitrile bound **LCu**^{II} complex.

Procedure for LCuCl and LCuBr: **LCuCl** (2.9 mg, 5.0 μmol) was dissolved in CD$_2$Cl$_2$ and added to a J Young NMR tube inside the glovebox. The tube was removed and ^{1}H NMR was performed to establish the molar ratio of **LCuX** to diethyl ether residual in the sample. The tube was brought back into the glovebox, where 6 equivalents of azobisisobutyronitrile (2.5 mg, 15 μmol) was dissolved in CD$_2$Cl$_2$ and added to the NMR tube. The sample was removed from the glovebox and placed into a preheated oil bath at 80 °C for 20 minutes. The reaction was indicated complete by the disappearance of the dark purple color of **LCuX** and appearance of a red-brown solution, indicative of a nitrile bound **LCu**^{II} complex.
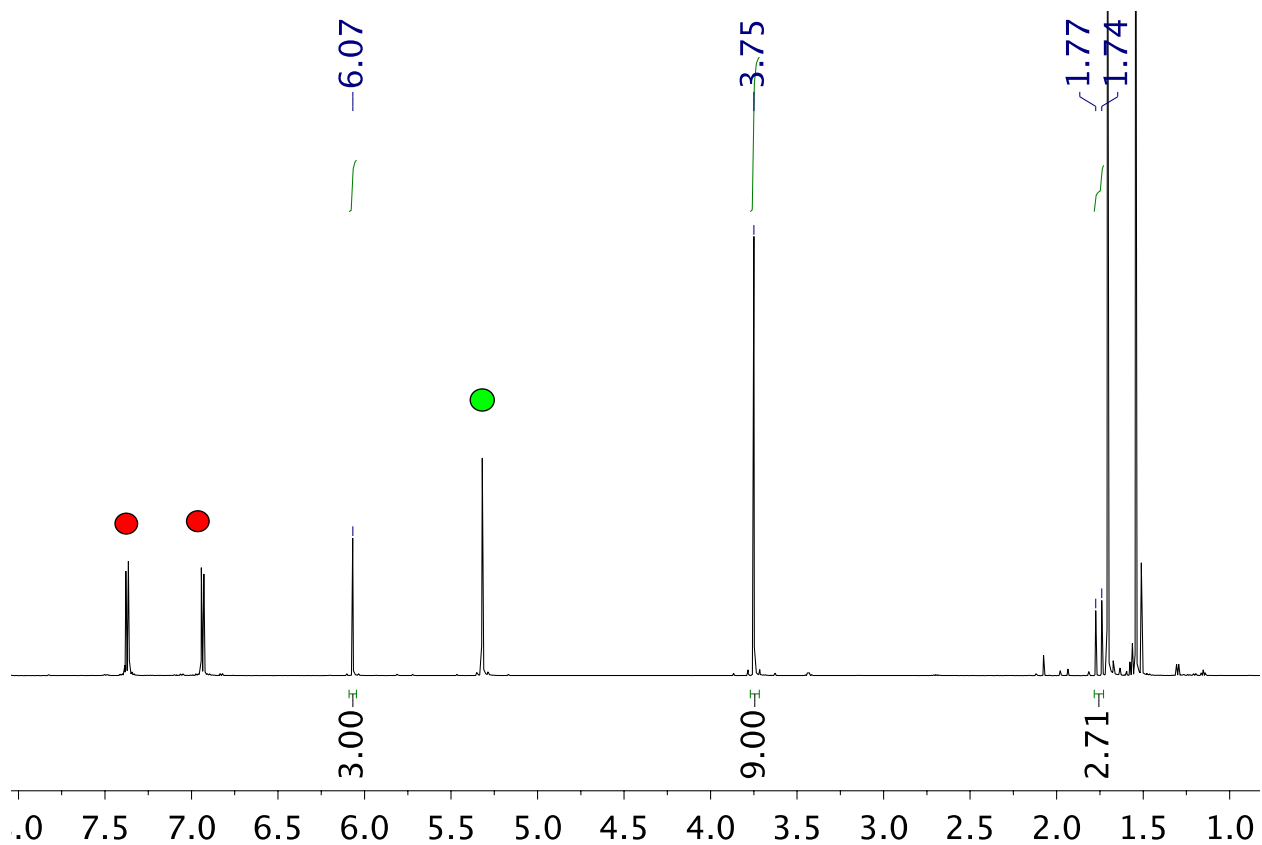
Supplementary Fig. 23. ^{1}H NMR (600 MHz, CD$_2$Cl$_2$, 27 °C) of the crude mixture following the reaction between **LCuF** and AIBN, revealing the formation of 2-fluoro-2-methylpropanenitrile at 1.76 ppm (d, J = 21 Hz).[13] A yield of 45% was obtained as an average of two runs, referenced to trimethoxybenzene internal standard (6.07 ppm and 3.75 ppm). Red dots indicate tris(4-bromophenyl)amine, and green dot indicates the solvent residual peak.
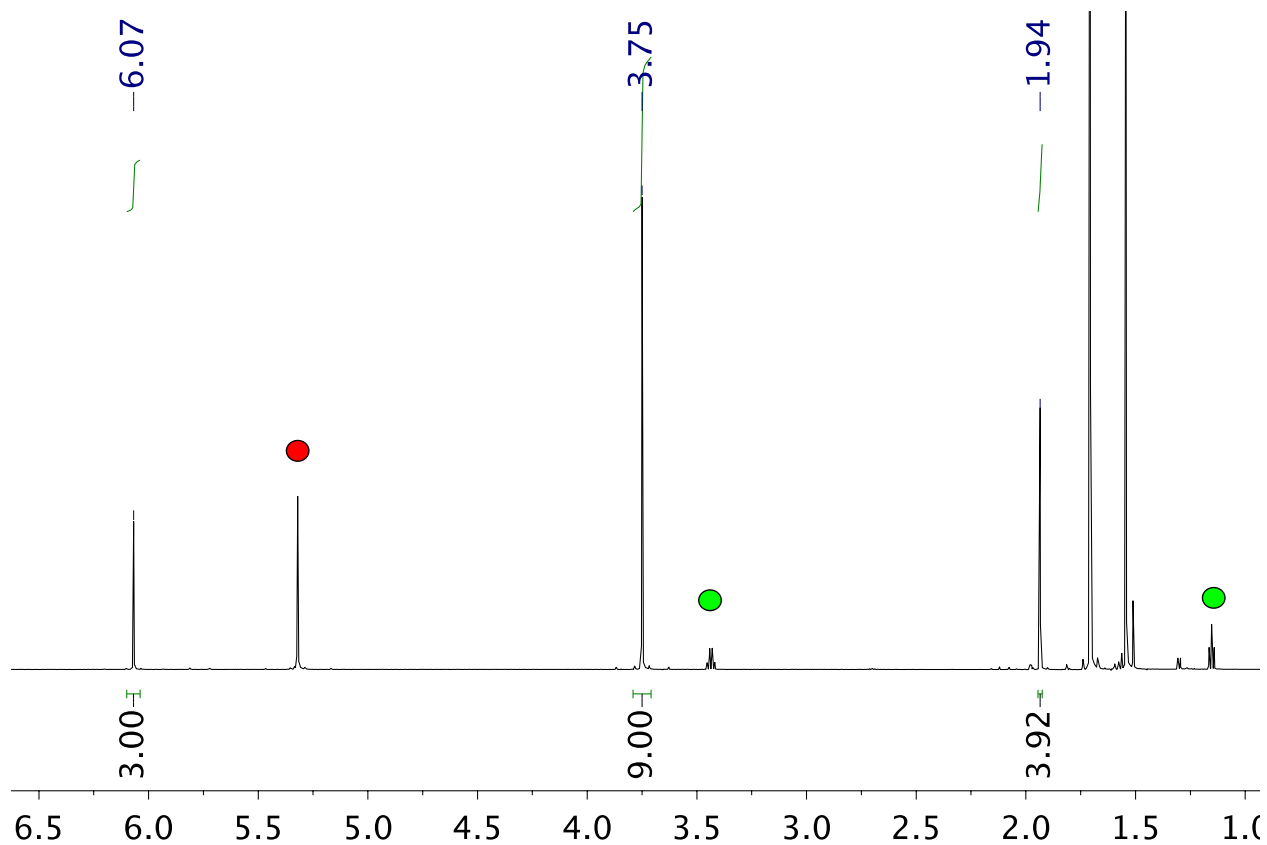
Supplementary Fig. 24. ^{1}H NMR (600 MHz, CD$_2$Cl$_2$, 27 °C) of the crude mixture following the reaction between **L**CuCl and AIBN, revealing the formation of 2-chloro-2-methylpropanenitrile at 1.94 ppm (s). A yield of 60% was obtained as an average of two runs, referenced to trimethoxybenzene internal standard (6.07 ppm and 3.75 ppm). The green dots indicate diethyl ether, and red dot indicates the solvent residual proton peak.
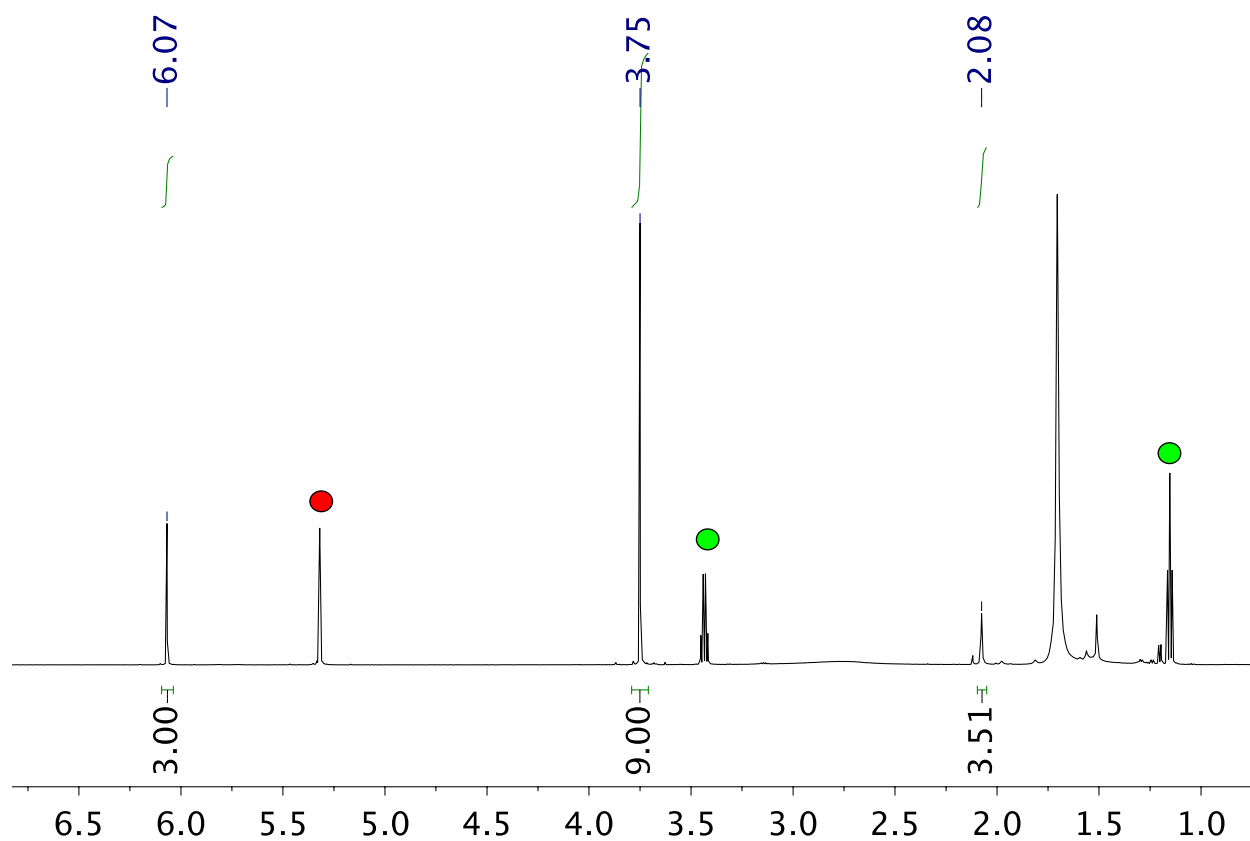
Supplementary Fig. 25. ^{1}H NMR (600 MHz, CD$_2$Cl$_2$, 27 °C) of the crude mixture following the reaction between **LCuBr** and AIBN, revealing the formation of 2-bromo-2-methyl-propionitrile at 2.08 ppm (s).[14] A yield of 68% was obtained as an average of two runs, referenced to trimethoxybenzene internal standard (6.07 ppm and 3.75 ppm). The green dots indicate diethyl ether, and red dot indicates the solvent residual proton peak.

Trityl radical capture
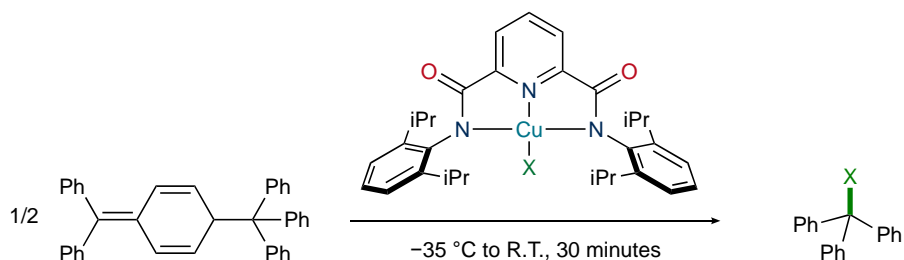
Procedure for LCuF: [TBA]**L**Cu^{II}F (0.250 mL, 10 mM) in CDCl$_3$ was added to an NMR tube inside the glovebox and cooled to −35 °C. A cold solution of [NAr$_3$]PF$_6$ (0.125 mL, 20mM) was added to generate **L**CuF. The NMR tube was inverted and stored at −35 °C for 30 minutes. Then, a cold solution of Gomberg's dimer (0.250 mL, 5 mM, CH$_2$Cl$_2$) was added by autopipette. The tube was inverted and allowed to sit at room temperature for 30 minutes prior to removal for NMR analysis.

Procedure for LCuCl and LCuBr: A sample of **L**CuX (~2.0 mg) was dissolved in CD$_2$Cl$_2$ and added to a J Young NMR tube inside the glovebox. The tube was removed from the glove box and ^{1}H NMR was performed to establish the molar ratio of **L**CuX to diethyl ether residual in the sample. The tube was brought back into the glovebox, where 0.5 equivalents of Gomberg's dimer (18 mM) dissolved in CD$_2$Cl$_2$ was injected by autopipette into the NMR tube. The sample was inverted, allowed to react for 30 minutes at room temperature. One equivalent of trimethoxybenzene was added as the internal standard prior to NMR analysis.
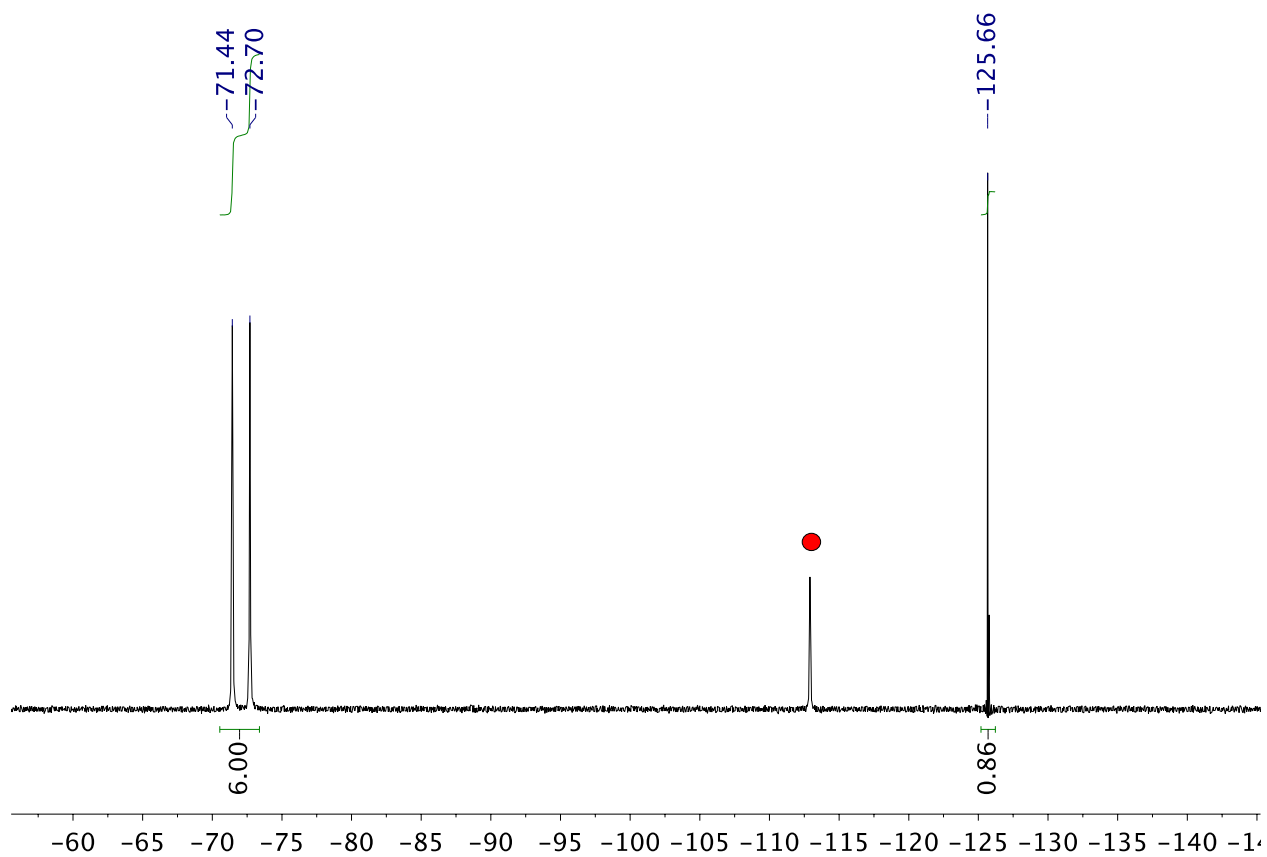
Supplementary Fig. 26. $^{19}F\{^{1}H\}$ NMR (565 MHz, 1:1 CDCl$_3$/CH$_2$Cl$_2$, 27 °C) of the reaction between **L**CuF (generated from [TBA]**L**Cu^{II}F and [NAr$_3$]PF$_6$ at −35 °C) and 0.5 equivalents of Gomberg's dimer, revealing the formation of trityl fluoride at 125.9 ppm (s).[15] A yield of 86% was obtained, referenced to the PF$_6^-$ peak of the [TBA]PF$_6$ byproduct. The red dot indicates fluorobenzene, the internal reference standard.
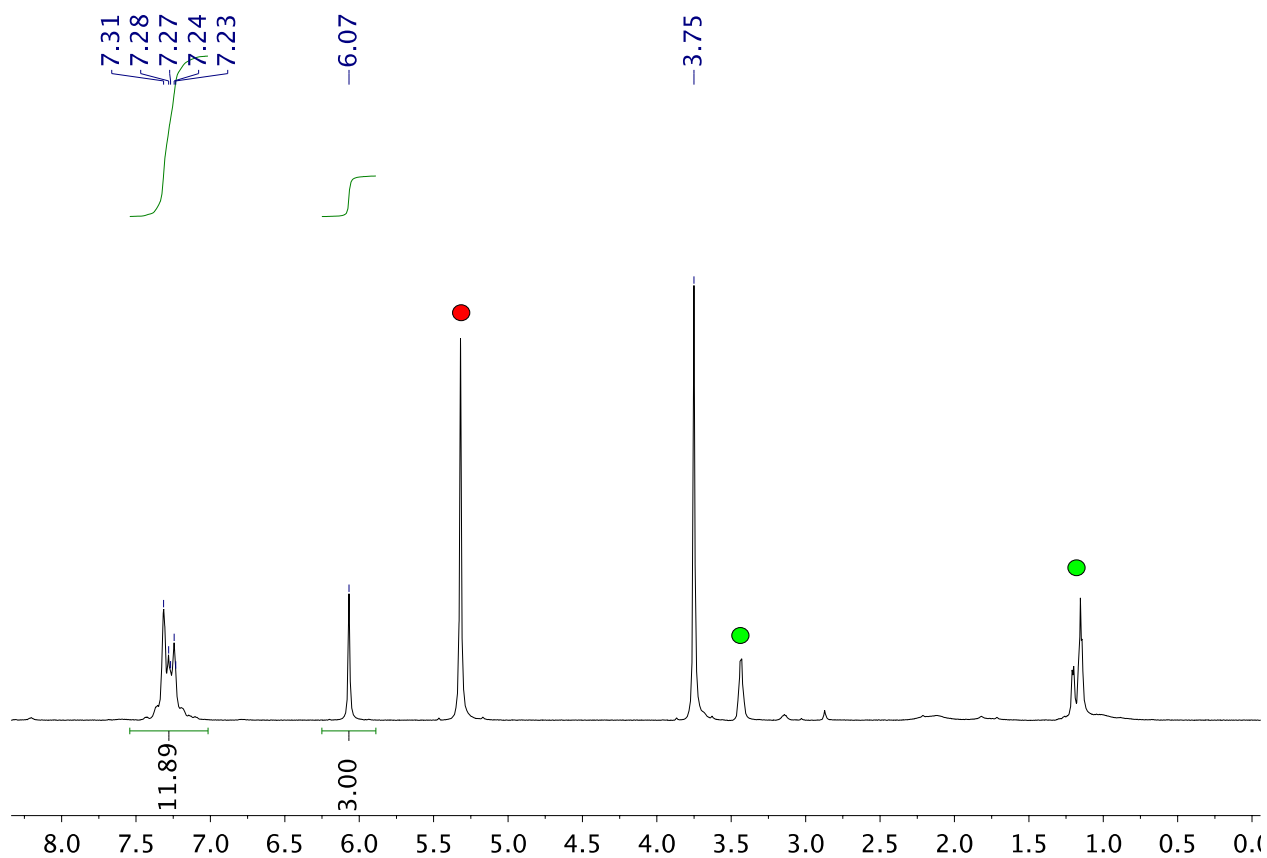
Supplementary Fig. 27. ^{1}H NMR (600 MHz, CD$_2$Cl$_2$, 27 °C) of the crude mixture from the reaction of **L**CuCl and 0.5 equivalents of Gomberg's dimer, revealing the formation of trityl chloride by comparison with an authentic sample. A yield of 79.2% was obtained, referenced to the internal standard trimethoxybenzene (6.07 ppm and 3.75 ppm). The red dot indicates the solvent residual peak. Green dots indicate residual diethyl ether from the sample of **L**CuCl.
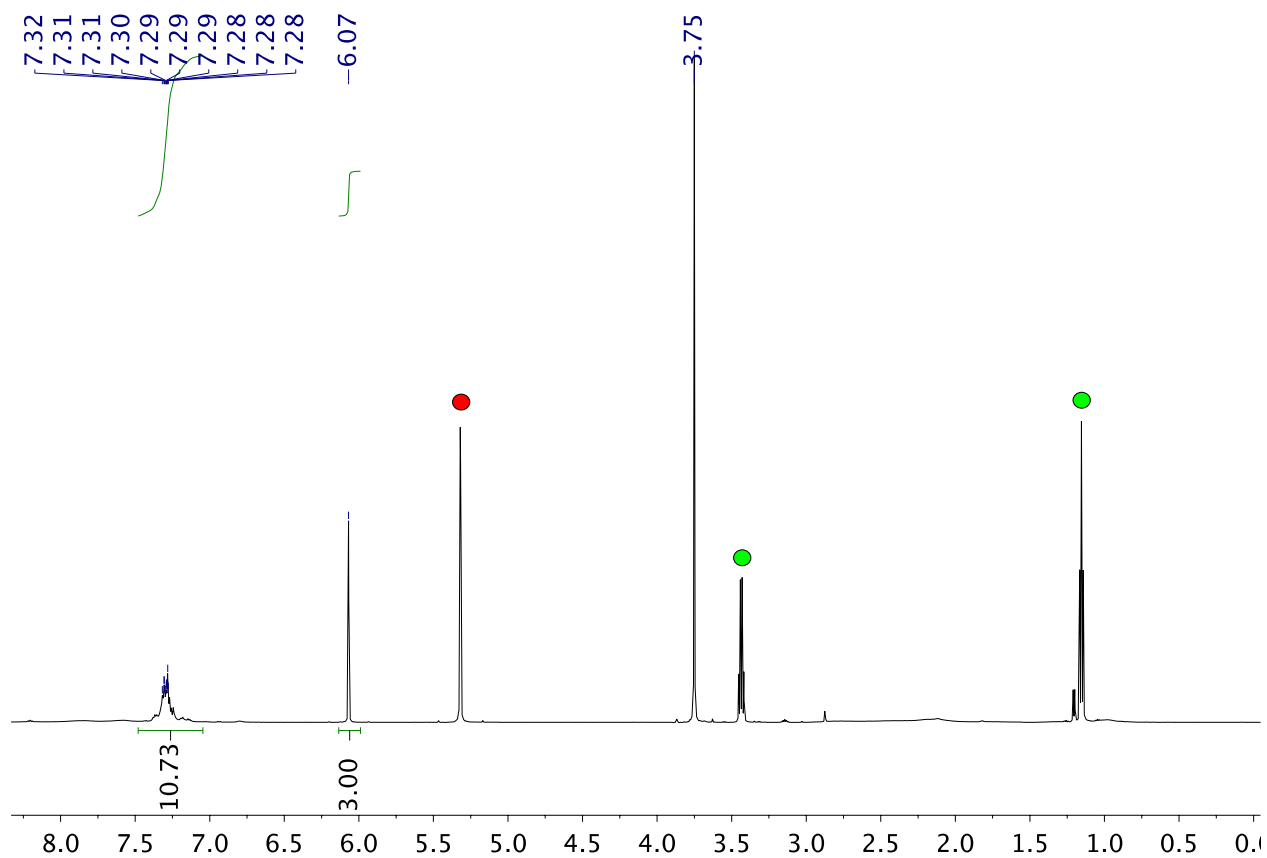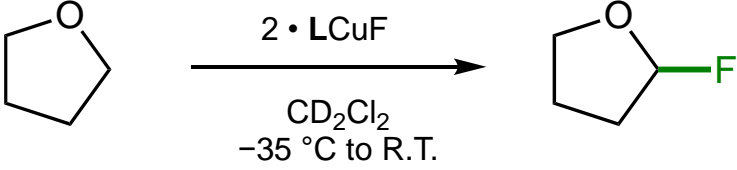
Supplementary Fig. 28. ^{1}H NMR (600 MHz, CD$_2$Cl$_2$, 27 °C) of the crude mixture from the reaction of **LCuBr** and 0.5 equivalents of Gomberg's dimer, revealing the formation of trityl bromide.[16] A yield of 71.5% was obtained, referenced to the internal standard trimethoxybenzene (6.07 ppm and 3.75 ppm). The red dot indicates the solvent residual peak. Green dots indicate residual diethyl ether from the sample of **LCuBr**.

Direct C(sp^3)-H fluorination by LCuF

An aliquot of [TBA]**LCu**^{II}**F** in CD$_2$Cl$_2$ (0.200 mL, 25 mM) was added to an NMR tube and cooled to −35 °C in the glovebox freezer. An aliquot of precooled [NAr$_3$]PF$_6$ (0.400 mL, 12.5mM) was rapidly added and the solution was inverted and stored in the freezer for one hour. The tube was then injected with 100 equivalents (1 mmol) of the desired substrate and allowed to warm to room temperature. The deep blue color of the solution gradually gave way to forest green, indicating the end of the reaction. The reported ^{19}F NMR yields (average of two trials) in Table 1 were calculated by comparison of the product integral with the byproduct [TBA]PF$_6$, based on the requirement of two equivalents of **LCuF** to furnish one equivalent of product.

Supplementary Table 4. Stoichiometry optimized for the reaction between **LCuF** and tetrahydrofuran. Yields determined by ^{19}F NMR.

Equivalents of THF	Yield (%)
25	35
50	54
100	69
1000	59
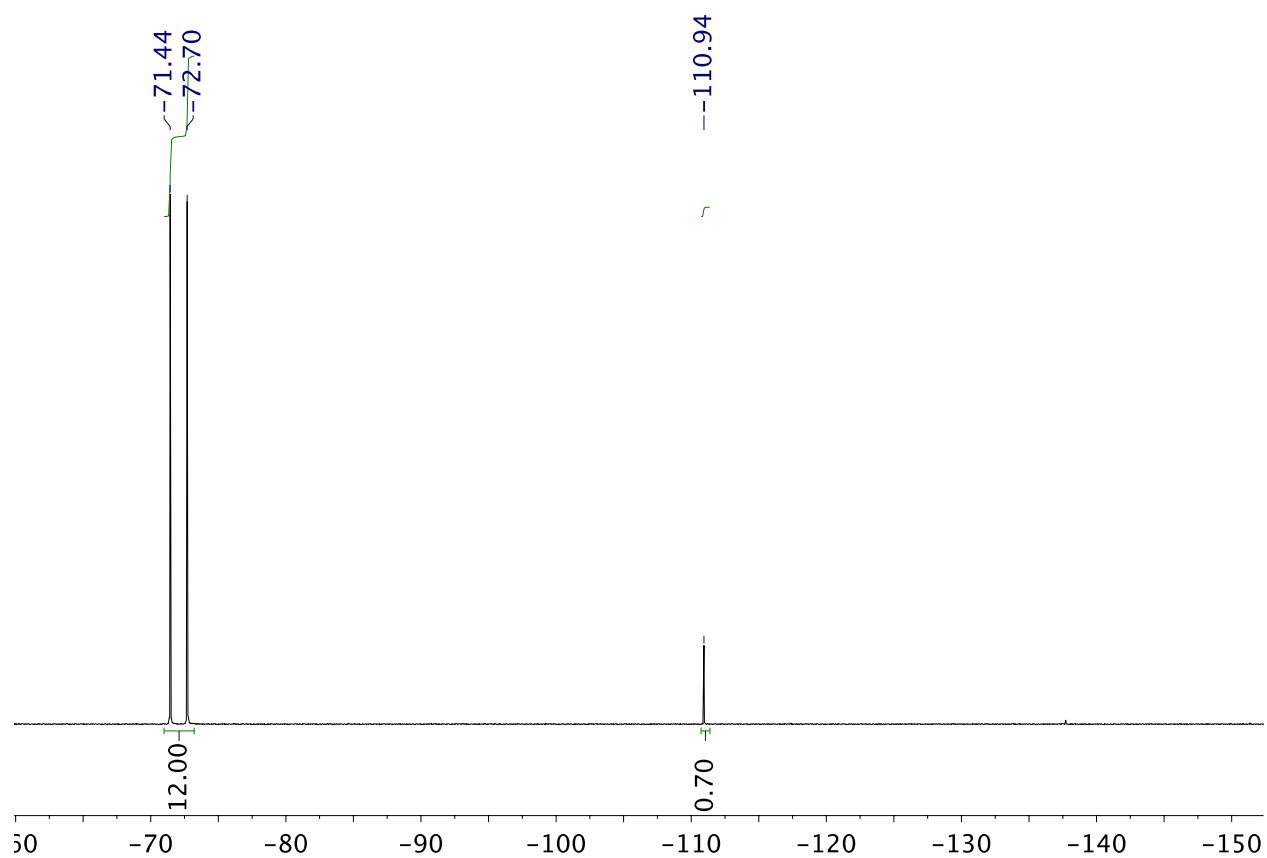
Supplementary Fig. 29. ^{19}F[^{1}H] NMR spectrum (565 MHz, CD$_2$Cl$_2$, 27 °C) of the reaction between **L**CuF and tetrahydrofuran, showing the formation of 2-fluorotetrahydyrofuran at −111.7 ppm.[17]
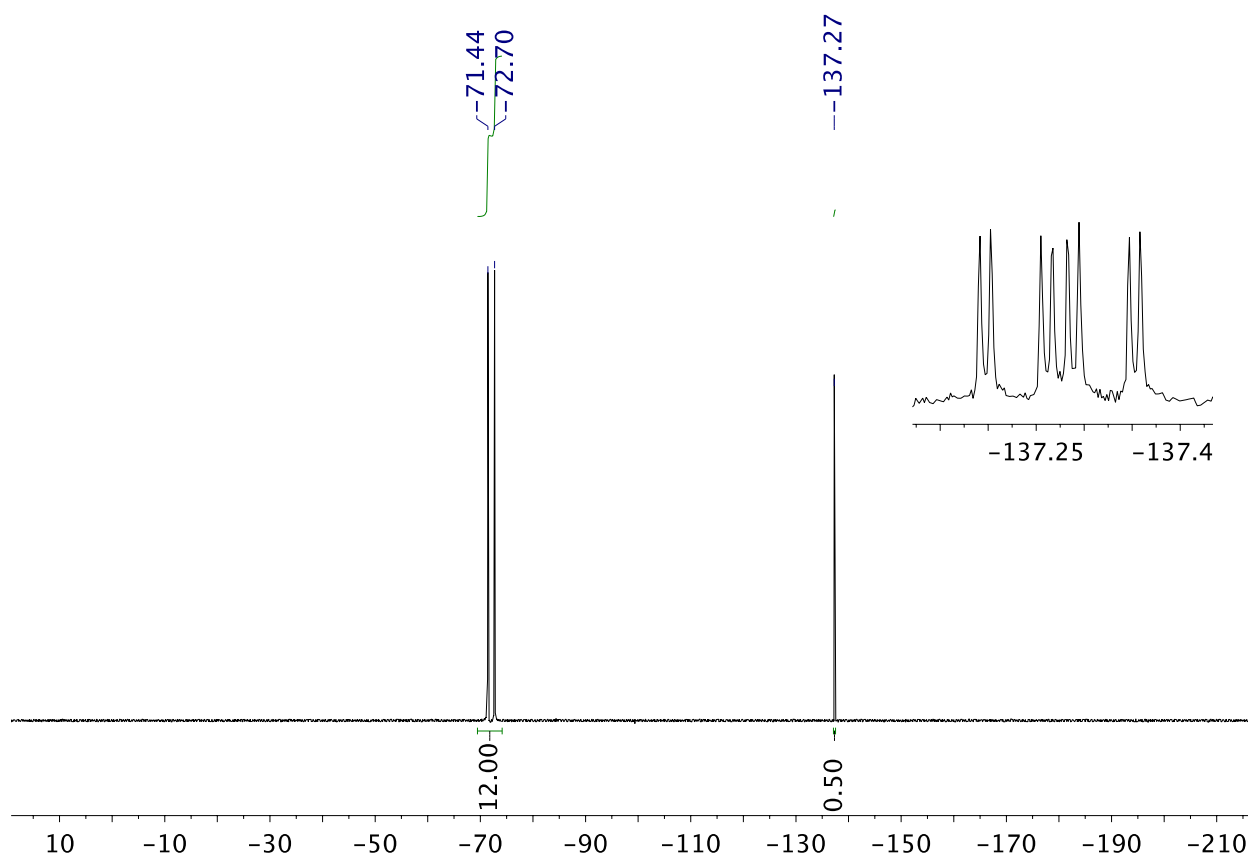
Supplementary Fig. 30. ^{19}F{^{1}H} NMR spectrum (565 MHz, CD$_2$Cl$_2$, 27 °C) of the reaction between **LCuF** and 1,4-dioxane, showing the formation of 2-fluoro-1,4-dioxane at −137.3 ppm.[18] The inset shows the proton-coupled ^{19}F NMR signal.
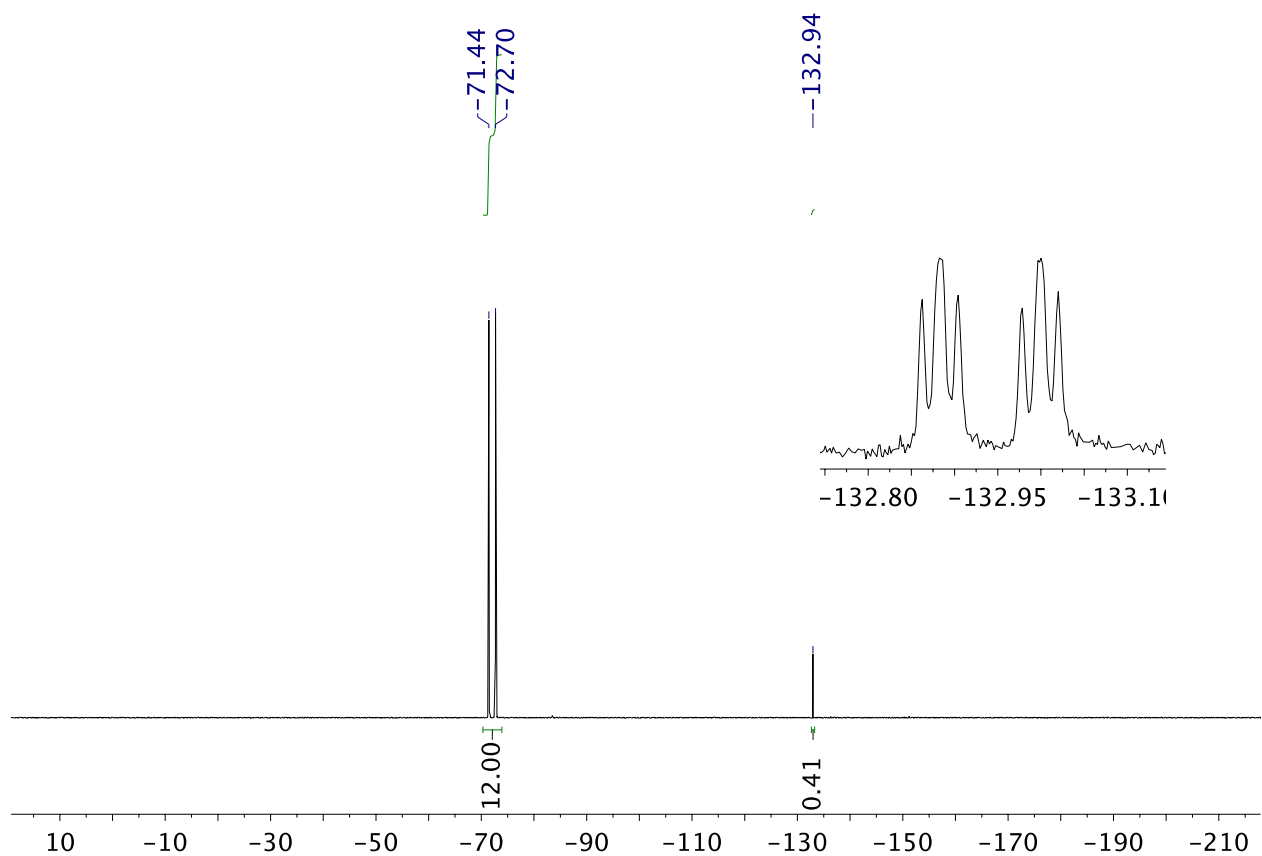
Supplementary Fig. 31. $^{19}F\{^1H\}$ NMR spectrum (565 MHz, CD_2Cl_2, 27 °C) of the reaction between **LCuF** and 18-crown-6, showing the formation of the monofluorinated product at −132.9 ppm.[18] The inset shows the proton-coupled ^{19}F NMR signal.
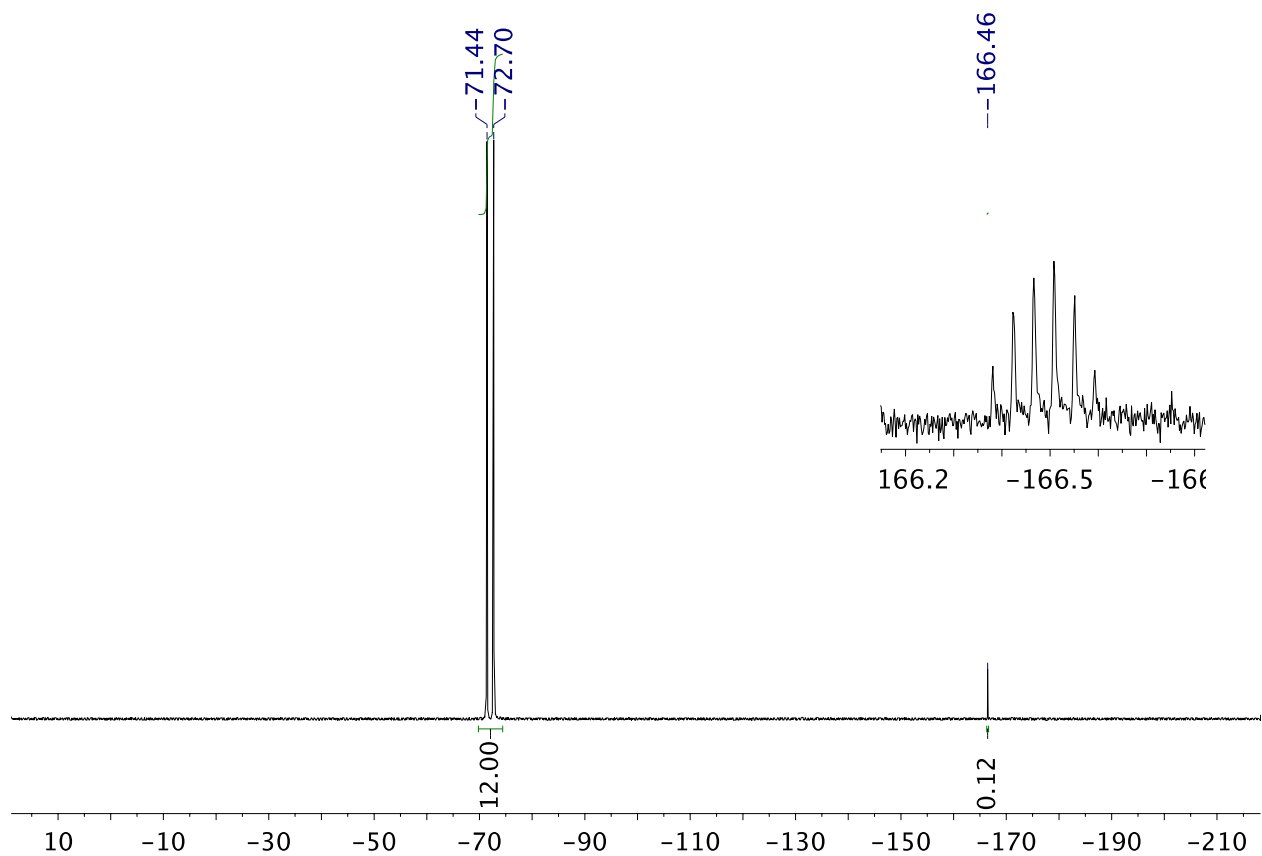
Supplementary Fig. 32. ^{19}F{^{1}H} NMR spectrum (565 MHz, CD$_2$Cl$_2$, 27 °C) of the reaction between **LCuF** and ethyl benzene, showing the formation of (1-fluoroethyl)benzene at −166.5 ppm.[19] The inset shows the proton-coupled ^{19}F NMR signal.
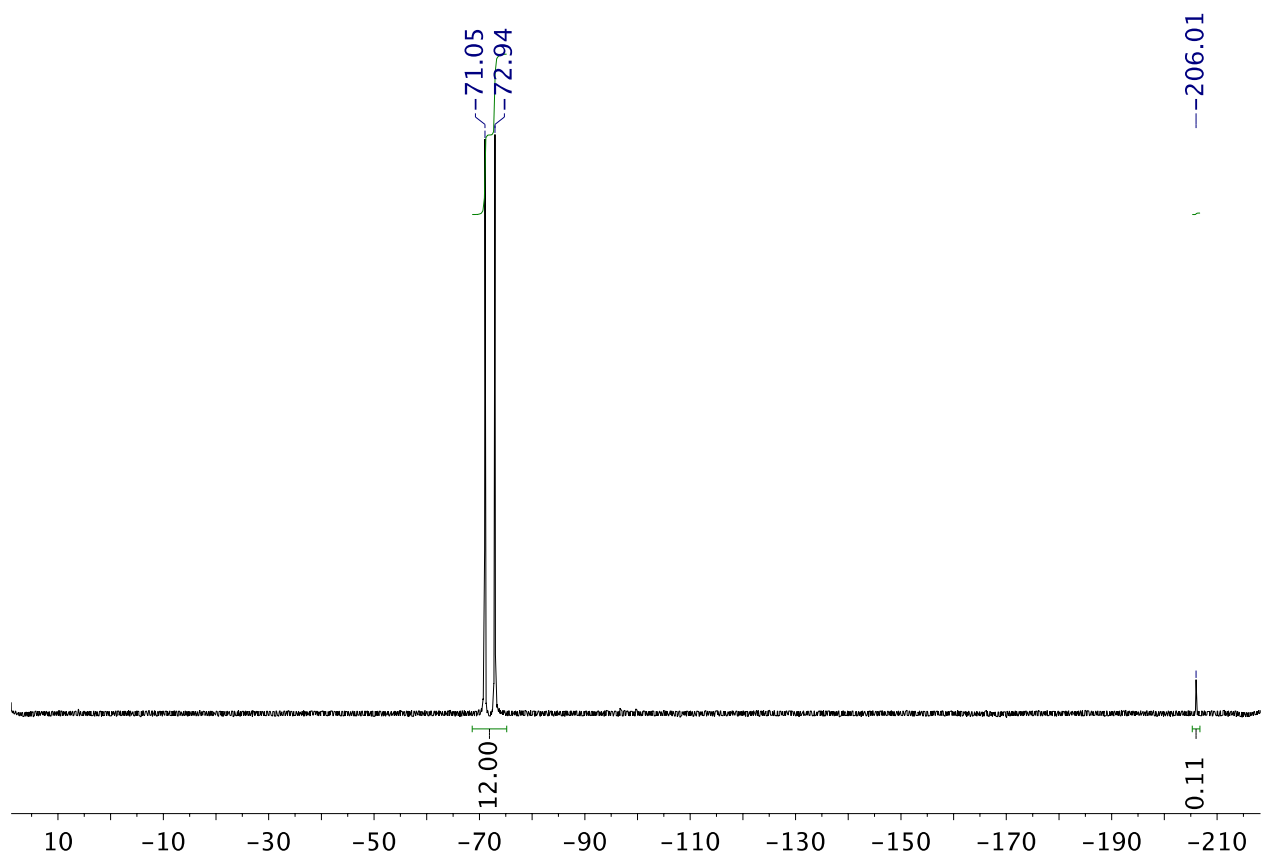
Supplementary Fig. 33. $^{19}F\{^1H\}$ NMR spectrum (377 MHz, CD$_2$Cl$_2$, 27 °C) of the reaction between **LCuF** and toluene, showing the formation of benzyl fluoride at −206.0 ppm.[20]
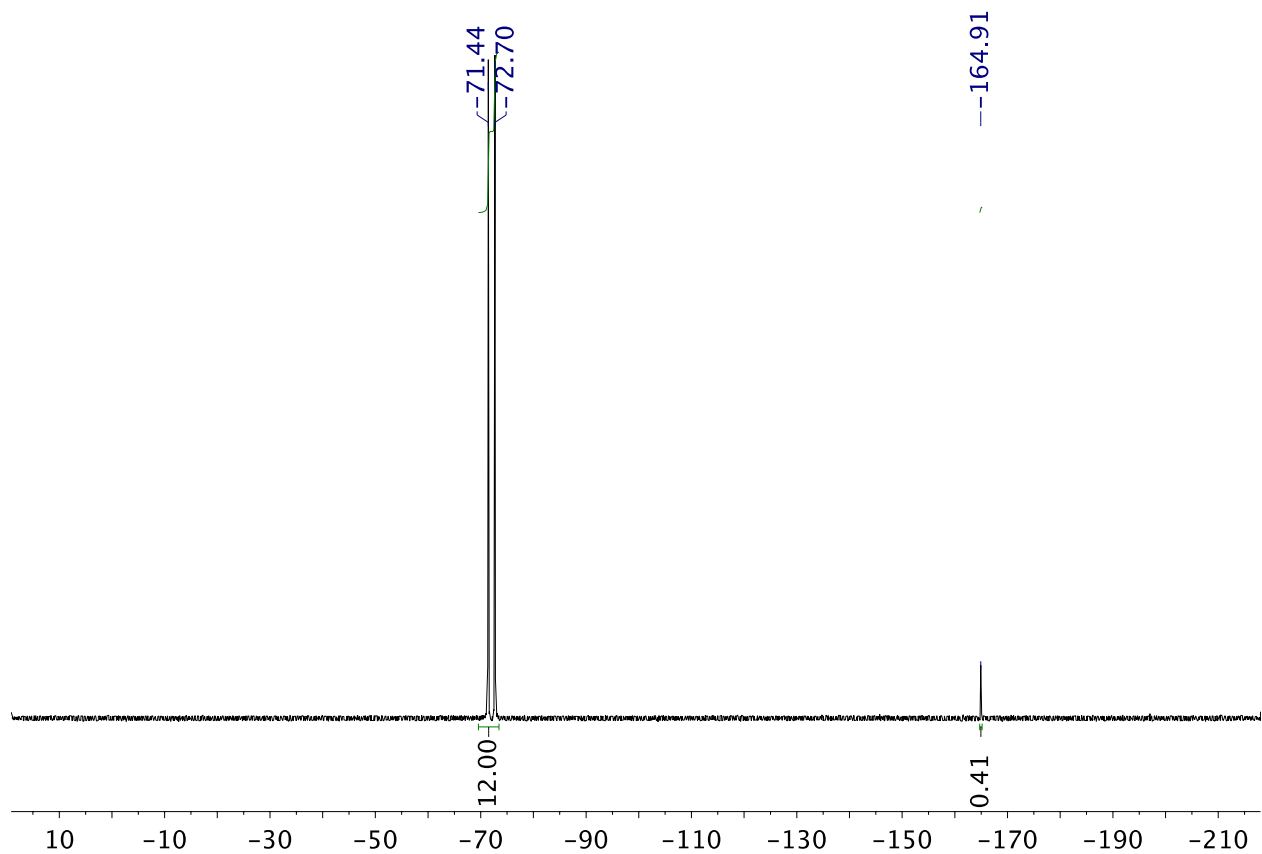
Supplementary Fig. 34. ^{19}F{^{1}H} NMR spectrum (565 MHz, CD$_2$Cl$_2$, 27 °C) of the reaction between **LCuF** and cyclohexene, showing the formation of 3-fluorocyclohexene at −164.9 ppm.[21]
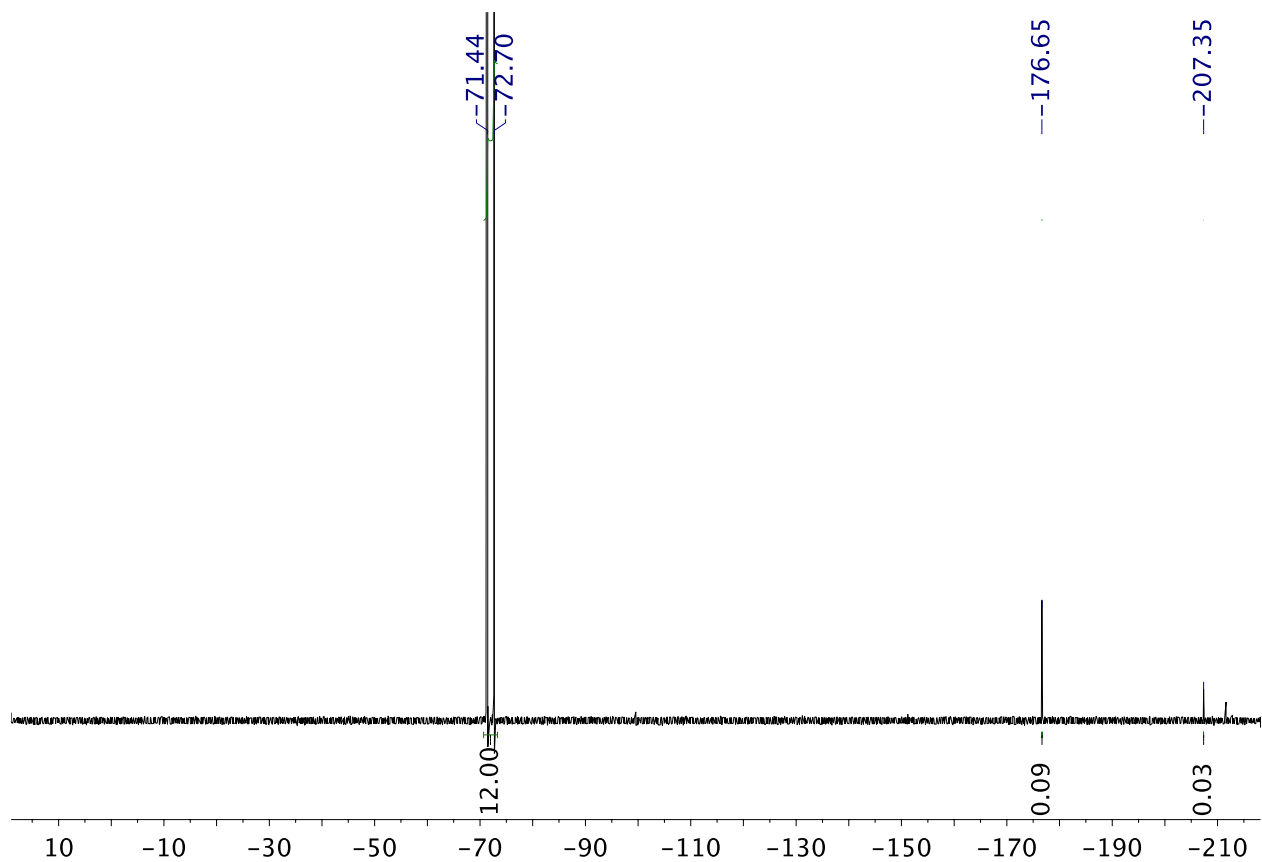
Supplementary Fig. 35. $^{19}F\{^1H\}$ NMR spectrum (565 MHz, CD_2Cl_2, 27 °C) of the reaction between **LCuF** and 1-decene, showing the formation of 3-fluorodec-1-ene (−176.7 ppm) and 1-fluorodec-2-ene (−207.4 ppm).[21]

X-ray Absorption Spectroscopy (XAS)

Cu K-edge XAS experiments were conducted on beamline 7-3 (3 GeV, 60-100 mA) at the Stanford Synchrotron Radiation Lightsource (SSRL) under standard operating conditions. Beamline 7-3 is equipped with a 20-pole, 2.0 tesla wiggler, a liquid nitrogen-cooled double-crystal Si[220] monochromator, a Rh-coated harmonic rejection mirror and a cylindrical Rh-coated bent focusing mirror with the energy cutoff set to 13 keV. A single energy was selected from the white beam with Si[220] (φ = 0) crystals and detuned by 50% at 9000 eV. A liquid He Oxford cryostat was used to maintain a sample temperature of 10 K. Samples were measured in fluorescence mode with a Canberra 30-element Ge solid state detector (liquid N_2 cooled), Ni-3 filters, Soller slits, and with simultaneous measurement of the calibration foil. The first inflection point of the copper foil was set to 8980.3 eV to calibrate each scan. Samples were assessed for radiation damage with aluminum filters added as necessary to minimize damage. One scan was collected per spot, with a minimum of 3 spots per sample, and each sample was measured in duplicate. Data were energy calibrated and normalized using Athena.[22] To prepare each sample, a Teflon Mössbauer cup with a Kapton window was deposited and set upright inside a 100 mL Schlenk flask with a septum in the 24/40 joint and a stopcock side attachment. The flask was evacuated for 10 minutes and backfilled with N_2. For the copper(II) samples, a solution of the compound in CH_2Cl_2 (typically 0.4 mL, 10 mM) was added by syringe and long steel needle at room temperature. The flask was then lowered into a liquid nitrogen bath for 5 minutes in order to freeze the liquid in the sample cup. For the copper(III) samples, a CH_2Cl_2 solution of [NAr$_3$]PF$_6$ (0.2mL, 22 mM, 1.1eq) was added to the cup at room temperature. The flask was then lowered into a dry ice acetone and allowed to cool for 20 minutes. Then, a CH_2Cl_2 solution of the copper(II) complex (0.2 mL, 20mM) was added dropwise. The mixture was allowed to sit for 15 minutes to ensure a complete reaction. The flask was then carefully transferred to a liquid nitrogen bath to freeze the sample. Samples were shipped to SSRL in a dewar shipper, secured on the sample rod at the beamline under liquid N_2, and quickly transferred to the liquid He cryostat for measurement.
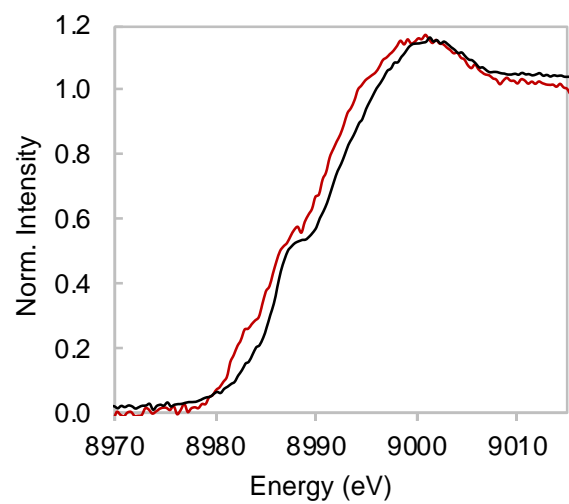
Supplementary Fig. 36. Copper K-edge X-ray absorption spectrum of [TBA]**L**Cu^{II}Cl (red trace) overlaid with **L**CuCl (black trace) in CH_2Cl_2 solution at 10 K, showing a rising edge shift of 1.4 eV.

X-Band Electron Paramagnetic Resonance (EPR)

Spectra were recorded on a Bruker EMXPlus X-band EPR spectrometer equipped with Coldedge variable temperature cryostat at 30 K. Under nitrogen atmosphere, a 1 mM solution in 3:1 toluene/acetone was prepared, of which 0.2 mL was added to a 4 mm quartz EPR tube (Wilmad Glass Company) prior to being frozen in liquid nitrogen for analysis. Spectra were simulated with the W95EPR software.[23]
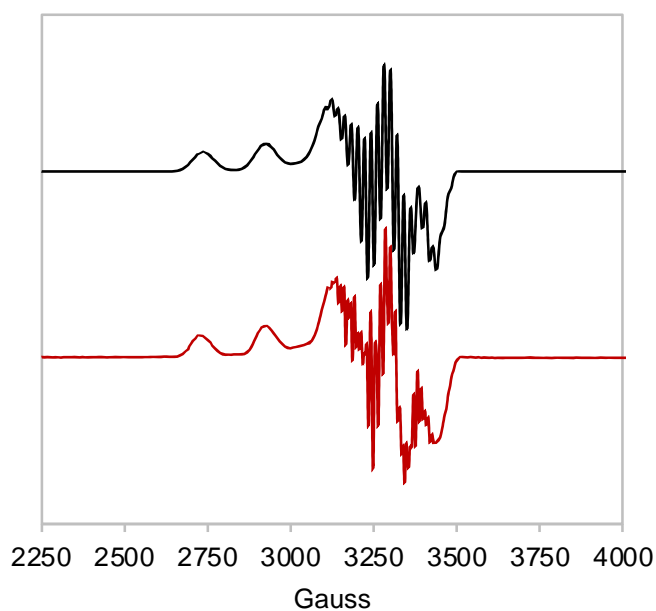
Supplementary Fig. 37. Experimental (red) and simulated (black) X-band EPR spectrum of [TBA]**L**Cu^{II}F (9.373461 GHz, Power = 0.06325 mW, ModWidth = 0.5000 mT).
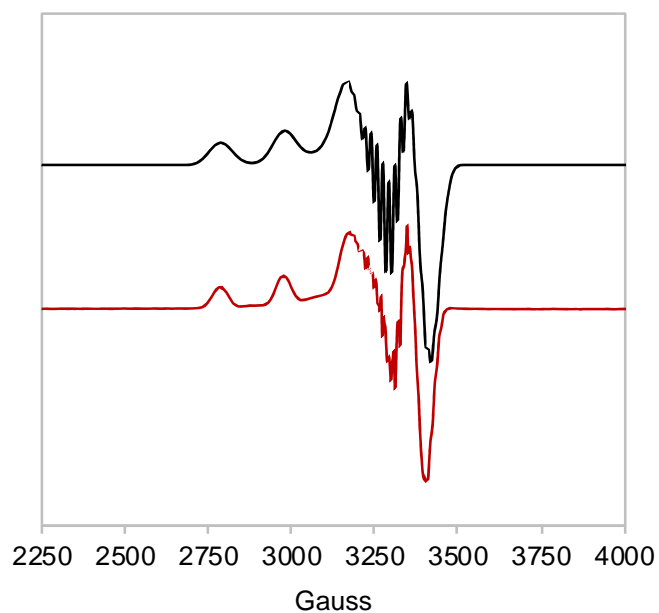
Supplementary Fig. 38. Experimental (red) and simulated (black) X-band EPR spectrum of [TBA]**L**Cu^{II}Cl (9.373939 GHz, Power = 0.06325 mW, ModWidth = 0.5000 mT).
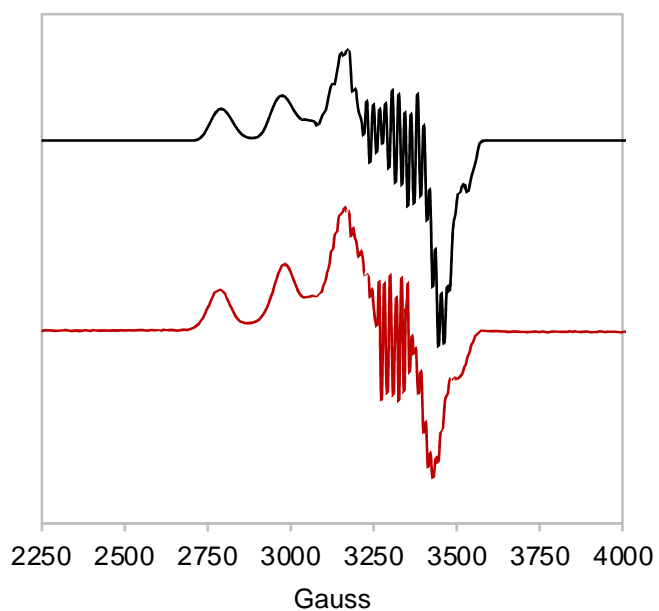
Supplementary Fig. 39. Experimental (red) and simulated (black) X-band EPR spectrum of [TBA]**L**Cu^{II}Br (9.373586 GHz, Power = 0.06325 mW, ModWidth = 0.5000 mT).

Supplementary Table 5. Simulated EPR parameters. Hyperfine couplings (A) given in MHz. Linewidths (W) given in mT.

Complex	[TBA]**L**Cu^{II}F	[TBA]**L**Cu^{II}Cl	[TBA]**L**Cu^{II}Br
g(x), g(y), g(z)	2.025, 2.080, 2.220	2.043, 2.048, 2.180	2.010, 2.030, 2.180
Cu: A(x), A(y), A(z)	170, 110, 560	160, 90, 560	150, 140, 520
N$_{py}$: A(x), A(y), A(z)	50, 50, 50	45.9, 45.9, 46	52, 68, 53
N$_{amide}$: A(x), A(y), A(z)	58, 58, 59	54.6, 54.6, 55	49, 35, 37
X: A(x), A(y), A(z)	48, 48, 48	45.9, 45.9, 46	48, 220, 50
W(x), W(y), W(z)	0.7, 0.8, 0.9	1.0, 0.8, 1.0	0.8, 0.8, 0.9

X-ray Diffraction Structures and Refinement Details

Single crystals were mounted with Paratone oil on glass fibers and immediately placed under a cold nitrogen stream (Oxford Cryosystems Cryostream) at 100(2) K or 150(2) K on either a Bruker D8 Venture instrument and a Photon II detector or a Kappa Nonius instrument and a APEX-II CCD area detector, both with Mo Kα radiation source (λ = 0.7107 Å). The data was integrated with the Bruker SAINT program. Structure solutions were performed using the SHELXTL/PC suite[24] in the Olex2 program, and were corrected for Lorentz and polarization effects. An empirical absorption correction was applied using Blessing's method as incorporated into the program SADABS.[25] Non-hydrogen atoms were refined with anisotropic thermal parameters and hydrogen atoms were included in idealized positions. All crystal structures were rendered in Olex2 using 50% probability ellipsoids. Details of solvent disorder refinement are included in the CIF files, which are available free of charge from the Cambridge Structural Database. The CHECKCIF routine reported no A- or B-level alerts for all structures except for **L**CuF. In the case of LCuF, three B- level alerts were reported that stem from the disorder of the co-crystallized fluorobenzene molecule in the unit cell.
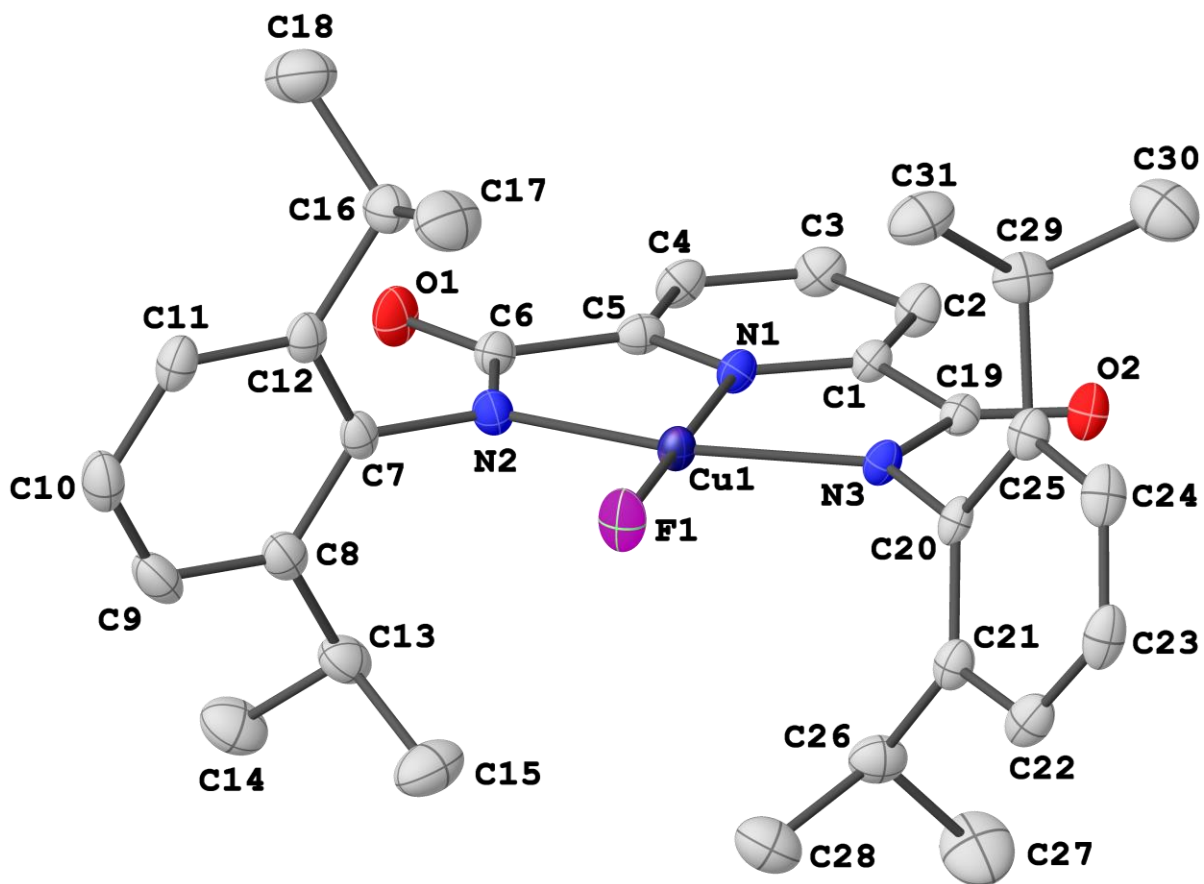
Supplementary Fig. 40. Solid-state structure of the anionic portion of [PPN]**L**Cu^{II}F with thermal ellipsoids represented at the 50% probability level. Hydrogens, the bis(triphenylphosphine)iminium cation, and co-crystallized tetrahydrofuran molecules are omitted for clarity. Selected bond distances (Å) and angles (°): Cu1-F1 1.8280(19), Cu1-N1 1.929(3), Cu1-N2 1.997(3), Cu1-N3 2.005(3), N1-Cu1-F1 178.95(11), N2-Cu1-N3 160.09(11). CCDC: 1985735
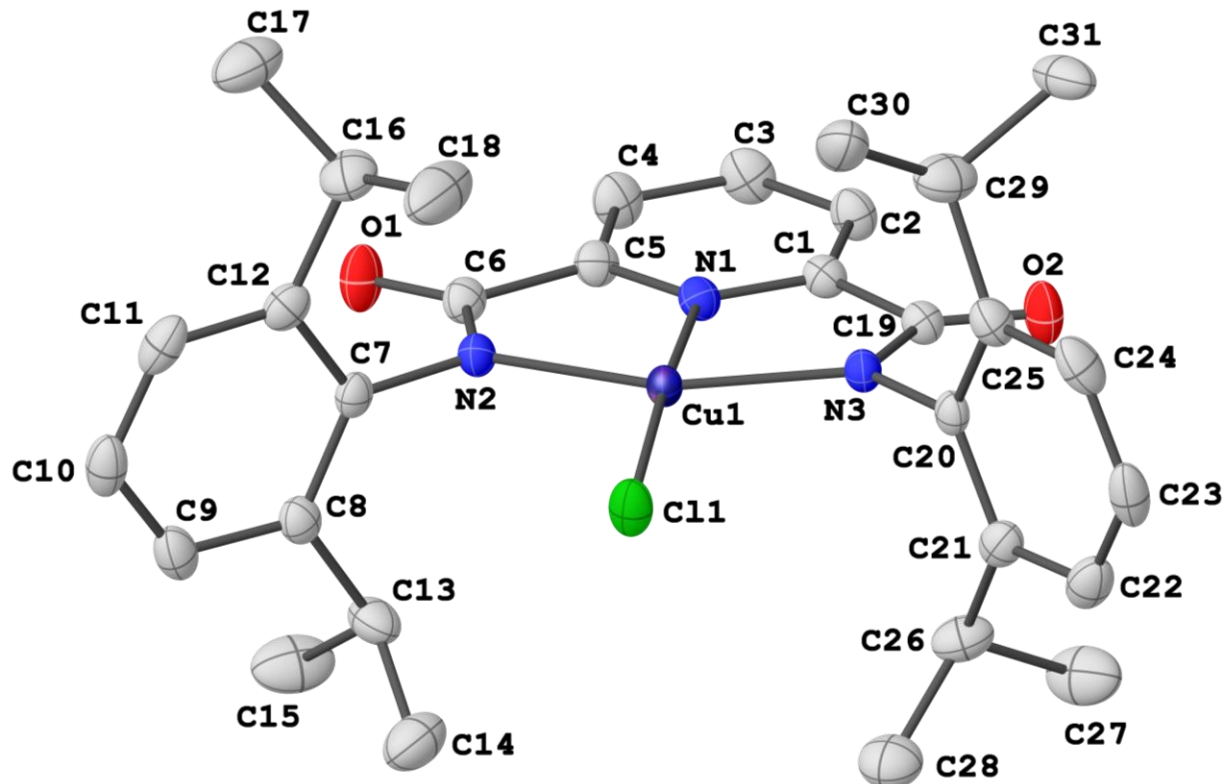
Supplementary Fig. 41. Solid-state structure of the anionic portion of [TBA]**L**Cu^{II}Cl with thermal ellipsoids represented at the 50% probability level. Hydrogens, minor components of disorder, the tetrabutylammonium cation, and co-crystallized tetrahydrofuran molecules are omitted for clarity. Selected bond distances (Å) and angles (°): Cu1-Cl1 2.2074(5), Cu1-N1 1.9439(14), Cu1-N2 2.0150(13), Cu1-N3 2.0028(13), N1-Cu1-Cl1 173.22(4), N2-Cu1-N3 158.74(6). CCDC: 1985736
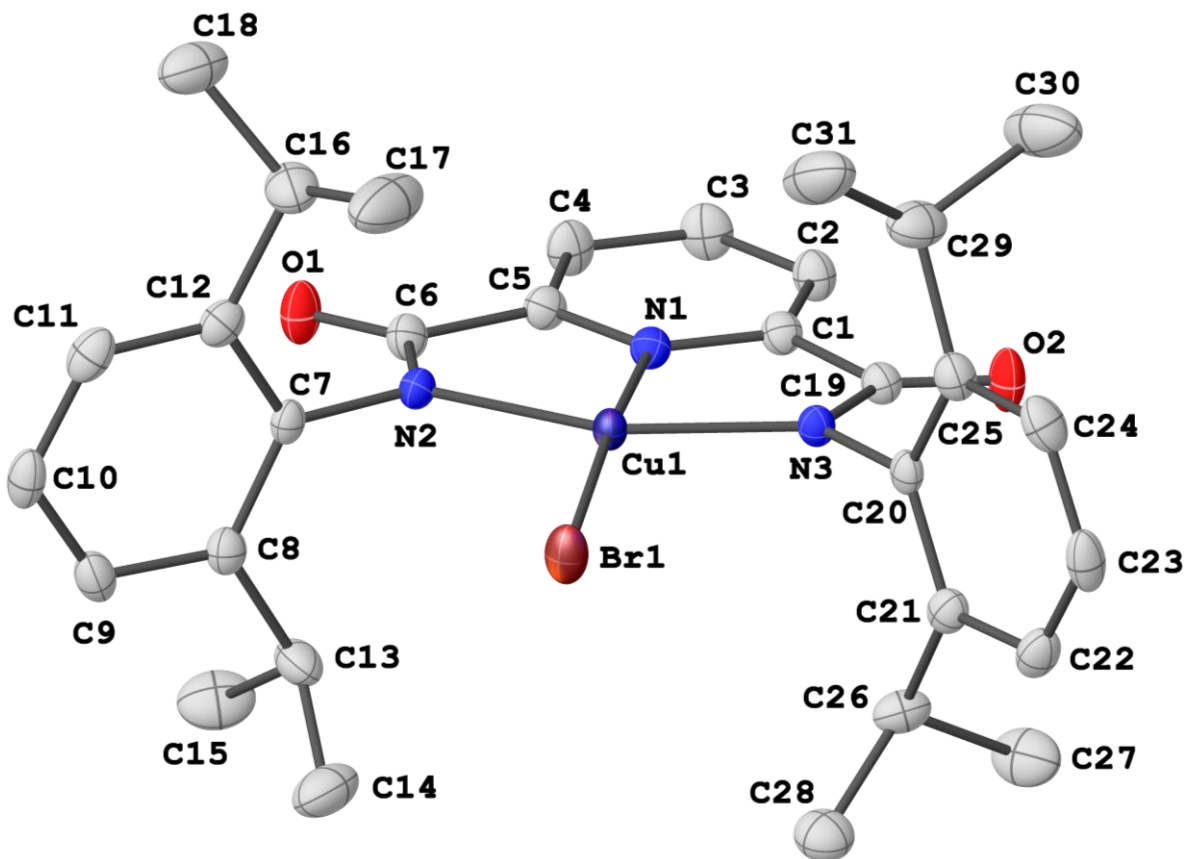
Supplementary Fig. 42. Solid-state structure of the anionic portion of [TBA]LCu^{II}Br with thermal ellipsoids represented at the 50% probability level. Hydrogens, the tetrabutylammonium cation and co-crystallized tetrahydrofuran molecules are omitted for clarity. Selected bond distances (Å) and angles (°): Cu1-Br1 2.3475(3), Cu1-N1 1.9417(17), Cu1-N2 2.0059(16), Cu1-N3 1.9969(16), N1-Cu1-Br1 172.89(5), N2-Cu1-N3 158.99(7). CCDC: 1985737
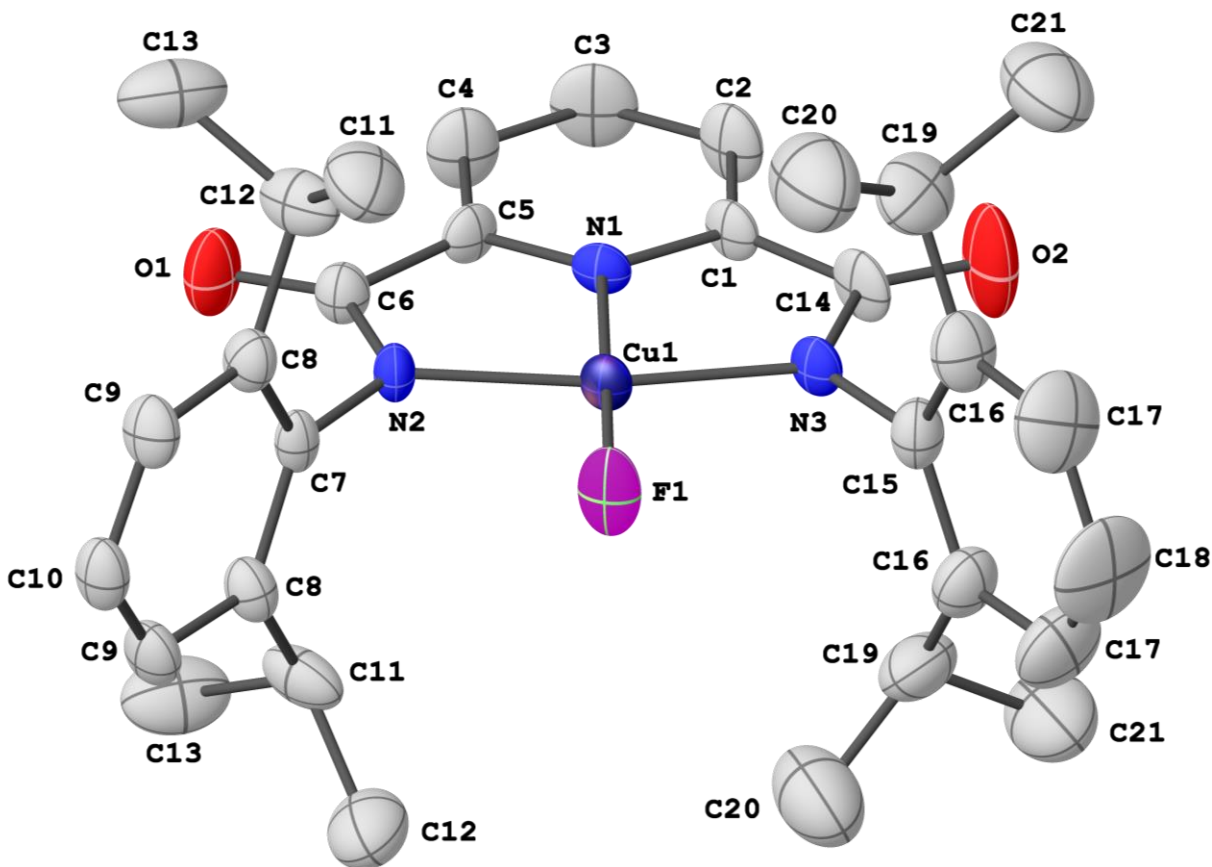
Supplementary Fig. 42. Solid-state structure of **LCuF** with thermal ellipsoids represented at the 50% probability level. Hydrogens and co-crystallized fluorobenzene molecules are omitted for clarity. Selected bond distances (Å) and angles (°): Cu1-F1 1.755(3), Cu1-N1 1.841(4), Cu1-N2 1.901(4), Cu1-N3 1.899(4), N1-Cu1-F1 179.68(17), N2-Cu1-N3 167.21(18). CCDC: 1985738
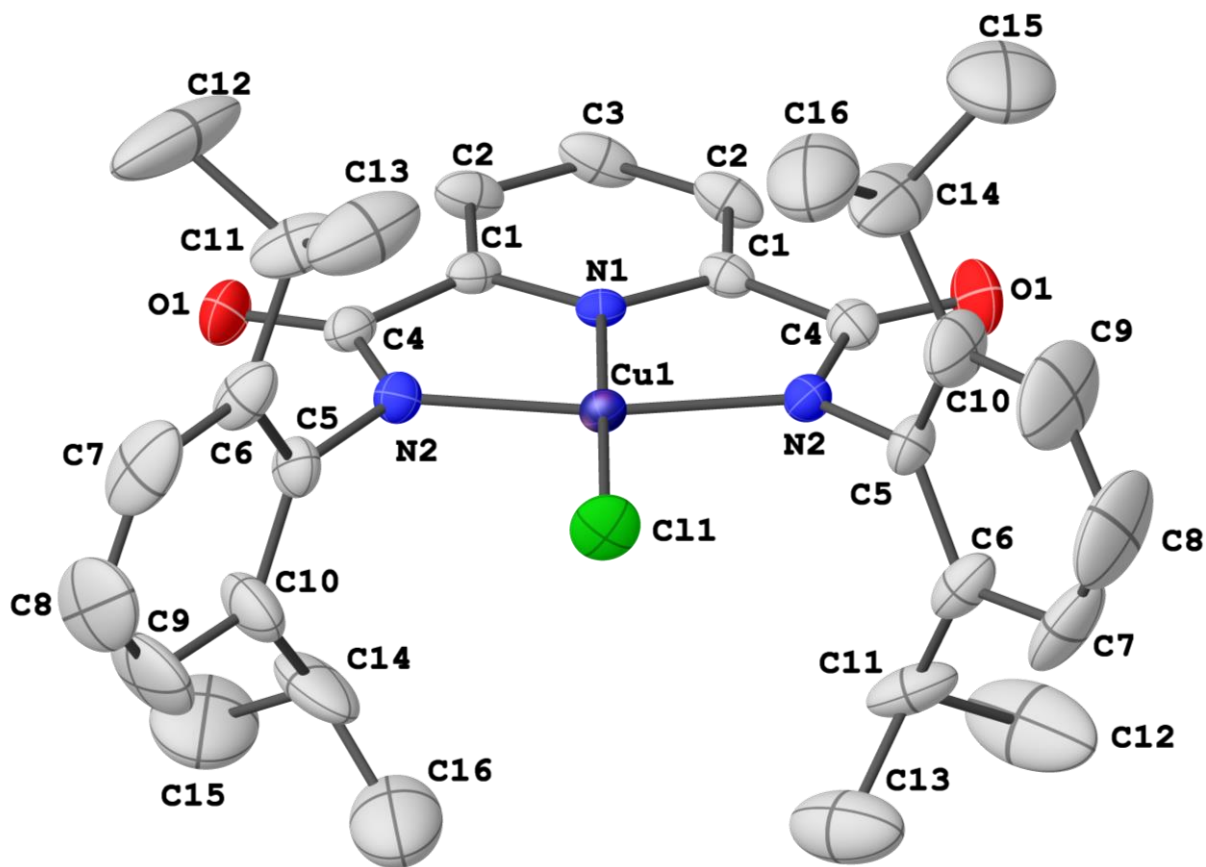
Supplementary Fig. 44. Solid-state structure of **LCuCl** with thermal ellipsoids represented at the 50% probability level. Hydrogens and co-crystallized diethyl ether molecules are omitted for clarity. Due to a crystallographic mirror plane, atoms related by symmetry are denoted in this diagram with an apostrophe. Selected bond distances (Å) and angles (°): Cu1-Cl1 2.1085(8), Cu1-N1 1.859(2), Cu1-N2/N2' 1.9132(16), N1-Cu1-Cl1 180, N2-Cu1-N2' 165.908. CCDC: 1985739
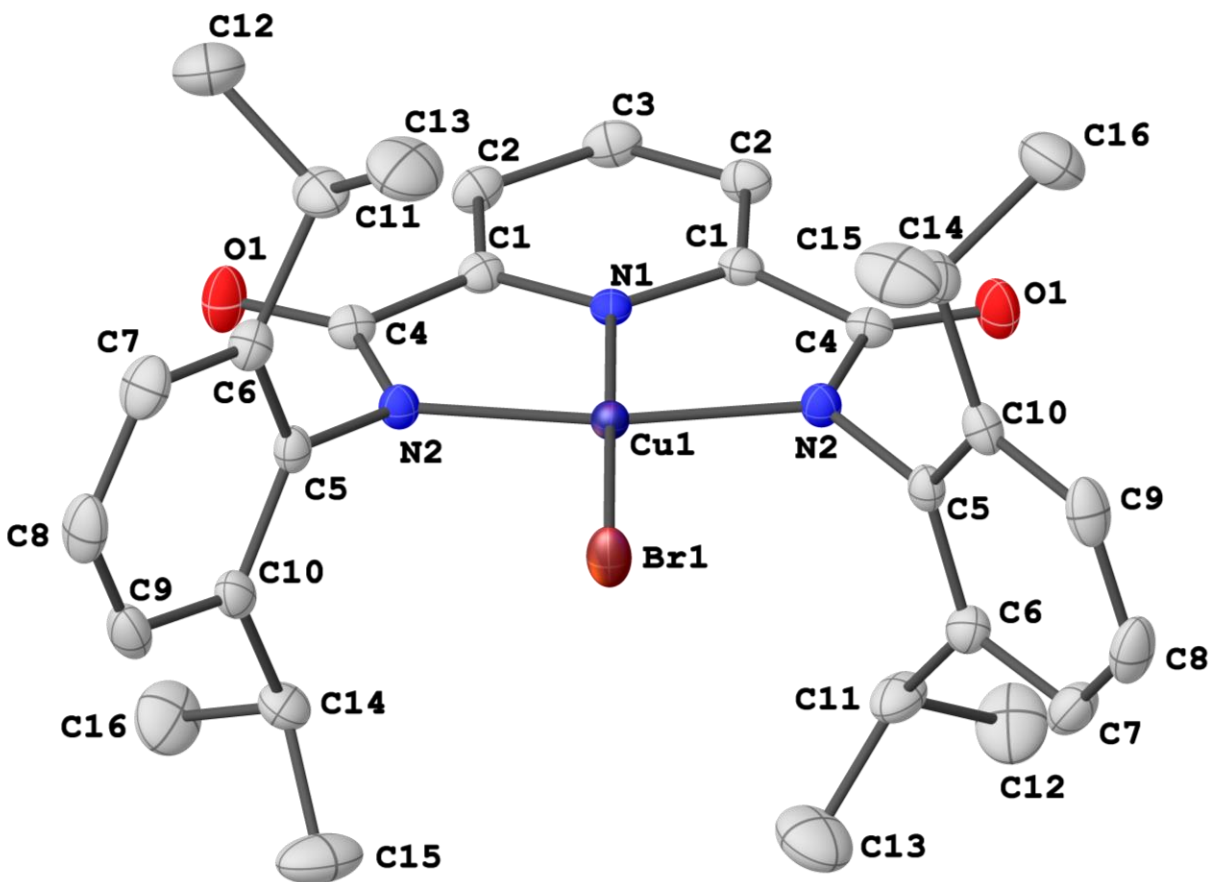
Supplementary Fig. 45. Solid-state structure of **LCuBr** with thermal ellipsoids represented at the 50% probability level. Hydrogens and co-crystallized diethyl ether molecules are omitted for clarity. Due to a crystallographic mirror plane, atoms related by symmetry are denoted in this diagram with an apostrophe. Selected bond distances (Å) and angles (°): Cu1-Br1 2.2562(4), Cu1-N1 1.8623(18), Cu1-N2/N2' 1.9159(13), N1-Cu1-Cl1 180, N2-Cu1-N2' 166.088. CCDC: 1985740

Supplementary Table 6: Crystallographic details for X-ray diffraction structures.

	[PPN]LCu^{II}F	[TBA]LCu^{II}Cl	[TBA]LCu^{II}Br	LCuF	LCuCl	LCuBr
CCDC Number	1985735	1985736	1985737	1985738	1985739	1985740
Empirical formula	$C_{67}H_{67}FCuP_2N_4O_2$	$C_{47}H_{73}ClCuN_4O_2$	$C_{47}H_{73}BrCuN_4O_2$	$C_{31}H_{37}FCuN_3O_2$	$C_{31}H_{37}ClCuN_3O_2$	$C_{31}H_{37}BrCuN_3O_2$
	$*5(C_4H_8O)$	$*2(C_4H_8O), 0.33(H_2O)$	$*2(C_4H_8O)$	$*2(C_6H_5F)$	$*2(C_4H_{10}O)$	$*2(C_4H_{10}O)$
Formula weight (g mol^{-1})	1465.24	974.87	1013.75	758.37	730.86	775.32
Color / Morphology	Blue / block	Green / block	Green / block	Dark blue / block	Violet / block	Dark blue / needle
Crystal size (mm)	0.50x0.20x0.15	0.75x0.23x0.18	0.50x0.20x0.15	0.22x0.11x0.06	0.34x0.29x0.15	0.39x0.29x0.26
Temperature (K)	100(2)	100(2)	100(2)	150(2)	100(2)	100(2)
Wavelength (Å)	0.71073	0.71073	0.71073	0.71073	0.71073	0.71073
Crystal system	Orthorhombic	Monoclinic	Monoclinic	Monoclinic	Monoclinic	Monoclinic
Space group (Z)	$P2_12_12_1$ (4)	$P2_1/c$ (4)	$P2_1/c$ (4)	$P2_1/m$ (2)	$C2/c$ (4)	$C2/c$ (4)
a (Å)	15.0248(16)	10.1912(4)	10.228(4)	9.1436(9)	19.3809(9)	19.5193(18)
b (Å)	17.643(2)	26.8069(9)	16.7001(10)	13.9372(13)	13.1487(6)	13.3270(13)
c (Å)	30.044(3)	20.4707(7)	20.4820(8)	15.6750(13)	15.3938(7)	15.3535(14)
α (°)	90	90	90	90	90	90
β (°)	90	100.862(2)	101.079(2)	97.531(4)	95.551(2)	94.521(3)
γ (°)	90	90	90	90	90	90
Volume (Å^3)	7964.1(15)	5492.3(3)	5486.4(4)	1980.3(3)	3904.5(3)	3981.5(6)
Density (calc., g cm^{-3})	1.222	1.179	1.227	1.272	1.243	1.293
Absorption coefficient (mm^{-1})	0.393	0.493	1.172	0.604	0.669	1.593
$F(000)$	3124	2112	2172	796	1560	1632
Theta range for data collection (°)	25.242	25.242	25.242	25.242	25.242	25.242
Index ranges	$-18 \leq h \leq 18$	$-12 \leq h \leq 12$	$-12 \leq h \leq 12$	$-11 \leq h \leq 11$	$-24 \leq h \leq 24$	$-24 \leq h \leq 24$
	$-22 \leq k \leq 22$	$-33 \leq k \leq 33$	$-33 \leq k \leq 33$	$-16 \leq k \leq 16$	$-16 \leq k \leq 16$	$-16 \leq k \leq 16$
	$-37 \leq l \leq 37$	$-25 \leq l \leq 25$	$-25 \leq l \leq 25$	$-18 \leq l \leq 18$	$-19 \leq l \leq 19$	$-19 \leq l \leq 19$
Reflections	97748	155019	115502	43052	64529	33300
C-C Bond precision (Å)	0.0058	0.0030	0.0036	0.0082	0.0042	0.0026
Completeness to θ_{max}	0.999	1.00	1.00	0.997	1.00	1.00
Goodness-of-fit	1.031	1.036	1.054	1.057	1.042	1.041
Largest diff. peak and hole ($e \cdot$ Å^{-3})	0.386 and −0.334	0.488 and −0.343	0.781 and −0.351	0.392 and −0.304	0.480 and −0.317	0.793 and −0.380
R_1, wR_2* [I >2σ(I)]	0.0396, 0.1030	0.0371, 0.0980	0.0366, 0.0989	0.0474, 0.0992	0.0370, 0.0978	0.0244, 0.0663

Computational Details

All computations were performed in parallel on 16 processors using the ORCA[26] program and structures were visualized in the ChemCraft program. DFT geometry optimizations were performed on a truncated model of LCuX complexes in which the (2,6)-diisopropylphenyl group is replaced with (2,6)-dimethylphenyl, denoted as ^{Me}**LCuX**, to enhance computational expediency. These optimizations were carried out using the B3LYP method[27,28] with the def2-TZVP(-f) basis set and the ZORA relativistic correction.[29] Energy minima were confirmed by a vibrational frequency calculation, and no imaginary frequencies were observed. Time-dependent density functional (TD-DFT) calculations for the UV-vis spectra of **LCuX** complexes utilized the truncated DFT optimized structures and calculated 50 roots. All DFT calculations were performed using very tight convergence thresholds for the energy (10^{-9} E_h).
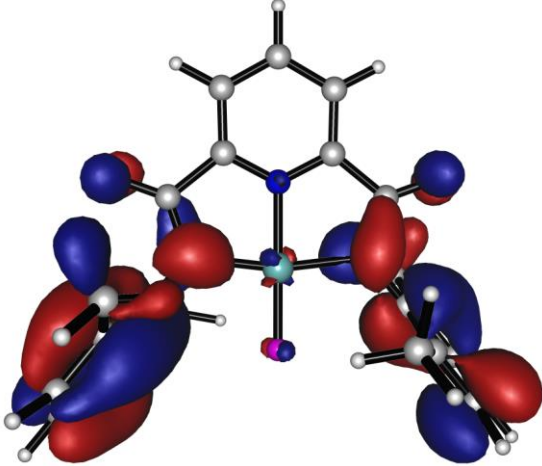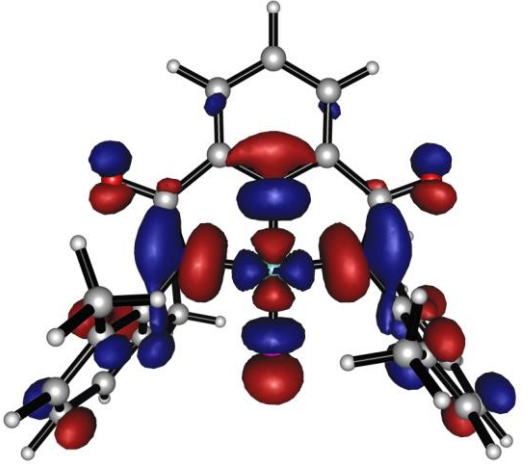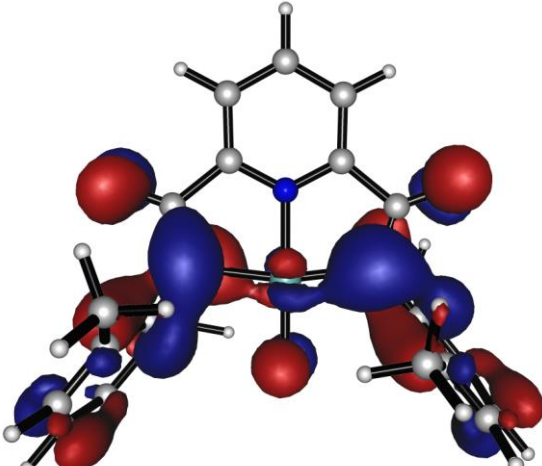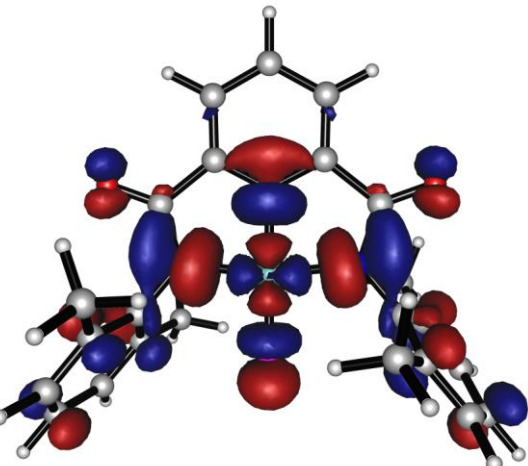
To investigate the multireference character of **LCuX** complexes, computations were performed using the complete active space self-consistent field (CASSCF) method[30,31]. The basis set on N, Cu, and X was def2-TZVP(-f), while all other atoms were calculated with def2-SVP. The keyword ZORA was included to account for relativistic effects. For CASSCF calculations, truncated crystallographic coordinates were utilized for **LCuF**, **LCuCl**, and **LCuBr** in which the isopropyl groups were replaced with hydrogens, and all hydrogens were then optimized with the B3LYP functional (denoted as ^{H}**LCuX**). Input orbitals for CASSCF were calculated from a quasi-restricted B3LYP calculation. Regardless of the size and composition of the input active space, the CASSCF output indicated that the only orbitals that participated in the active space were the σ_B HOMO and σ^* LUMO. A state-specific CASSCF calculation of one singlet root with a (2 electrons, 2 orbitals) active space was performed. The orbitals were localized with an IBO-BOYS localization procedure, and the CAS wavefunction was recalculated with the same parameters.[32]

According to the protocol outlined by Lancaster et al.,[33] full crystallographic coordinates of **LCuX** complexes were used to calculate DFT orbitals that were benchmarked to reflect experimental Cu L^{2,3} edge spectroscopic data in order to determine the contribution of Cu 3d character in the LUMO. For these calculations, the CP(PPP) basis set[34] with special integration accuracy was used on copper while scalar relativistically recontracted basis set ZORA-def2-TZVP(-f) was used on all other atoms. To finish, a subsequent natural bond orbital (NBO) calculation was performed to obtain natural population analysis (NPA) results.[35,36] An identical procedure was performed for the copper(II) complexes, [**LCu^{II}X**]$^-$, using hydrogen-optimized crystallographic coordinates to obtain comparable NBO results.
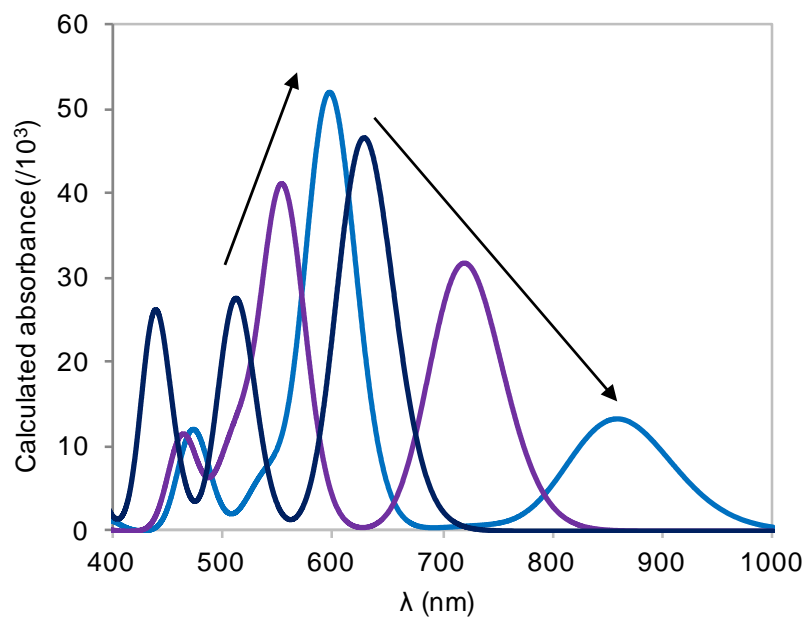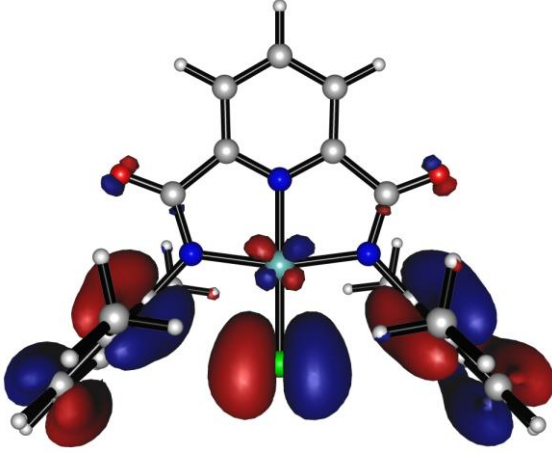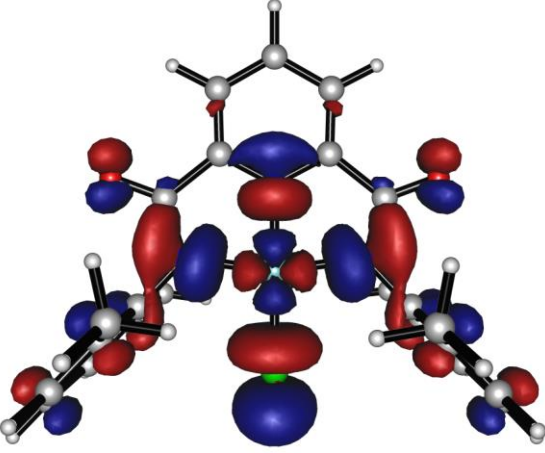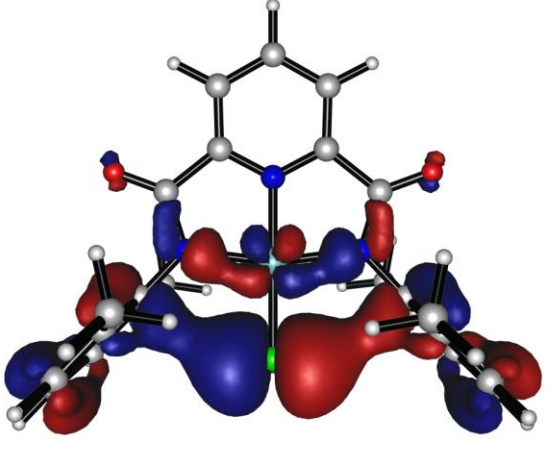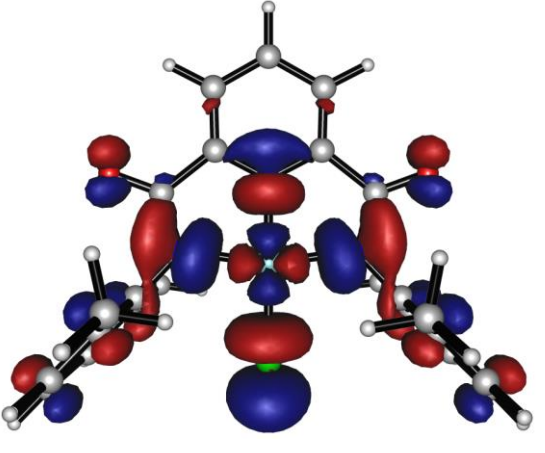
Supplementary Fig. 46. TD-DFT calculated absorption spectra of ^{Me}**L**CuF (dark blue), ^{Me}**L**CuCl (purple trace), and ^{Me}**L**CuBr (light blue trace). Arrows included as visual cues to illustrate decreasing intensity in the low-energy peak and increasing intensity of the high-energy peak across the series from **L**CuF to **L**CuCl to **L**CuBr.
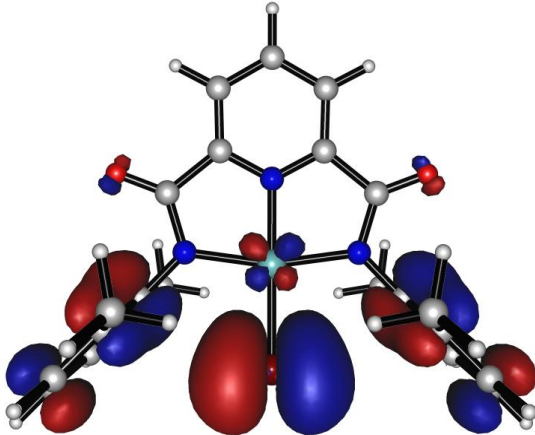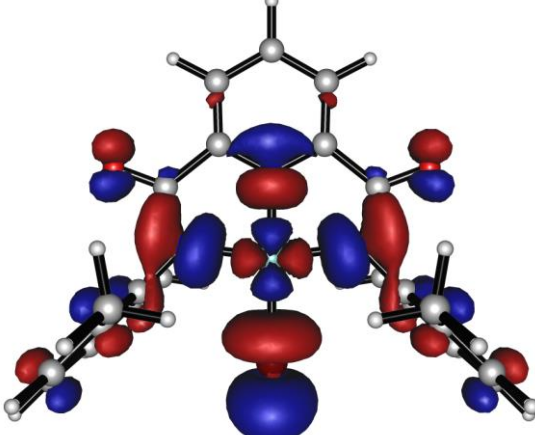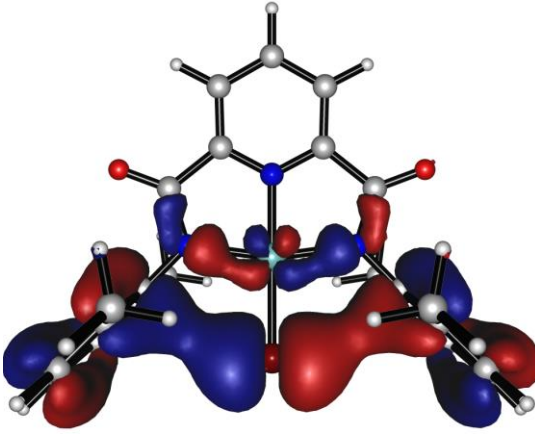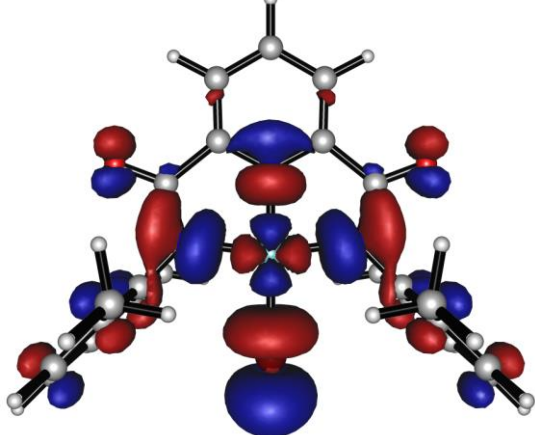
Supplementary Table 7. Highest intensity TD-DFT transitions for ^{Me}**L**CuF. Orbitals plotted at a 0.03 isosurface value.

Transition (nm)	Donor Orbital	Acceptor Orbital
624		
512		

Supplementary Table 8. Highest intensity TD-DFT transitions for ^MeLCuCl. Orbitals plotted at a 0.03 isosurface value.

Transition (nm)	Donor Orbital	Acceptor Orbital
720		
554		

Supplementary Table 9. Highest intensity TD-DFT transitions for ^{Me}**L**CuBr. Orbitals plotted at a 0.03 isosurface value.

Transition (nm)	Donor Orbital	Acceptor Orbital
858		
597		

HOMO   LUMO
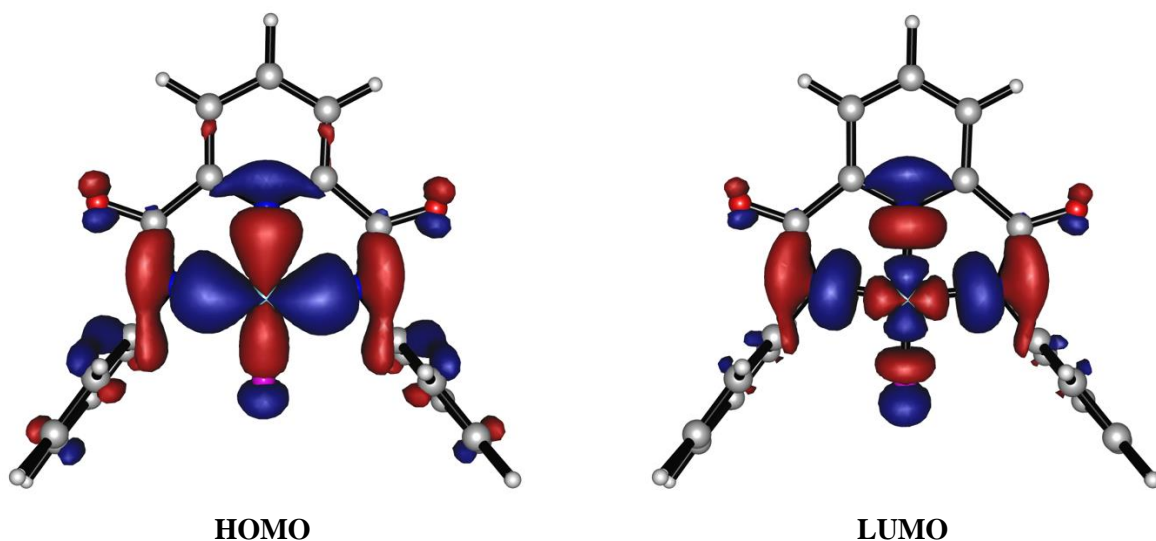
Supplementary Fig. 47. CASSCF(2, 2) orbitals of **L**CuF before the localization procedure. Orbitals were plotted with an isosurface value of 0.03. The orbitals of **L**CuF after the localization are shown in Fig. 3b.

Supplementary Table 10. Parameters obtained from the state-specific CASSCF calculations of (2 electrons, 2 orbitals) active space before localization. The percentages of orbital contributions were obtained from Loewdin orbital analysis. The electronic configuration [2 0] denotes two electrons occupying the HOMO, while [0 2] denotes two electrons occupying the LUMO.

	[H]**LCuF**	[H]**LCuCl**	[H]**LCuBr**
[2 0] (%)	92.3	91.4	90.5
[0 2] (%)	7.7	8.6	9.5
HOMO population	1.84503	1.82791	1.81084
LUMO population	0.15497	0.17209	0.18916
HOMO % Cu	49.9	54.6	55.7
HOMO % X	2.6	8.6	14.0
HOMO % L	47.5	36.8	30.3
LUMO % Cu	57.8	56.1	55.1
LUMO % X	4.4	9.1	13.0
LUMO % L	37.8	34.8	31.9

Supplementary Table 11. Parameters obtained from Natural Bond Orbital calculations of [LCu^{II}X]$^-$ and LCuX complexes. NAO – Natural Orbital; NPA – Natural Population Analysis.

	[**LCuF**]$^-$	[**LCuCl**]$^-$	[**LCuBr**]$^-$	^{Me}**LCuF**	^{Me}**LCuCl**	^{Me}**LCuBr**
NPA Cu 3d electrons	9.29	9.35	9.36	9.26	9.33	9.35
NPA X valence electrons	7.72	7.75	7.49	7.70	7.55	7.49
NAO charge Cu	1.35	1.25	1.23	1.39	1.26	1.23
NAO charge X	−0.82	−0.75	−0.73	−0.71	−0.59	−0.50
NAO charge L	−0.53	−0.50	−0.50	−0.68	−0.67	−0.73

Supplementary Table 12. Singlet-triplet gaps calculated with DFT for the optimized truncated ^{Me}LCuX structures.

Compound	Singlet triplet gap (kcal mol^{-1})
LCuF	21.1
LCuCl	17.3
LCuBr	10.7

Benchmarked calculations of LUMO % Cu 3d character
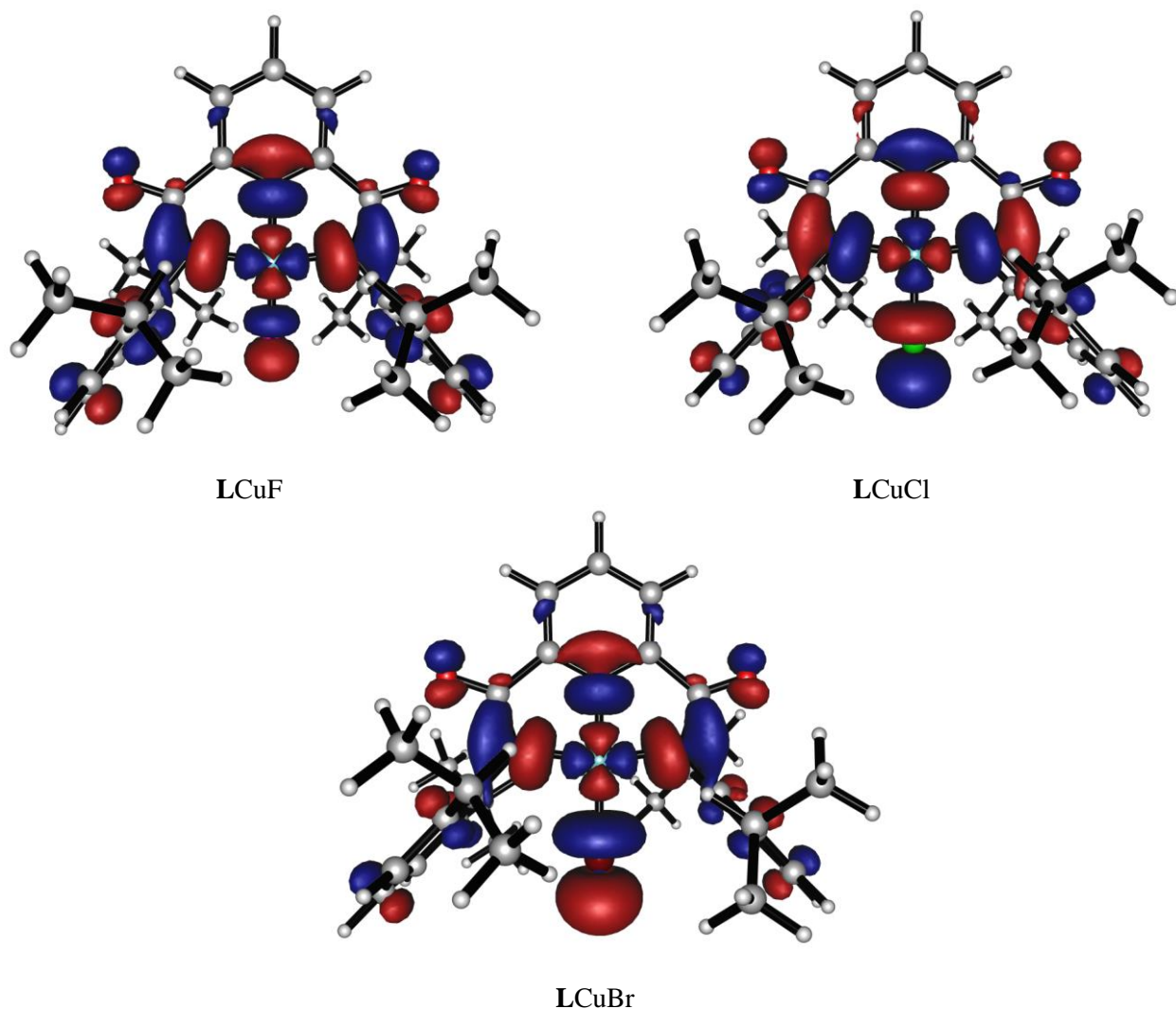
LCuF

LCuCl

LCuBr

Supplementary Fig. 48. Lowest unoccupied molecular orbitals (LUMOs) (alpha spin) of **L**CuF, **L**CuCl, and **L**CuBr from the experimentally benchmarked computational procedure by Lancaster et al. to reflect the Cu $L^{2,3}$ edge spectra. Orbitals were plotted with an isosurface value of 0.03.

Supplementary Table 13. LUMO compositions from Löewdin population analysis based on the computational procedure by Lancaster et al.

Compound	LUMO % Cu 3d	LUMO % X	LUMO % L
LCuF	37.5	7.8	54.7
LCuCl	35.2	12.8	52.0
LCuBr	33.9	15.1	51.0

Cartesian coordinates of complexes used in computations

Complex – Level of theory optimized (Calculations used for)
Charge, spin multiplicity

^{Me}**L**CuF – B3LYP/def2-TZVPP (TD-DFT/DFT/NBO)
0, 1

29	4.563168000	15.792000000	15.369021000
8	1.736821000	18.597916000	15.085920000
8	4.329874000	12.800386000	18.002775000
9	5.961051000	15.880155000	14.294674000
7	3.100256000	15.703176000	16.493022000
7	3.697564000	17.404530000	14.736756000
7	5.075256000	14.158174000	16.273136000
6	3.040311000	14.692424000	17.350099000
6	4.187998000	18.165227000	13.659065000
6	2.500060000	17.676313000	15.325113000
6	4.223679000	13.762040000	17.259071000
6	2.182381000	16.655246000	16.388551000
6	5.272088000	19.038399000	13.876403000
6	1.070724000	16.618470000	17.213569000
1	0.320740000	17.391692000	17.120783000
6	3.614490000	18.021424000	12.379549000
6	1.960196000	14.597338000	18.211532000
1	1.917898000	13.776565000	18.914018000
6	5.905769000	19.162327000	15.232491000
1	5.164464000	19.379135000	16.004452000
6	0.969747000	15.575081000	18.132470000
1	0.112681000	15.523605000	18.791955000
6	6.295680000	13.498883000	16.034947000
6	6.426778000	12.699297000	14.882509000
6	4.123445000	18.786434000	11.336566000
1	3.686729000	18.691476000	10.349667000
6	5.749515000	19.782566000	12.803614000
1	6.578444000	20.462370000	12.959277000
6	2.469234000	17.078356000	12.141345000
1	2.703874000	16.068928000	12.487269000
6	7.372115000	13.669607000	16.928657000
6	5.182569000	19.660801000	11.542440000
1	5.568631000	20.246056000	10.716932000
6	5.290264000	12.548716000	13.912124000
1	5.086728000	13.498237000	13.410989000
6	7.240466000	14.535521000	18.149521000
1	6.891800000	15.538537000	17.892541000

1	2.232660000	17.023577000	11.078995000
6	7.637044000	12.053230000	14.657832000
1	7.748115000	11.430037000	13.778752000
1	1.572603000	17.408864000	12.671295000
6	8.563246000	13.003478000	16.664710000
1	9.395997000	13.119568000	17.347926000
6	8.699022000	12.201021000	15.539438000
1	9.635881000	11.692410000	15.348043000
1	4.372788000	12.233477000	14.413422000
1	6.525782000	14.108868000	18.857483000
1	5.532546000	11.809365000	13.148902000
1	8.200618000	14.632203000	18.655778000
1	6.647069000	19.961264000	15.238284000
1	6.409081000	18.231721000	15.505836000

^{Me}**L**CuCl – B3LYP/def2-TZVPP (TD-DFT/DFT/NBO)

0, 1

29	4.494348000	15.786065000	15.420120000
8	1.677611000	18.637174000	15.230412000
8	4.177639000	12.749236000	18.023350000
17	6.196138000	15.888701000	14.115405000
7	3.012597000	15.697420000	16.559748000
7	3.602415000	17.417803000	14.801827000
7	4.985571000	14.129228000	16.344626000
6	2.939374000	14.680554000	17.405682000
6	4.067045000	18.281753000	13.787793000
6	2.424739000	17.693145000	15.430894000
6	4.102189000	13.732399000	17.304093000
6	2.102829000	16.656343000	16.471650000
6	4.921184000	19.347781000	14.127094000
6	0.992823000	16.625101000	17.299541000
1	0.255846000	17.412060000	17.218996000
6	3.672145000	18.059516000	12.455225000
6	1.858653000	14.582356000	18.266373000
1	1.809110000	13.749184000	18.953611000
6	5.350685000	19.569043000	15.549332000
1	4.491264000	19.726220000	16.205237000
6	0.879022000	15.571428000	18.204325000
1	0.022554000	15.520964000	18.864569000
6	6.147175000	13.363400000	16.110450000
6	6.119009000	12.346718000	15.137485000
6	4.130405000	18.931599000	11.474431000
1	3.830088000	18.775785000	10.445316000
6	5.356237000	20.195784000	13.115035000

1	6.009705000	21.023644000	13.362365000
6	2.770489000	16.912056000	12.099013000
1	3.218573000	15.956444000	12.381541000
6	7.314016000	13.632376000	16.850247000
6	4.966951000	19.991845000	11.797782000
1	5.317503000	20.660101000	11.020934000
6	4.875111000	12.076456000	14.339977000
1	4.588179000	12.952114000	13.752582000
6	7.340682000	14.727809000	17.877787000
1	7.112872000	15.696614000	17.426836000
1	2.580241000	16.891749000	11.026198000
6	7.269593000	11.593787000	14.932664000
1	7.260444000	10.804197000	14.191040000
1	1.808373000	16.989253000	12.611093000
6	8.442287000	12.855645000	16.613305000
1	9.345755000	13.048167000	17.179199000
6	8.424390000	11.844033000	15.662068000
1	9.313123000	11.250119000	15.487819000
1	4.032743000	11.824239000	14.988150000
1	6.606002000	14.549987000	18.666705000
1	5.032503000	11.245647000	13.652544000
1	8.324159000	14.794590000	18.342385000
1	5.996430000	20.443680000	15.623977000
1	5.902923000	18.706798000	15.930886000

^{Me}**L**CuBr – B3LYP/def2-TZVPP (TD-DFT/DFT/NBO)

0, 1

29	4.512832000	15.782428000	15.395843000
8	1.695279000	18.638895000	15.224657000
8	4.183025000	12.743879000	18.001202000
35	6.318341000	15.874651000	13.982604000
7	3.026084000	15.694799000	16.542286000
7	3.616265000	17.419144000	14.781611000
7	5.005286000	14.126245000	16.331768000
6	2.951080000	14.677276000	17.385834000
6	4.063383000	18.307433000	13.777692000
6	2.440529000	17.691877000	15.418416000
6	4.112572000	13.729403000	17.284546000
6	2.117161000	16.653345000	16.455280000
6	4.895343000	19.385952000	14.131197000
6	1.006188000	16.622243000	17.282198000
1	0.270387000	17.410407000	17.202764000
6	3.663485000	18.101845000	12.444251000
6	1.869353000	14.576982000	18.245310000

1	1.818643000	13.741998000	18.930256000
6	5.323750000	19.595535000	15.555620000
1	4.462775000	19.737706000	16.213054000
6	0.890434000	15.566772000	18.184562000
1	0.033236000	15.515492000	18.843805000
6	6.158920000	13.338924000	16.116793000
6	6.115274000	12.290130000	15.179486000
6	4.099054000	18.999653000	11.476083000
1	3.794948000	18.855998000	10.446298000
6	5.308022000	20.259723000	13.131588000
1	5.945018000	21.096932000	13.390271000
6	2.780327000	16.944884000	12.072964000
1	3.250164000	15.992284000	12.329443000
6	7.328800000	13.613807000	16.848978000
6	4.916367000	20.070488000	11.812870000
1	5.249034000	20.759012000	11.045926000
6	4.865870000	12.007653000	14.394907000
1	4.578270000	12.870651000	13.789352000
6	7.371564000	14.740286000	17.841818000
1	7.173744000	15.699780000	17.357576000
1	2.578053000	16.944370000	11.002136000
6	7.255471000	11.515296000	14.998732000
1	7.234386000	10.701657000	14.283792000
1	1.822956000	16.991653000	12.597372000
6	8.446370000	12.814299000	16.637057000
1	9.352197000	13.011933000	17.197420000
6	8.414400000	11.773163000	15.718802000
1	9.294692000	11.161609000	15.563803000
1	4.026680000	11.773490000	15.053989000
1	6.623719000	14.607474000	18.627075000
1	5.015721000	11.160512000	13.725961000
1	8.351238000	14.797287000	18.315717000
1	5.960752000	20.475731000	15.639581000
1	5.884300000	18.735120000	15.929172000

^{H}**LCuF** – B3LYP/def2-SVP [C, H, O]/def2-TZVP(-f) [Cu, N, F] (CASSCF)

0, 1

6	1.383008000	9.226000000	12.709135000
6	1.911009000	9.215000000	6.350218000
1	1.831098000	8.289339000	12.384332000
6	0.881152000	9.251000000	5.442055000
1	0.462149000	8.312957000	5.073860000
1	2.332909000	8.283077000	6.720463000
6	0.246882000	9.267000000	13.512956000

1	-0.209926000	8.328710000	13.830854000
29	3.070491000	10.453000000	9.639400000
9	1.322515000	10.453000000	9.487125000
8	4.631919000	10.453000000	13.278646000
8	5.250010000	10.453000000	6.345743000
7	3.449784000	10.453000000	7.778460000
7	3.113192000	10.453000000	11.539407000
7	4.904465000	10.453000000	9.808689000
6	4.365105000	10.453000000	12.092604000
6	1.957067000	10.453000000	12.333225000
6	1.383008000	11.680000000	12.709135000
6	1.911009000	11.691000000	6.350218000
6	-0.290182000	10.453000000	13.919871000
1	-1.175321000	10.453000000	14.556568000
6	5.594642000	10.453000000	8.684797000
6	5.396273000	10.453000000	11.025766000
1	1.831098000	12.616661000	12.384332000
6	6.771249000	10.453000000	11.180982000
1	7.201294000	10.453000000	12.180010000
6	7.001625000	10.453000000	8.790019000
1	7.615418000	10.453000000	7.892785000
6	7.529426000	10.453000000	10.057102000
1	8.615008000	10.453000000	10.160151000
6	4.776834000	10.453000000	7.464669000
6	0.881152000	11.655000000	5.442055000
1	0.462148000	12.593043000	5.073861000
6	0.330221000	10.453000000	5.001969000
1	-0.499021000	10.453000000	4.296369000
1	2.332909000	12.622923000	6.720464000
6	2.425938000	10.453000000	6.803299000
6	0.246882000	11.639000000	13.512956000
1	-0.209926000	12.577290000	13.830854000

<u>HLCuCl – B3LYP/def2-SVP [C, H, O]/def2-TZVP(-f) [Cu, N, Cl] (CASSCF)</u>

0, 1

8	12.634278000	5.232958000	2.785902000
7	11.140341000	6.910924000	3.311188000
6	11.544386000	5.621932000	3.166236000
6	10.446587000	4.669904000	3.525774000
6	12.014123000	7.959932000	2.925716000
6	10.477693000	3.286906000	3.529971000
1	11.407898000	2.784983000	3.269661000
6	12.804425000	8.588137000	3.895337000
1	12.749263000	8.282058000	4.936936000

6	12.036611000	8.356732000	1.585648000
6	13.662190000	9.602135000	3.454876000
1	14.303308000	10.104682000	4.180132000
1	11.390510000	7.864664000	0.862584000
6	13.709686000	9.974941000	2.131803000
1	14.388070000	10.770289000	1.822680000
6	12.906403000	9.374743000	1.222182000
1	12.940977000	9.688820000	0.177769000
29	9.317515000	7.144866000	3.843809000
17	9.317356000	9.253866000	3.843493000
8	6.001040000	5.232775000	4.903290000
7	9.317655000	5.285866000	3.844088000
7	7.495724000	6.910809000	4.377500000
6	7.091874000	5.621800000	4.522839000
6	8.188816000	4.669829000	4.163587000
6	9.317857000	2.603866000	3.844491000
1	9.317761000	1.514183000	3.844379000
6	6.620784000	7.959800000	4.761658000
6	8.158919000	3.286826000	4.159805000
1	7.228932000	2.784670000	4.420547000
6	5.831387000	8.587596000	3.792847000
1	5.886481000	8.281719000	2.751343000
6	6.598236000	8.357000000	6.102606000
6	4.973469000	9.601597000	4.233004000
1	4.332527000	10.104065000	3.507557000
1	7.244296000	7.864842000	6.825622000
6	4.925917000	9.974792000	5.555965000
1	4.247447000	10.770326000	5.864477000
6	5.728290000	9.374989000	6.465767000
1	5.693531000	9.689237000	7.510127000

^H**L**CuBr – B3LYP/def2-SVP[C, H, O]/def2-TZVP(-f) [Cu, N, Br] (CASSCF)

0, 1

8	12.196220000	7.894342000	10.497985000
7	10.687196000	6.210344000	10.978914000
6	11.099206000	7.508344000	10.852940000
6	9.989197000	8.462345000	11.197907000
6	11.549209000	5.177345000	10.515937000
6	12.340171000	4.470334000	11.437960000
6	10.029202000	9.846345000	11.196921000
1	10.967116000	10.346359000	10.963139000
6	11.553258000	4.869357000	9.141934000
6	13.189186000	3.480334000	10.942983000
1	13.826242000	2.925570000	11.632182000

6	13.223235000	3.188346000	9.589982000
1	13.889988000	2.407824000	9.223787000
1	12.288012000	4.714419000	12.495987000
6	12.413271000	3.870357000	8.699958000
1	12.445476000	3.619539000	7.639280000
1	10.906854000	5.418184000	8.461124000
35	8.852167000	3.722348000	11.478824000
29	8.852176000	5.978348000	11.478843000
8	5.508147000	7.894353000	12.459735000
7	7.017158000	6.210351000	11.978777000
7	8.852184000	7.841348000	11.478860000
6	6.605159000	7.508351000	12.104773000
6	7.715176000	8.462350000	11.759823000
6	6.155137000	5.177350000	12.442736000
6	5.364168000	4.470362000	11.519700000
6	7.675181000	9.846350000	11.760833000
1	6.737263000	10.346366000	11.994588000
6	8.852195000	10.534348000	11.478883000
1	8.852201000	11.623938000	11.478895000
6	6.150084000	4.869338000	13.816733000
6	4.515146000	3.480361000	12.014660000
1	3.878007000	2.925430000	11.325671000
6	4.481094000	3.188349000	13.368656000
1	3.814488000	2.407718000	13.734814000
1	5.416846000	4.714585000	10.461753000
6	5.291064000	3.870338000	14.257692000
1	5.258887000	3.619485000	15.318411000
1	6.796123000	5.418207000	14.497872000

LCuF – B3LYP/def2-TZVPP (Procedure according to Lancaster et al.)

0, 1

6	0.960634000	9.226002000	12.692248000
6	1.489921000	9.214977000	6.333438000
6	1.557775000	7.906997000	12.277467000
1	2.333363000	8.106081000	11.538622000
6	0.533002000	6.985001000	11.628102000
1	-0.222504000	6.653593000	12.343724000
1	1.028499000	6.093384000	11.235553000
1	0.018933000	7.478045000	10.801140000
6	0.460248000	9.250981000	5.425067000
1	0.040355000	8.321839000	5.055973000
6	2.052744000	7.916975000	6.802645000
1	2.901209000	8.134406000	7.450980000
6	2.215343000	7.226997000	13.464706000

1	2.965088000	7.868985000	13.930557000
1	2.711780000	6.305248000	13.148180000
1	1.476488000	6.963010000	14.225482000
6	-0.175655000	9.267012000	13.495839000
1	-0.634896000	8.338605000	13.813977000
6	2.586153000	7.081968000	5.650840000
1	1.788204000	6.762083000	4.975897000
1	3.074221000	6.181380000	6.032987000
1	3.320141000	7.637400000	5.063029000
6	1.044443000	7.161984000	7.626285000
1	0.665148000	7.772635000	8.447568000
1	1.491815000	6.260776000	8.055042000
1	0.188966000	6.849133000	7.020743000
29	2.648746000	10.452981000	9.622851000
9	0.900801000	10.452992000	9.470222000
8	4.209437000	10.452983000	13.262412000
8	4.828930000	10.452956000	6.329635000
7	3.028415000	10.452972000	7.761987000
7	2.691062000	10.452987000	11.522866000
7	4.482685000	10.452970000	9.792510000
6	3.942863000	10.452981000	12.076316000
6	1.534777000	10.452997000	12.316450000
6	0.960649000	11.680002000	12.692240000
6	1.489937000	11.690977000	6.333430000
6	-0.712794000	10.453017000	13.902642000
1	-1.596167000	10.453016000	14.531409000
6	5.173089000	10.452962000	8.668759000
6	4.974247000	10.452971000	11.009687000
6	1.557807000	12.998997000	12.277450000
1	2.333285000	12.799934000	11.538474000
6	6.349191000	10.452963000	11.165182000
1	6.780303000	10.452918000	12.156317000
6	6.580051000	10.452953000	8.774265000
1	7.192936000	10.452902000	7.884978000
6	7.107595000	10.452954000	10.041455000
1	8.186664000	10.452876000	10.142346000
6	0.533047000	13.921001000	11.628078000
1	-0.222776000	14.252145000	12.343485000
1	1.028480000	14.812729000	11.235736000
1	0.019143000	13.428024000	10.800989000
6	4.355528000	10.452963000	7.448465000
6	0.460263000	11.654981000	5.425059000
1	0.040385000	12.584110000	5.055931000
6	-0.090586000	10.452983000	4.984865000

1	-0.913835000	10.452983000	4.281973000
6	2.052776000	12.988975000	6.802628000
1	2.901153000	12.771617000	7.451048000
6	2.215385000	13.678997000	13.464684000
1	2.965671000	13.037259000	13.930016000
1	2.711122000	14.601198000	13.148400000
1	1.476595000	13.941829000	14.225901000
6	2.004766000	10.452975000	6.786619000
6	-0.175640000	11.639012000	13.495831000
1	-0.634708000	12.567440000	13.814173000
6	2.586196000	13.823968000	5.650817000
1	1.788218000	14.143772000	4.975882000
1	3.074230000	14.724578000	6.032935000
1	3.320180000	13.268502000	5.063036000
6	1.044485000	13.743984000	7.626262000
1	0.664914000	13.133152000	8.447278000
1	1.491908000	14.645011000	8.055320000
1	0.189171000	14.057052000	7.020613000

LCuCl – B3LYP/def2-TZVPP (Procedure according to Lancaster et al.)

0, 1

8	6.000789000	5.626517000	4.887183000
7	7.495912000	7.304527000	4.362562000
6	7.091880000	6.015524000	4.507450000
6	8.188968000	5.063531000	4.148703000
6	6.620817000	8.353520000	4.746364000
6	8.158972000	3.680531000	4.144680000
1	7.243010000	3.165308000	4.398413000
6	5.832049000	8.981530000	3.777181000
6	5.890397000	8.566547000	2.332190000
1	6.677055000	7.817703000	2.242685000
6	6.597493000	8.750505000	6.087363000
6	4.973941000	9.995523000	4.216987000
1	4.336008000	10.495963000	3.497982000
6	7.525250000	8.138495000	7.105579000
1	8.142915000	7.405919000	6.586703000
6	4.925622000	10.368507000	5.539979000
1	4.249283000	11.158455000	5.846146000
6	5.727404000	9.768499000	6.450165000
1	5.689507000	10.086540000	7.485778000
6	8.462102000	9.146490000	7.711816000
1	9.025547000	9.684458000	6.947526000
1	9.178028000	8.644883000	8.368414000
1	7.926917000	9.885771000	8.314872000

6	6.246624000	9.696558000	1.380289000
1	5.473274000	10.469505000	1.368565000
1	6.341918000	9.305043000	0.364808000
1	7.190330000	10.170015000	1.654055000
6	6.766992000	7.378481000	8.184388000
1	6.140505000	8.048765000	8.780045000
1	7.465567000	6.884901000	8.865123000
1	6.121224000	6.613353000	7.748876000
6	4.603503000	7.918549000	1.898873000
1	4.344111000	7.067304000	2.532811000
1	4.676785000	7.556759000	0.869629000
1	3.769745000	8.625349000	1.941633000
29	9.318039000	7.538537000	3.830003000
17	9.318035000	9.647537000	3.830028000
8	12.635298000	5.626556000	2.773779000
7	9.318043000	5.679537000	3.829982000
7	11.141168000	7.304547000	3.298439000
6	11.545206000	6.015550000	3.153521000
6	10.447121000	5.063543000	3.512246000
6	9.318049000	2.997537000	3.829951000
1	9.317859000	1.915527000	3.829660000
6	12.015258000	8.353553000	2.913662000
6	10.478123000	3.680543000	3.516238000
1	11.394225000	3.165512000	3.262770000
6	12.805023000	8.981544000	3.883859000
6	12.745677000	8.566527000	5.328840000
1	11.958844000	7.817810000	5.417934000
6	12.038580000	8.750569000	1.573672000
6	13.663127000	9.995551000	3.444077000
1	14.301534000	10.495249000	4.163216000
6	11.111826000	8.138579000	0.555442000
1	10.494094000	7.405961000	1.074302000
6	13.711444000	10.368566000	2.121093000
1	14.387770000	11.158386000	1.814596000
6	12.908665000	9.768575000	1.210893000
1	12.945654000	10.086025000	0.175081000
6	10.173969000	9.146584000	-0.050772000
1	9.610098000	9.683771000	0.713756000
1	9.458479000	8.644665000	-0.707619000
1	10.709498000	9.886232000	-0.653079000
6	12.389445000	9.696515000	6.279767000
1	13.162931000	10.469344000	6.291760000
1	12.293304000	9.305589000	7.295427000
1	11.446108000	10.170351000	6.005352000

6	11.869087000	7.378593000	-0.523385000
1	12.495432000	8.049132000	-1.118908000
1	11.169993000	6.885287000	-1.203811000
1	12.514738000	6.613096000	-0.088281000
6	14.032574000	7.918525000	5.762142000
1	14.291402000	7.066757000	5.128667000
1	13.959692000	7.557486000	6.791714000
1	14.866144000	8.625427000	5.718169000

LCuBr – B3LYP/def2-TZVPP (Procedure according to Lancaster et al.)

0, 1

8	6.000789000	5.626517000	4.887183000
7	7.495912000	7.304527000	4.362562000
6	7.091880000	6.015524000	4.507450000
6	8.188968000	5.063531000	4.148703000
6	6.620817000	8.353520000	4.746364000
6	8.158972000	3.680531000	4.144680000
1	7.243010000	3.165308000	4.398413000
6	5.832049000	8.981530000	3.777181000
6	5.890397000	8.566547000	2.332190000
1	6.677055000	7.817703000	2.242685000
6	6.597493000	8.750505000	6.087363000
6	4.973941000	9.995523000	4.216987000
1	4.336008000	10.495963000	3.497982000
6	7.525250000	8.138495000	7.105579000
1	8.142915000	7.405919000	6.586703000
6	4.925622000	10.368507000	5.539979000
1	4.249283000	11.158455000	5.846146000
6	5.727404000	9.768499000	6.450165000
1	5.689507000	10.086540000	7.485778000
6	8.462102000	9.146490000	7.711816000
1	9.025547000	9.684458000	6.947526000
1	9.178028000	8.644883000	8.368414000
1	7.926917000	9.885771000	8.314872000
6	6.246624000	9.696558000	1.380289000
1	5.473274000	10.469505000	1.368565000
1	6.341918000	9.305043000	0.364808000
1	7.190330000	10.170015000	1.654055000
6	6.766992000	7.378481000	8.184388000
1	6.140505000	8.048765000	8.780045000
1	7.465567000	6.884901000	8.865123000
1	6.121224000	6.613353000	7.748876000
6	4.603503000	7.918549000	1.898873000
1	4.344111000	7.067304000	2.532811000

1	4.676785000	7.556759000	0.869629000
1	3.769745000	8.625349000	1.941633000
29	9.318039000	7.538537000	3.830003000
17	9.318035000	9.647537000	3.830028000
8	12.635298000	5.626556000	2.773779000
7	9.318043000	5.679537000	3.829982000
7	11.141168000	7.304547000	3.298439000
6	11.545206000	6.015550000	3.153521000
6	10.447121000	5.063543000	3.512246000
6	9.318049000	2.997537000	3.829951000
1	9.317859000	1.915527000	3.829660000
6	12.015258000	8.353553000	2.913662000
6	10.478123000	3.680543000	3.516238000
1	11.394225000	3.165512000	3.262770000
6	12.805023000	8.981544000	3.883859000
6	12.745677000	8.566527000	5.328840000
1	11.958844000	7.817810000	5.417934000
6	12.038580000	8.750569000	1.573672000
6	13.663127000	9.995551000	3.444077000
1	14.301534000	10.495249000	4.163216000
6	11.111826000	8.138579000	0.555442000
1	10.494094000	7.405961000	1.074302000
6	13.711444000	10.368566000	2.121093000
1	14.387770000	11.158386000	1.814596000
6	12.908665000	9.768575000	1.210893000
1	12.945654000	10.086025000	0.175081000
6	10.173969000	9.146584000	-0.050772000
1	9.610098000	9.683771000	0.713756000
1	9.458479000	8.644665000	-0.707619000
1	10.709498000	9.886232000	-0.653079000
6	12.389445000	9.696515000	6.279767000
1	13.162931000	10.469344000	6.291760000
1	12.293304000	9.305589000	7.295427000
1	11.446108000	10.170351000	6.005352000
6	11.869087000	7.378593000	-0.523385000
1	12.495432000	8.049132000	-1.118908000
1	11.169993000	6.885287000	-1.203811000
1	12.514738000	6.613096000	-0.088281000
6	14.032574000	7.918525000	5.762142000
1	14.291402000	7.066757000	5.128667000
1	13.959692000	7.557486000	6.791714000
1	14.866144000	8.625427000	5.718169000

[**L**CuF]⁻ – B3LYP/def2-TZVPP (DFT/NBO)

−1, 2

29	6.708322000	5.360385000	3.958870000
9	5.614342000	5.697829000	5.383780000
8	5.159020000	3.877917000	0.478777000
8	10.730548000	5.990846000	4.169167000
7	8.467482000	5.926723000	4.713995000
7	7.845290000	4.974922000	2.448964000
7	5.343173000	4.707885000	2.642777000
6	3.931130000	4.635430000	2.836670000
6	7.294189000	4.491113000	1.339930000
6	5.796115000	4.317690000	1.445818000
6	9.441284000	4.528271000	0.299094000
1	10.071196000	4.354925000	-0.563773000
6	9.985388000	5.032083000	1.459127000
1	11.038374000	5.263825000	1.537809000
6	9.150386000	5.245423000	2.554059000
6	8.839136000	5.501623000	7.093031000
6	3.307640000	3.385671000	2.976644000
6	1.809538000	5.735246000	3.006488000
1	1.216636000	6.643200000	3.020801000
6	9.039156000	8.253555000	7.555997000
1	9.129894000	9.314216000	7.753534000
6	8.837084000	7.803609000	6.250989000
6	8.699583000	4.011672000	6.860046000
1	8.719450000	3.844335000	5.783934000
6	9.537481000	5.764299000	3.913079000
6	3.861118000	7.178454000	2.674619000
1	4.935360000	7.006539000	2.622618000
6	9.155729000	7.352529000	8.623022000
1	9.322936000	7.724880000	9.626648000
6	8.722567000	6.413649000	6.039005000
6	8.716544000	8.770635000	5.082963000
1	9.016213000	8.234350000	4.183995000
6	9.058230000	6.003562000	8.384038000
1	9.147720000	5.310258000	9.212311000
6	7.266721000	9.199188000	4.914844000
1	6.615073000	8.336043000	4.774468000
1	7.148377000	9.856433000	4.048506000
1	6.916798000	9.745985000	5.795168000
6	4.115144000	2.104363000	3.039729000
1	5.118301000	2.333919000	2.689395000
6	4.256857000	1.648334000	4.494748000
1	4.686187000	2.441199000	5.110169000

1	4.909730000	0.774008000	4.568822000
1	3.287176000	1.376872000	4.922020000
6	9.869231000	3.215234000	7.461150000
1	10.826049000	3.578876000	7.079033000
1	9.781477000	2.159757000	7.190235000
1	9.891474000	3.280118000	8.551425000
6	3.447468000	7.831589000	1.372576000
1	3.684807000	7.191751000	0.518965000
1	3.971352000	8.781183000	1.233194000
1	2.374218000	8.040485000	1.344493000
6	3.200586000	5.828710000	2.856593000
6	1.916620000	3.359207000	3.106538000
1	1.409870000	2.407236000	3.214091000
6	8.075180000	4.243794000	0.224994000
1	7.624414000	3.850696000	-0.674905000
6	1.178063000	4.518491000	3.119461000
1	0.099808000	4.475464000	3.225172000
6	3.611373000	8.085571000	3.878584000
1	2.547253000	8.296780000	4.014456000
1	4.123148000	9.042093000	3.744917000
1	3.993641000	7.618761000	4.787260000
6	9.650999000	9.982279000	5.212013000
1	9.353024000	10.646396000	6.026483000
1	9.629621000	10.569796000	4.290919000
1	10.681319000	9.668624000	5.393093000
6	3.566795000	1.015557000	2.134706000
1	2.560309000	0.701801000	2.422982000
1	4.203412000	0.128016000	2.179484000
1	3.532693000	1.354274000	1.097571000
6	7.365349000	3.505193000	7.374953000
1	7.287471000	3.622887000	8.460106000
1	7.239216000	2.444067000	7.138904000
1	6.543146000	4.054422000	6.911858000

[**L**CuCl]⁻ – B3LYP/def2-TZVPP (DFT/NBO)

−*1, 2*

29	4.151466000	10.390127000	14.354304000
17	2.077402000	11.029081000	14.762055000
8	7.240264000	12.885458000	15.272083000
8	5.068755000	6.568988000	13.243021000
7	5.121340000	12.081260000	14.813079000
7	3.869616000	8.505998000	13.695608000
7	5.997508000	9.793208000	14.221530000
6	4.580246000	13.360286000	15.139823000

6	6.236604000	8.547154000	13.830760000
6	4.974666000	7.767036000	13.555809000
6	6.969440000	10.646315000	14.526449000
6	2.643670000	7.799892000	13.479647000
6	2.058639000	7.085040000	14.531731000
6	7.539637000	8.091208000	13.719926000
1	7.730178000	7.077129000	13.398096000
6	3.588062000	15.855343000	15.798328000
1	3.198298000	16.834122000	16.054122000
6	4.261141000	13.643498000	16.477753000
6	8.294467000	10.263375000	14.445603000
1	9.077891000	10.963835000	14.696626000
6	0.911813000	7.021541000	12.000664000
1	0.453579000	6.990162000	11.020568000
6	0.365787000	6.268685000	13.017757000
1	-0.509593000	5.656858000	12.832304000
6	8.575567000	8.963320000	14.031845000
1	9.601913000	8.629275000	13.951314000
6	0.922699000	6.319932000	14.274786000
1	0.472871000	5.748976000	15.078410000
6	3.911167000	15.563136000	14.484400000
1	3.784167000	16.324978000	13.723460000
6	2.051756000	7.798640000	12.201608000
6	4.427260000	14.317104000	14.132648000
6	3.761050000	14.903522000	16.781503000
1	3.515293000	15.150863000	17.808370000
6	4.881372000	14.017886000	12.708730000
1	5.423380000	13.073635000	12.768390000
6	1.643439000	7.842420000	16.880573000
1	1.400427000	8.841434000	16.517186000
1	2.082158000	7.940103000	17.877881000
1	0.714482000	7.275053000	16.982235000
6	2.957585000	5.745422000	16.466021000
1	2.064168000	5.122898000	16.553695000
1	3.414834000	5.806558000	17.457532000
1	3.659303000	5.232347000	15.804765000
6	5.564031000	13.121926000	18.547930000
1	6.476374000	13.424662000	18.030626000
1	5.822911000	12.342241000	19.269591000
1	5.195891000	13.982721000	19.113530000
6	2.060701000	10.044457000	11.134223000
1	0.993482000	10.038329000	10.888482000
1	2.557813000	10.687943000	10.402361000
1	2.175245000	10.497389000	12.117467000

6	2.414910000	8.055228000	9.685588000
1	2.775763000	7.026765000	9.612789000
1	2.956350000	8.653675000	8.949476000
1	1.361864000	8.068698000	9.394980000
6	5.885350000	15.035854000	12.197623000
1	5.422004000	16.012876000	12.028252000
1	6.306868000	14.705025000	11.244428000
1	6.708917000	15.171568000	12.901318000
6	3.773448000	13.813660000	11.758691000
1	3.085884000	13.035980000	12.100352000
1	4.149525000	13.509130000	10.777146000
1	3.182667000	14.725273000	11.613050000
6	6.445338000	12.002352000	14.916181000
6	4.514125000	12.616699000	17.566946000
1	4.919871000	11.729593000	17.083939000
6	2.617542000	7.138313000	15.939759000
1	3.536742000	7.721044000	15.915966000
6	2.627783000	8.641480000	11.083502000
1	3.704440000	8.707120000	11.250846000
6	3.248100000	12.198752000	18.290933000
1	2.789662000	13.041572000	18.816972000
1	3.469913000	11.431038000	19.037275000
1	2.514719000	11.789538000	17.594785000

[**LCuBr**]⁻ – B3LYP/def2-TZVPP (DFT/NBO)

− 1, 2

35	4.394846000	11.021629000	5.312133000
29	2.192578000	10.335171000	5.751635000
8	1.295310000	6.512215000	6.825735000
8	-0.894563000	12.828229000	4.850617000
7	0.351385000	9.733671000	5.877213000
7	2.482935000	8.460959000	6.405314000
7	1.225134000	12.019537000	5.289807000
6	-0.624323000	10.584008000	5.581220000
6	-1.939447000	10.198366000	5.664927000
1	-2.726430000	10.896345000	5.416808000
6	-2.219886000	8.899364000	6.080626000
1	-3.245531000	8.564428000	6.164405000
6	-1.181186000	8.030007000	6.391626000
1	-1.370470000	7.016408000	6.715920000
6	0.118964000	8.484659000	6.272929000
6	1.378701000	7.714249000	6.532985000
6	3.709700000	7.751570000	6.603377000
6	4.291678000	7.054614000	5.533336000

6	5.419417000	6.281245000	5.776369000
1	5.865115000	5.720530000	4.963067000
6	5.979188000	6.204838000	7.034446000
1	6.851224000	5.584607000	7.206620000
6	5.440229000	6.942789000	8.063503000
1	5.900423000	6.891968000	9.042099000
6	4.304484000	7.730149000	7.880471000
6	3.728930000	7.129051000	4.130257000
1	2.848754000	7.769806000	4.156519000
6	4.726266000	7.749956000	3.167544000
1	5.044728000	8.735003000	3.509937000
1	4.274764000	7.866135000	2.177740000
1	5.613118000	7.121181000	3.051962000
6	3.288618000	5.750274000	3.635914000
1	4.137801000	5.066097000	3.568017000
1	2.837114000	5.818432000	2.642054000
1	2.552703000	5.305863000	4.308856000
6	3.733531000	8.551089000	9.015538000
1	2.654381000	8.600508000	8.850441000
6	4.259937000	9.958944000	8.987902000
1	5.330313000	9.980930000	9.221245000
1	3.755180000	10.573851000	9.739006000
1	4.124171000	10.433314000	8.018212000
6	3.948133000	7.951756000	10.392456000
1	3.596577000	6.919042000	10.453141000
1	3.402312000	8.533984000	11.138457000
1	5.000865000	7.968228000	10.686441000
6	-0.103871000	11.943936000	5.192573000
6	1.766554000	13.297449000	4.954148000
6	2.098851000	13.569616000	3.625256000
6	2.602262000	14.833532000	3.319588000
1	2.855929000	15.074075000	2.293056000
6	2.769374000	15.792292000	4.297804000
1	3.161710000	16.769366000	4.040094000
6	2.434076000	15.502131000	5.604691000
1	2.555638000	16.265603000	6.365180000
6	1.913663000	14.259209000	5.959361000
6	1.851740000	12.548902000	2.531014000
1	1.473499000	11.647233000	3.009882000
6	0.767040000	13.048399000	1.574934000
1	-0.141395000	13.317888000	2.116451000
1	0.513709000	12.275935000	0.843651000
1	1.104838000	13.928308000	1.020445000
6	3.112756000	12.170690000	1.778148000

1	3.537782000	13.027907000	1.247551000
1	2.896015000	11.402317000	1.030866000
1	3.871292000	11.777514000	2.455663000
6	1.459347000	13.971059000	7.380230000
1	0.929578000	13.019528000	7.340118000
6	0.453555000	14.994247000	7.886265000
1	0.916467000	15.974071000	8.037296000
1	0.040970000	14.675644000	8.847335000
1	-0.376481000	15.118429000	7.187832000
6	2.578142000	13.805551000	8.339381000
1	3.282212000	13.037674000	8.009684000
1	2.206890000	13.509608000	9.325127000
1	3.147187000	14.732887000	8.467551000

References

1. Donoghue, P. J. *et al.* Rapid C–H bond activation by a monocopper(III)–hydroxide complex. *J. Am. Chem. Soc.* **133**, 17602–17605 (2011).

2. Bolli, C. *et al.* Bis(triphenyl-λ^5-phosphanylidene)ammonium fluoride: a reactive fluoride source to access the hypervalent silicates [Me$_n$SiF$_{5-n}$]$^-$ (n = 0–3). *Dalt. Trans.* **43**, 4326–4334 (2014).

3. Jang, E. S. *et al.* Copper(II) anilides in sp^3 C-H amination. *J. Am. Chem. Soc.* **136**, 10930–10940 (2014).

4. Barham, J. P., John, M. P. & Murphy, J. A. Contra-thermodynamic hydrogen atom abstraction in the selective C–H functionalization of trialkylamine N-CH$_3$ groups. *J. Am. Chem. Soc.* **138**, 15482–15487 (2016).

5. Bordwell, F. G. Equilibrium acidities in dimethyl sulfoxide solution. *Acc. Chem. Res.* **21**, 456–463 (1988).

6. Olmstead, W. N., Margolin, Z. & Bordwell, F. G. Acidities of water and simple alcohols in dimethyl sulfoxide solution. *J. Org. Chem.* **45**, 3295–3299 (1980).

7. Izutsu, K. *Acid-Base Dissociation Constants in Dipolar Aprotic Solvents*. (Blackwell Scientific Publications, 1990).

8. Mandal, M. *et al.* Mechanisms for hydrogen-atom abstraction by mononuclear copper(III) cores: Hydrogen-atom transfer or concerted proton-coupled electron transfer? *J. Am. Chem. Soc.* **141**, 17236–17244 (2019).

9. Wang, Z., Deng, H., Li, X., Ji, P. & Cheng, J.-P. Standard and Absolute pK$_a$ Scales of Substituted Benzoic Acids in Room Temperature Ionic Liquids. *J. Org. Chem.* **78**, 12487–12493 (2013).

10. Elwell, C. E. *et al.* Carboxylate structural effects on the properties and proton-coupled electron transfer reactivity of [CuO$_2$CR]$^{2+}$ cores. *Inorg. Chem.* **58**, 15872–15879 (2019).

11. Olmstead, W. N. & Bordwell, F. G. Ion-pair association constants in dimethyl sulfoxide. *J. Org. Chem.* **45**, 3299–3305 (1980).

12. Bordwell, F. G. & Algrim, D. Nitrogen acids. 1. Carboxamides and sulfonamides. *J. Org. Chem.* **41**, 2507–2508 (1976).

13. Bumgardner, C. L., Lawton, E. L., McDaniel, K. G. & Carmichael, H. Photodifluoramination of alkanes and alkenes. *J. Am. Chem. Soc.* **92**, 1311–1317 (1970).

14. Takolpuckdee, P., Mars, C. A. & Perrier, S. Merrifield resin-supported chain transfer agents, precursors for RAFT polymerization. *Org. Lett.* **7**, 3449–3452 (2005).

15. Bloom, S., McCann, M. & Lectka, T. Photocatalyzed benzylic fluorination: shedding "light" on the involvement of electron transfer. *Org. Lett.* **16**, 6338–6341 (2014).

16. Gazizov, M. B. *et al.* Reaction of acyl halides and P(III) chlorides with alkyl diphenyl(or triphenyl)methyl ethers. *Russ. J. Gen. Chem.* **77**, 309–311 (2007).

17. Jordan, A. J., Thompson, P. K. & Sadighi, J. P. Copper(I)-mediated borofluorination of alkynes. *Org. Lett.* **20**, 5242–5246 (2018).

18. Beniazza, R. *et al.* Light-promoted metal-free cross dehydrogenative couplings on ethers mediated by NFSI: reactivity and mechanistic studies. *Chem. Commun.* **53**, 12708–12711 (2017).

19. Emer, E., Pfeifer, L., Brown, J. M. & Gouverneur, V. cis-Specific hydrofluorination of alkenylarenes under palladium catalysis through an ionic pathway. *Angew. Chem. Int. Ed.* **53**, 4181–4185 (2014).

20. Xu, P., Wang, F., Fan, G., Xu, X. & Tang, P. Hypervalent iodine(III)-mediated oxidative fluorination of alkylsilanes by fluoride ions. *Angew. Chem. Int. Ed.* **56**, 1101–1104 (2017).

21. Braun, M.-G. & Doyle, A. G. Palladium-catalyzed allylic C–H fluorination. *J. Am. Chem. Soc.* **135**, 12990–12993 (2013).

22. Ravel, B. & Newville, M. ATHENA, ARTEMIS, HEPHAESTUS: data analysis for X-ray absorption spectroscopy using IFEFFIT. *J. Synchrotron Radiat.* **12**, 537–541 (2005).

23. Neese, F. W95EPR. *QCPE Bull.* **15**, 5 (1995).

24. Bruker-Analytical X-ray Services. SHELXTL-PC, Vers. 5.10. (1998).

25. Blessing, R. H. An empirical correction for absorption anisotropy. *Acta Crystallogr. Sect. A* **51**, 33–38 (1995).

26. Neese, F. Software update: the ORCA program system, version 4.0. *Wiley Interdiscip. Rev. Comput. Mol. Sci.* **8**, e1327 (2018).

27. Becke, A. D. Density-functional thermochemistry. III. The role of exact exchange. *J. Chem. Phys.* **98**, 5648–5652 (1993).

28. Miehlich, B., Savin, A., Stoll, H. & Preuss, H. Results obtained with the correlation energy density functionals of becke and Lee, Yang and Parr. *Chem. Phys. Lett.* **157**, 200–206 (1989).

29. Weigend, F. & Ahlrichs, R. Balanced basis sets of split valence, triple zeta valence and quadruple zeta valence quality for H to Rn: Design and assessment of accuracy. *Phys. Chem. Chem. Phys.* **7**, 3297–3305 (2005).

30. Werner, H. J. & Knowles, P. J. A second order multiconfiguration SCF procedure with optimum convergence. *J. Chem. Phys.* **82**, 5053–5063 (1985).

31. Knowles, P. J. & Werner, H. J. An efficient second-order MC SCF method for long configuration expansions. *Chem. Phys. Lett.* **115**, 259–267 (1985).

32. Radoń, M., Broclawik, E. & Pierloot, K. Electronic structure of selected {FeNO}[7] complexes in heme and non-heme architectures: A density functional and multireference ab initio study. *J. Phys. Chem. B* **114**, 1518–1528 (2010).

33. DiMucci, I. M. *et al.* The myth of d[8] copper(III). *J. Am. Chem. Soc.* **141**, 18508–18520 (2019).

34. Neese, F. Prediction and interpretation of the [57]Fe isomer shift in Mössbauer spectra by density functional theory. *Inorganica Chim. Acta* **337**, 181–192 (2002).

35. Glendening, E. D., Landis, C. R. & Weinhold, F. NBO 6.0: Natural bond orbital analysis program. *J. Comput. Chem.* **34**, 1429–1437 (2013).

36. Reed, A. E., Weinstock, R. B. & Weinhold, F. Natural population analysis. *J. Chem. Phys.* **83**, 735–746 (1985).